

Recent Advances in Synthesis, Properties, and Applications of Metal Halide Perovskite Nanocrystals/Polymer Nanocomposites

Shuang Liang, Mingyue Zhang, Gill M. Biesold, Woosung Choi, Yanjie He, Zili Li, Dingfeng Shen, and Zhiqun Lin*

Metal halide perovskite nanocrystals (PNCs) have recently garnered tremendous research interest due to their unique optoelectronic properties and promising applications in photovoltaics and optoelectronics. Metal halide PNCs can be combined with polymers to create nanocomposites that carry an array of advantageous characteristics. The polymer matrix can bestow stability, stretchability, and solution-processability while the PNCs maintain their size-, shape- and composition-dependent optoelectronic properties. As such, these nanocomposites possess great promise for next-generation displays, lighting, sensing, biomedical technologies, and energy conversion. The recent advances in metal halide PNC/polymer nanocomposites are summarized here. First, a variety of synthetic strategies for crafting PNC/polymer nanocomposites are discussed. Second, their array of intriguing properties is examined. Third, the broad range of applications of PNC/polymer nanocomposites is highlighted, including light-emitting diodes (LEDs), lasers, and scintillators. Finally, an outlook on future research directions and challenges in this rapidly evolving field are presented.

1. Introduction

Metal halide perovskites, an emerging class of semiconducting materials with outstanding optoelectronic properties, have the general chemical formula ABX_3 . A^+ (commonly methylammonium ($CH_3NH_3^+$) (MA^+), formamidinium ($CH(NH_2)_2^+$) (FA^+), or Cs^+) and B^{2+} (commonly Pb^{2+} or Sn^{2+}) are cations of different sizes and X^- are halide anions (Cl^- , Br^- , I^-) that coordinate with the B^{2+} ions. The coordination of the X^- and B^{2+} ions results in corner sharing BX_6 octahedrons that constitute

a 3D framework. The A-site cations occupy the cavity within the framework. Metal halide perovskites have a relatively soft lattice and a dynamically disordered crystal structure which results in tunable charge-carrier recombination rates and other nonclassical semiconductor characteristics.^[1] Metal halide perovskites have been extensively studied for solar energy conversion over the past decade due to their intriguing optoelectronic properties, including near-perfect crystalline structures,^[2] tunable direct bandgaps,^[3] large absorption coefficient ($1.5 \times 10^4 \text{ cm}^{-1}$ at 550 nm),^[4] high ambipolar mobility ($\approx 20 \text{ cm}^2 \text{ V}^{-1} \text{ s}^{-1}$),^[5] long carrier diffusion lengths (100–1000 nm; $\approx 175 \text{ }\mu\text{m}$ in $MAPbI_3$ single crystals) ($L_{\text{eff,e}}/L_{\text{eff,h}} < 1$),^[6] small exciton binding energy ($\approx 30 \text{ meV}$),^[7] high defect tolerance,^[8] solution processability, and low processing cost.^[9] Notably, the certified power conversion efficiency


(PCE) of single-junction perovskite solar cells has rapidly increased from 3.8% in 2009 to 25.2% in 2019.^[10]

It is also notable that charge carriers within metal halide perovskites can undergo radiative recombination to emit light, making them promising candidates as next-generation light sources for light-emitting diodes (LEDs)^[11] and lasers.^[12] Bulk perovskite, however, exhibits limited photoluminescence quantum yield (PLQY) due to the presence of mobile ionic defects and small exciton binding energy.^[13] In contrast, perovskite nanocrystals (PNCs) possess strong quantum confinement and display improved optoelectronic properties from their bulk counterparts.^[14] Notably, metal halide PNCs possess high luminescence, narrow full width at half maximum, and a composition- and size-dependent bandgap.^[15] The photoluminescence (PL) of metal halide PNCs can be readily tuned from ultraviolet (UV) to near-infrared wavelengths by simply tailoring their composition or altering their size relative to their Bohr diameters.

Hot-injection and ligand-assisted reprecipitation methods represent the two most-developed colloidal synthesis approaches of metal halide PNCs.^[13,16] The use of organic capping ligands in synthesis enables nanoscale growth of metal halide perovskite crystals and actively passivates their surface defects, in a manner similar to that of conventional NC

S. Liang, M. Zhang, G. M. Biesold, W. Choi, Dr. Y. He, Dr. Z. Li, D. Shen, Prof. Z. Lin
 School of Materials Science and Engineering
 Georgia Institute of Technology
 Atlanta, GA 30332, USA
 E-mail: zhiqun.lin@mse.gatech.edu

S. Liang, W. Choi
 School of Chemical and Biomolecular Engineering
 Georgia Institute of Technology
 Atlanta, GA 30332, USA

 The ORCID identification number(s) for the author(s) of this article can be found under <https://doi.org/10.1002/adma.202005888>.

DOI: 10.1002/adma.202005888

synthesis.^[13] To date, a wide range of nanostructures have been achieved, including quantum dots (QDs), nanoplatelets (NPLs), nanosheets (NSs), and nanowires (NWs).^[17] Similar to conventional semiconducting NCs, the composition, size, and structural engineering of metal halide PNCs can be realized via either in situ synthesis or postsynthesis methods.^[18] Specific bulky organic cations (aliphatic or aromatic alkylammonium) can be inserted into 3D perovskite framework and function as spacers that isolate single (or multiple) inorganic perovskite layers.^[19] These low-dimensional perovskites (particularly 2D perovskite) possess relaxed limits of cation dimensions, expanded compositional diversity, and high environmental stability.^[19,20] Numerous desirable properties (e.g., large exciton binding energy) can be achieved by tuning the composition and chain length of the bulky organic cations and by changing the number of layers of 2D perovskite.^[20b]

Despite recent significant advances in metal halide PNCs research, their instability remains a daunting issue that limits their widespread application.^[21] Exposure to light, elevated temperature, moisture, and other polar solvents can easily destroy the crystal structure of perovskite materials.^[22] In addition, metal halide PNCs also experience inevitable agglomeration when transitioning from liquid state to solid state during processing for technological applications, which may lead to reduced performance of as-prepared optoelectronic devices.^[23] Polymers have been widely employed to eliminate the issues described above by producing PNC/polymer nanocomposites.^[23b,24] In this context, polymers possess a myriad of unique advantageous attributes, such as the ability to chemically interact with perovskites,^[25] the capability of passivating surface defects of PNCs,^[26] favorable mechanical properties,^[27] low weight and solution processability,^[28] low diffusion rates of oxygen and moisture,^[29] high chemical resistance,^[30] and often transparent within visible wavelengths. In addition, conjugated polymers can facilitate favorable band energy level alignment,^[31] which enables charge separation at the PNCs/conjugated polymer interface and increases the lifetime of charge carriers.^[31,32] PNC/polymer nanocomposites simultaneously bestow enhanced control over the size and morphology of PNCs,^[17a] improved stability,^[30] decreased agglomeration of PNCs in the solid state,^[33] and efficient charge separation. In addition to the superior optoelectronic properties, devices made from these nanocomposites possess processing flexibility, stretchability, and self-healing properties inherited from the polymers.^[30,34]

In this review, we aim to summarize the recent advances in metal halide PNC/polymer nanocomposites (all polymers and PNCs mentioned in this review have been summarized in **Table 1**). First, the state-of-the-art synthetic strategies of metal halide PNC/polymer nanocomposites will be introduced. Subsequently, the optical, optoelectronic, and electronic properties of metal halide PNCs and PNC/polymer nanocomposites will be presented. Next, the mechanical properties of as-prepared nanocomposites and stabilities of metal halide PNCs in these nanocomposites will be discussed. Moreover, the applications of metal halide PNC/polymer nanocomposites in LEDs, lasers, scintillators, biosensors and bioimaging, photocatalysis, and piezoelectric nanogenerators will be highlighted. Finally, a perspective on future research opportunities and challenges in this rich and rapidly developing field will be provided.

2. Synthesis of Metal Halide PNC/Polymer Nanocomposites

2.1. Chemical Anchoring of Polymers onto PNCs

2.1.1. *In Situ Synthesis of PNCs in the Presence of Polymerizable Capping Agents*

The large surface area to volume ratio of NCs results in high surface energies that promote aggregation of NCs. As noted above, capping ligands, such as small organic molecules and polymers, have been widely utilized in the colloidal synthesis of metal halide PNCs to stabilize their surface. The interaction between the small organic molecule capping agents and PNCs is, however, primarily through weak, noncovalent, dynamic bonding^[90] which can easily be broken by high temperature and UV irradiation. Variation in ion strength and solvent composition have also been found to degrade PNCs.^[22b,91] Therefore, encapsulating PNCs with polymeric capping ligands (with stronger binding than conventional small organic molecular capping ligands) has been introduced as an alternative.^[64] Chemically anchoring polymers onto PNCs can also eliminate phase separation between polymers and PNCs due to their strong chemical interactions, which yields starkly different samples than physical mixing.

The in situ synthesis of PNCs in the presence of polymerizable species was among the first feasible approaches to produce PNC/polymer nanocomposites with strong chemical bonding between the perovskite NCs and polymer capping ligands. Recently, crosslinked methylammonium lead bromide (MAPbBr₃) PNCs were crafted through a modified ligand-assisted reprecipitation method using the trifunctional 4-vinyl-benzyl-dimethyloctadecylammonium chloride (V-18) as the polymerizable ligand.^[64] In V-18, the center of the ligand (an ammonium group with two methyl groups) was found to induce sufficient ionic interactions with PNCs to anchor the ligands onto the NC surfaces, and the styryl groups and long alkyl side chain were found to facilitate radical polymerization and high colloidal stability, respectively.^[64] As shown in **Figure 1a,b**, when synthesized in the presence of other inorganic ligands V-18-capped MAPbBr₃ NCs exhibit monodisperse morphology, excellent PLQY, high film conductivity, and optical homogeneity due to enhanced surface passivation. Further study demonstrated that the as-prepared MAPbBr₃ NCs could be thermally polymerized, or copolymerized with styrene and methyl methacrylate to obtain homogeneous MAPbBr₃ PNC/polymer nanocomposites that could be applied in LEDs with excellent performance.^[64] This in situ method has been further extended to include other commercially available monomers, such as methyl methacrylate,^[56] lauryl methacrylate,^[59] and styrene.^[75]

In situ synthesis of PNCs (e.g., CsPbBr₃ NCs) has also been conducted in pure monomer solutions. After formation of the NCs, the surface capped monomers can be polymerized via thermal polymerization or UV light-induced photopolymerization, both of which provide enhanced protection of the PNCs.^[56] The resulting nanocomposites have been found to be highly soluble in organic solvents, which enables solution-processability

Table 1. Polymers and PNCs used in PNC/polymer nanocomposites.

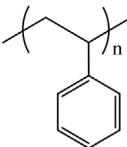
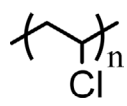
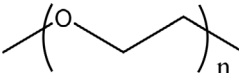
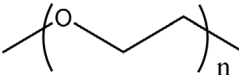
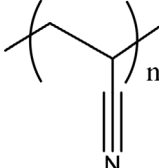
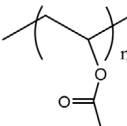
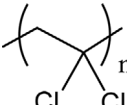

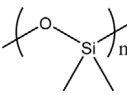
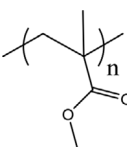
Polymer/monomer		Chemical structure	PNC	PLQY	Ref.
Polystyrene	PS		CsPbX ₃	75% ^[29] 44% ^[35] 25% ^[36] 68% ^[37] 34% ^[38] 48% ^[39] 27% ^[40] 79% ^[41]	[29,35–42]
Poly(vinyl chloride)	PVC		MAPbBr ₃ MAPbBr ₃	80% ^[43] 16% ^[38] 80% ^[43] 65% ^[45]	[43,44] [38,43,45]
Poly(ethylene glycol)	PEG		CsPbX ₃	41% ^[46]	[46]
Poly(ethylene oxide)	PEO		MAPbX ₃	N/A	[34a,47]
Polyacrylonitrile	PAN		FAPbBr ₃ CsPbBr ₃ MAPbX ₃	N/A 60% ^[49] 80% ^[43] 30.9% ^[50]	[48] [49] [43,50]
Poly(vinyl acetate)	PVAc		CsPbX ₃	N/A	[39]
Poly(vinylidene chloride)	PVDC		MAPbBr ₃	80% ^[43]	[43]
Poly(vinylidene fluoride)	PVDF		MAPbX ₃	80% ^[43] 94.6% ^[51] 80% ^[52]	[43,51–53]
Poly(dimethylsiloxane)	PDMS		CsPbBr ₃ MAPbX ₃	65% ^[54] 10% ^[23b]	[54] [23b]
Poly(methyl methacrylate)	PMMA		FAPbBr ₃ CsPbX ₃	N/A 54% ^[56] 45% ^[57]	[55] [14a,56–58]
			FAPbBr ₃ MAPbBr ₃	N/A 80% ^[43] 40.4% ^[45]	[58a] [38,43,45]

Table 1. Continued.

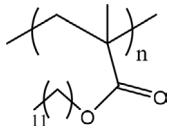
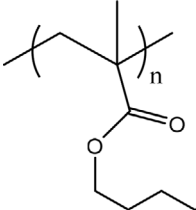
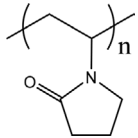
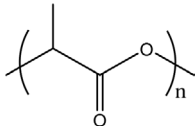
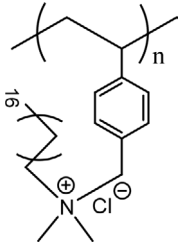
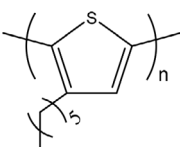
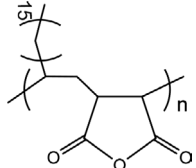
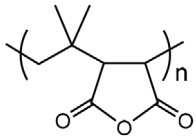
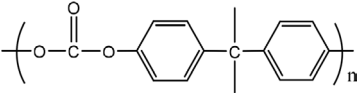
Polymer/monomer		Chemical structure	PNC	PLQY	Ref.
Poly(lauryl methacrylate)	PLMA		CsPbBr ₃	86% ^[59]	[29,59]
Poly(butyl methacrylate)	PBMA		CsPbBr ₃	N/A	[24a]
Poly(vinylpyrrolidone)	PVP		FAPbBr ₃	N/A	[58a]
Poly(lactic acid)	PLA		CsPbX ₃ CsPbX ₃	55% ^[60] 24% ^[61] 90% ^[63]	[58a,60–62] [63]
Poly(4-vinyl-benzyl-dimethyloctadecyl-ammonium chloride)	V-18		MAPbBr ₃	95% ^[64]	[64]
Poly(3-hexylthiophene)	P3HT		MAPbBr ₃	N/A	[65]
Poly(maleic anhydride- <i>alt</i> -1-octadecene)	PMAO		CsPbX ₃	88% ^[66] 69% ^[67] 88.8% ^[68]	[66–68]
Poly(isobutylene- <i>alt</i> -maleic anhydride)	PIMA		CsPbBr ₃	80% ^[69]	[69]
Polycarbonate	PC		MAPbBr ₃	31% ^[38] 43.6% ^[45]	[38,44,45]

Table 1. Continued.

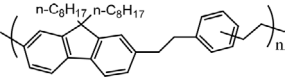
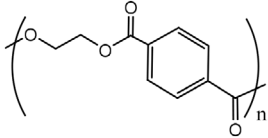
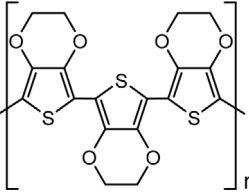
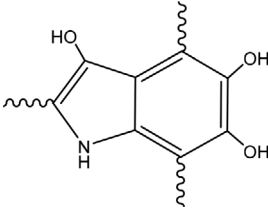
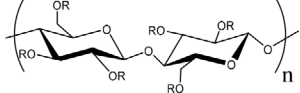
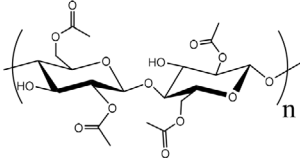
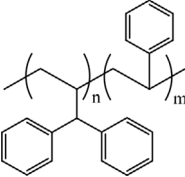
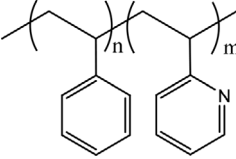
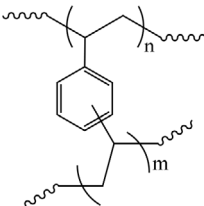
Polymer/monomer		Chemical structure	PNC	PLQY	Ref.
Poly(fluorene-co-divinylbenzene)	F8DVB		MAPbX ₃	N/A	[70]
Poly(ethylene terephthalate)	PET		CsPbBr ₃	N/A	[71]
Poly(3,4-ethylenedioxythiophene)	PEDOT		CsPbI ₃	N/A	[72]
Poly(norepinephrine)	PNE		MAPbBr ₃	N/A	[73]
Ethyl cellulose			CsPbBr ₃	37.2% ^[74]	[74]
Cellulose acetate	CA		MAPbBr ₃	47% ^[38]	[38,43]
Diphenylvinylphosphine-styrene copolymer	PDPEP-co-PS		CsPbBr ₃	90% ^[75]	[75]
Polystyrene-block-poly-2-vinylpyridine	PS-b-P2VP		CsPbX ₃	51% ^[76]	[76]
Poly(divinylbenzene)	PDVB		MAPbX ₃	63% ^[77]	[77,78]
			FAPbI ₃	N/A	[78]
			CsPbBr ₃	60% ^[79]	[79]

Table 1. Continued.

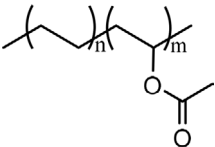
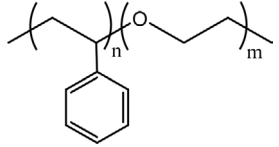
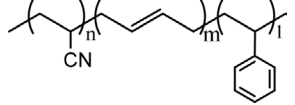
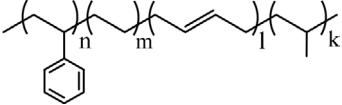
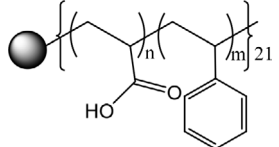
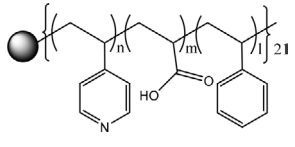
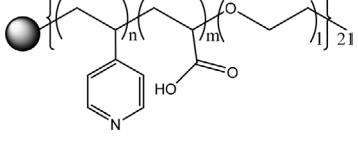
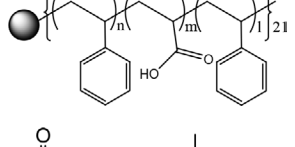
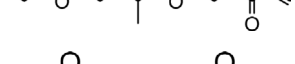
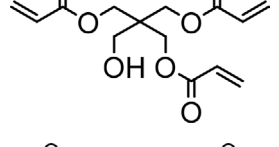
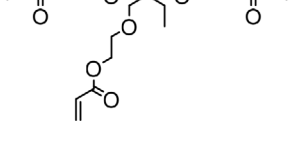
Polymer/monomer		Chemical structure	PNC	PLQY	Ref.
Poly(ethylene vinyl acetate)	PEVA		CsPbBr ₃	40.5% ^[80]	[80]
Polystyrene- <i>block</i> -poly(ethyl oxide)	PEO- <i>b</i> -PS		MAPbBr ₃	56% ^[81]	[81]
Poly(acrylonitrile butadiene styrene)	ABS		MAPbBr ₃	48% ^[38]	[38,44]
Poly(styrene-ethylene-butylene-styrene)	SEBS		CsPbBr ₃	N/A	[29]
Star-like poly(acrylic acid)- <i>block</i> -polystyrene	PAA- <i>b</i> -PS		CsPbBr ₃	91.4% ^[17a] 71% ^[82]	[17a,82]
Star-like poly(4-vinylpyridine)- <i>block</i> -poly(acrylic acid)- <i>block</i> -polystyrene	P4VP- <i>b</i> -PAA- <i>b</i> -PS		MAPbBr ₃	N/A	[83]
Star-like poly(4-vinylpyridine)- <i>block</i> -poly(acrylic acid)- <i>block</i> -poly(ethylene oxide)	P4VP- <i>b</i> -PAA- <i>b</i> -PEO		MAPbBr ₃	N/A	[83]
Star-like polystyrene- <i>block</i> -poly(acrylic acid)- <i>block</i> -polystyrene	PS- <i>b</i> -PAA- <i>b</i> -PS		CsPbBr ₃	67% ^[82]	[82]
Tri(propylene glycol) diacrylate	TPGDA		FAPbBr ₃	35% ^[84]	[84]
Pentaerythritol triacrylate	PETA		FAPbBr ₃	23.6% ^[84]	[84]
Trimethylolpropane ethoxylate triacrylate	ETPTA		FAPbBr ₃	N/A	[84]

Table 1. Continued.

Polymer/monomer		Chemical structure	PNC	PLQY	Ref.
poly(ethylenimine)	PEI		CsPbBr ₃	75% ^[85] 85% ^[86]	[85,86]
polyimide	PI		CsPbBr ₃	88.1% ^[87]	[87]
Poly(2-(dimethylamino)ethylmethacrylate)	PDMAEMA		CsPbBr ₃	60% ^[88]	[88]
Crosslinked alkynyl acid			CsPbBr ₃	N/A	[89]

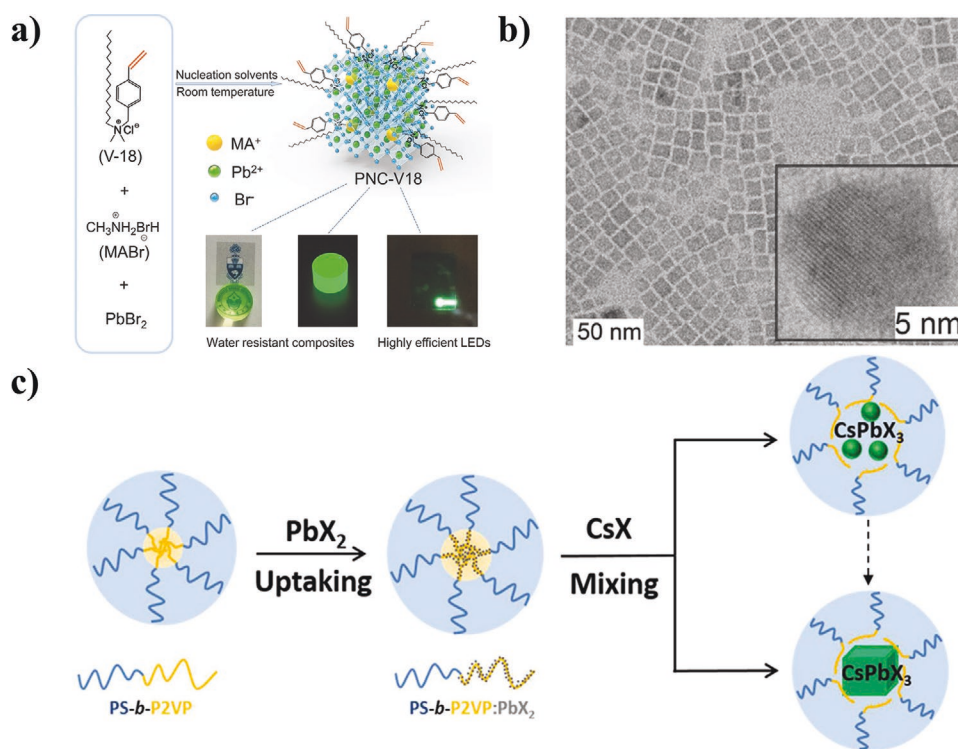


Figure 1. a) The design of perovskite NCs modified with polymerizable ligands, 4-vinyl-benzyl-dimethyloctadecylammonium chloride (V-18), and their application in light emitting diodes (LEDs) and water-resistant composite. b) Transmission electron microscopy (TEM) image and high-resolution transmission microscopy (HRTEM) image (insert) of PNCs-V18. a,b) Adapted with permission.^[64] Copyright 2017, Wiley-VCH. c) Synthetic strategy for perovskite NCs using linear amphiphilic block copolymer micelles as nanoreactors. c) Adapted with permission.^[76] Copyright 2017, American Chemical Society.

and the ability to be used as a luminescent ink to create optoelectronic devices with high luminous efficiency and excellent color-rendering index.^[56]

2.1.2. In Situ Synthesis of PNCs in the Presence of Polymer Capping Agents

In addition to polymerizable monomer capping ligands, polymer capping ligands can also be used in the colloidal synthesis of PNCs for in situ fabrication of PNC/polymer nanocomposites.^[41,66] Cesium lead halide (CsPbX_3) NCs were recently crafted via hot-injection colloidal synthesis using a combination of poly(maleic anhydride-*alt*-1-octadecene) (PMAO) and conventional small organic molecular ligands oleic acid and oleylamine.^[66] Diffusion-ordered nuclear magnetic resonance (NMR) measurements determined that PMAO was not directly connected to the surface of PNCs, but rather interacted with the bonded small organic molecular ligands via hydrophobic interactions. As a result, PMAO decreased the diffusion coefficient of ligands on CsPbX_3 NC surface and provided a tightly connected ligand outer shell, thereby limiting the interaction between PNC surfaces and the surrounding media.

PNCs with a protective polymer shell were also crafted by anchoring functionalized polymers onto their surfaces.^[41,81] For example, after the atom transfer radical polymerization (ATRP) of styrene, the as-prepared polystyrene (PS) can be functionalized via *tert*-butyloxycarbonyl deprotection to yield ammonium bromide-terminated PS ($\text{NH}_3\text{Br-PS}$).^[41] During the in situ synthesis of CsPbBr_3 NCs, the $\text{NH}_3\text{Br-PS}$ has been demonstrated to stabilize the surface of CsPbBr_3 NC via its ammonium cation and serve as a bromide source, thereby passivating the surface of the as-prepared CsPbBr_3 NCs.^[41]

2.1.3. In Situ Synthesis of PNCs in the Presence of Polymer Nanoreactors

The above-mentioned synthetic approaches often require the addition of conventional small organic molecule ligands to control the uniformity of size and morphology of PNCs. Notably, polymerizable and polymer capping ligands bind to PNC surfaces through a similar mechanism as conventional small organic molecule ligands. Therefore, the dynamic dissociation of ligands from PNCs surfaces remains an inevitable challenge that limits the stability of PNCs under high humidity and temperature.^[92] To this end, in situ synthesis of PNCs using linear polymer micelles as nanoreactors has been developed as an alternative approach.^[76]

Recently, the amphiphilic block copolymer polystyrene-*block*-poly-2-vinylpyridine (PS-*b*-P2VP) has been demonstrated to self-assemble into a reverse micelle structure in nonpolar solvents, with the P2VP and PS blocks as the core and shell, respectively. This reverse micellar structure was then utilized to craft PNCs. Perovskite precursors were mixed with PS-*b*-P2VP copolymers in nonpolar solvents, where the internal P2VP block efficiently bound to the metal precursors (i.e., cesium bromide and lead bromide) through the coordination interaction between the pyridine groups of P2VP and the metal moieties

of precursors. This selective loading of the metal precursors into the reverse micelles was found to lead to nucleation and growth of CsPbBr_3 NCs, as shown in Figure 1c.^[93] Moreover, the outside PS blocks were demonstrated to sterically stabilize the metal precursors during crystal nucleation and growth, enhancing the colloidal stability of CsPbBr_3 NCs after the reaction, and protecting the formed CsPbBr_3 NCs from moisture and polar solvents (e.g., methanol and ethanol).^[29,76]

Because the size and morphology of the as-prepared CsPbBr_3 PNCs can easily be controlled by tuning the size and structure of the self-assembled PS-*b*-P2VP micelles, no additional small organic molecule ligands are needed.^[76] This technique has also been found to eliminate ligand dissociation due to the covalent bond between the outer PS block and the inner P2VP block. Both all-inorganic (e.g., CsPbX_3) and organic-inorganic hybrid PNCs (e.g., MAPbI_3) have been synthesized using linear block copolymer nanoreactors.^[77,78]

The dynamic instability of conventional linear polymeric micelles has proven to be a challenge in using them to craft PNCs.^[94] As noted above, these micelles are thermodynamic aggregates of multiple amphiphilic molecules above critical micelle concentration, so their size and shape depend heavily on temperature, solvent properties, solution concentration, pH, and other experimental conditions.^[95] Even small variations in those parameters during PNCs synthesis can result in the dissociation of micellar structure, which leads to poor control over PNC size and morphology. Moreover, nanocomposites prepared from this approach often encapsulate multiple PNCs within one polymer micelle, which may be deleterious for biomedical applications where cellular uptake is more feasible for smaller NCs, or in optoelectronic devices that require uniform NCs dispersion.^[96]

Recently, an unconventional strategy for crafting PNCs that capitalizes on unimolecular star-shaped block copolymer micelle nanoreactors has been developed.^[17a,82,83,97] The amphiphilic multiarm block copolymer poly(acrylic acid)-*block*-polystyrene (PAA-*b*-PS) was synthesized by sequential ATRP, with the hydrophilic PAA block in the core and the hydrophobic PS block as the shell. The unimolecular nature of the nanoreactors endows them with enhanced spherical micellar structural stability compared with conventional self-assembled linear block copolymers micelles (Figure 2a). Perovskite precursors have been found to selectively bind to the inner PAA blocks of the star-shaped copolymers via strong coordination with the carboxylic groups of the PAA blocks. The loaded perovskite metal precursors can then easily form covalently ligated PNCs within the nanoreactor via a facile and rapid coprecipitation reaction (Figure 2b). Because the PNCs are confined within the micelles, their size and size distribution can be precisely tuned by controlling the molecular weight and polydispersity of each block of the nanoreactor, which is easily achieved during ATRP of the monomers (i.e., *tert*-butyl acrylate and styrene). Because the outer PS blocks are covalently connected to the inner PAA blocks, they are permanently capped on the surface of PNCs which prevents aggregation and endows the PNCs with remarkable stability, which will be discussed in the following section.

Enhanced protection of the final PNCs can be achieved by further functionalization and engineering of the star-shaped block copolymer nanoreactors. The addition of a small amount

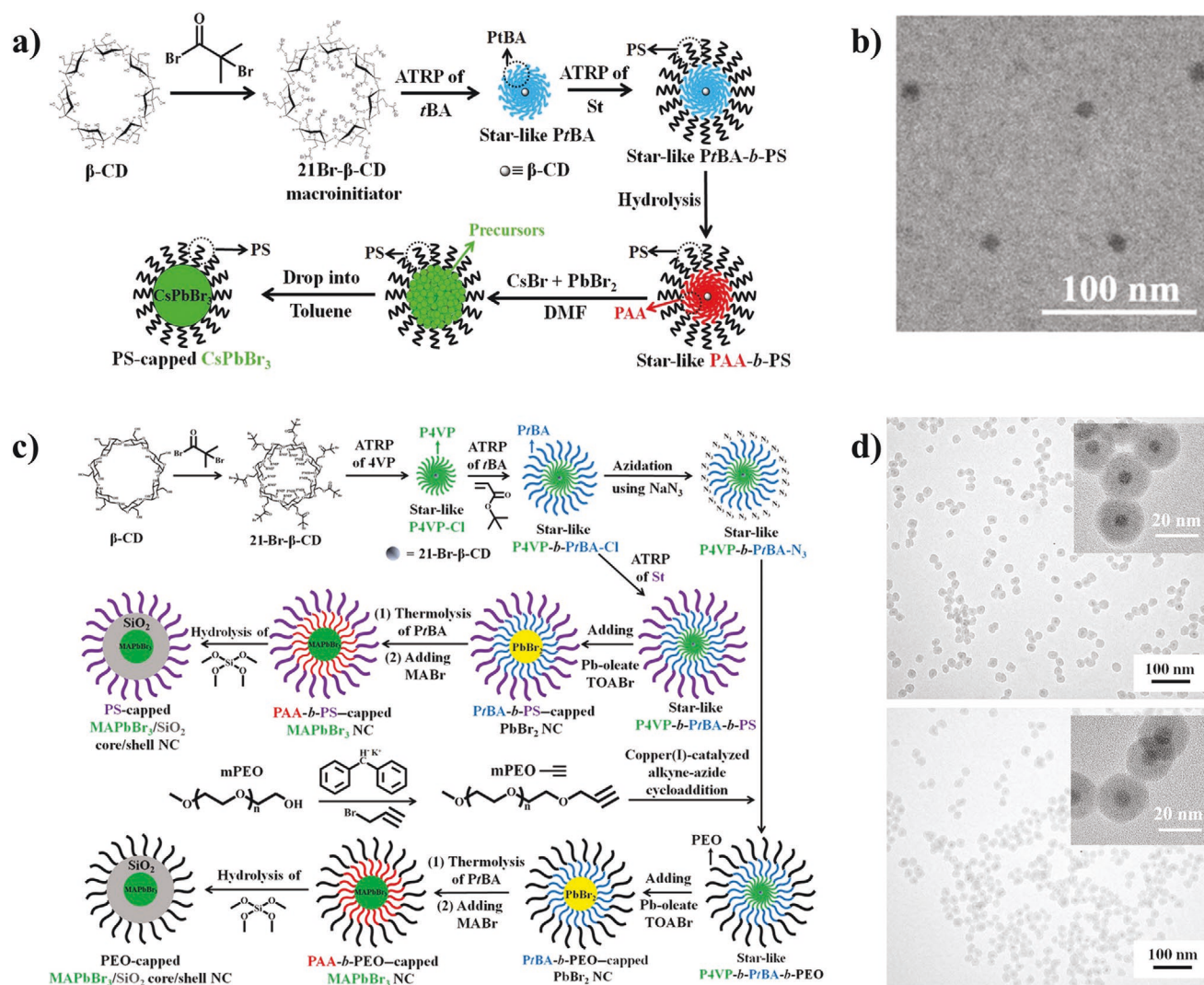


Figure 2. a) Stepwise representation of crafting "hairy" all-inorganic perovskite CsPbBr₃ QDs with intimately and permanently capped by PS chains via capitalizing on amphiphilic star-like PAA-*b*-PS diblock copolymers as nanoreactors. b) TEM image of PS-capped CsPbBr₃ QDs with diameter = 10.1 ± 0.6 nm. a,b) Adapted with permission.^[17a] Copyright 2019, Wiley-VCH. c) Stepwise representation of the synthetic route to PS-capped MAPbBr₃/SiO₂ core/shell NCs and PEO-capped MAPbBr₃/SiO₂ core/shell NCs by exploiting star-like P4VP-*b*-PtBA-*b*-PS and P4VP-*b*-PtBA-*b*-PEO as nanoreactors, respectively. d) TEM images of PEO-capped MAPbBr₃/SiO₂ core/shell NCs with MAPbBr₃ core diameter of 6.1 ± 0.3 nm and SiO₂ shell thickness of 8.9 ± 0.4 nm (top), and MAPbBr₃ core diameter of 6.8 ± 0.3 nm and SiO₂ shell thickness of 8.0 ± 0.3 nm (bottom). c,d) Adapted with permission.^[83] Copyright 2019, The Authors, published by American Association for the Advancement of Science.

of divinylbenzene as a crosslinker during the ATRP reaction of styrene has been found to yield partially crosslinked PS that forms a denser protective layer on the surface of CsPbBr₃ PNCs.^[97] In addition to diblock star-shaped amphiphilic copolymer nanoreactors, multiarm star-shaped triblock copolymers, namely poly(4-vinylpyridine)-*block*-poly(acrylic acid)-*block*-polystyrene (P4VP-*b*-PAA-*b*-PS), have been synthesized to craft PAA-*b*-PS-ligated PNCs (i.e., MAPbBr₃ NCs) via similar techniques and mechanisms as noted above (Figure 2c).^[83] A passivating SiO₂ shell was then formed around MAPbBr₃ NCs via the in situ hydrolysis of tetramethyl orthosilicate in the compartment occupied by the outer PAA blocks (Figure 2d). Water soluble poly(ethylene oxide)-ligated (PEO-ligated) dual-shelled MAPbBr₃ NCs were also formed by the substitution of hydrophobic PS to hydrophilic PEO through a click reaction.^[83]

Hollow PNCs with PS chains covalently tethered to their surface were crafted by tailoring the composition of multiarm star-shaped triblock copolymer from P4VP-*b*-PAA-*b*-PS to PS-*b*-PAA-*b*-PS.^[82]

2.1.4. Postsynthesis Anchoring of Polymers onto PNCs

In addition to in situ synthesis of PNCs with polymers or polymerizable ligands, postsynthesis modification of PNCs with polymers has been investigated. Polymeric capping ligands have been found to possess a substantially lower dissociation tendency than small organic molecule ligands due to the numerous anchoring groups on their backbones.^[24a,27] Ligand exchange has emerged as a common postsynthesis strategy to

tailor the surface capping ligands and surface chemistry of conventional QDs.^[98] Ligand exchange is, however, rarely used with PNCs because most conventional ligand exchange methods utilize polar solvents (e.g., dimethylformamide (DMF))^[99] that will result in detrimental transformation of perovskite crystals^[90b,100] or dissociation of ligands.^[101]

Until recently, two main postsynthesis methods have been developed to tether polymer capping ligands onto the surface of PNCs. One, the “grafting to” approach, involves the direct reaction between properly functionalized polymers and the NCs surface. The other, the “grafting from” approach, involves initiating polymer chain growth on functionalized NCs. For example, multidentate polymer zwitterionic ligands were grafted to PNCs, endowing PNCs with solubility in a wide range of organic solvents (Figure 3a,b).^[24a] The binding of multidentate polymeric ligands onto the surface of CsPbBr₃ PNCs can easily be triggered by simply mixing CsPbBr₃ PNC solution with multidentate polymeric ligands. This method has also been applied to the commercially available, multidentate poly(lactic acid) ligand.^[63]

PMAO, another multidentate polymeric ligand, has been anchored onto the surface of PNCs through a reaction with small organic molecule ligands.^[67] PMAO is simultaneously highly compatible in nonpolar, hydrocarbon solvents (due to its octadecane (ODE) unit) and highly reactive with surface oleylamine groups (due to its succinic units). The formed poly(succinamic acid) blocks in PMAO have been observed to release the oleylamine species from the surface of CsPbBr₃ PNCs and strongly tether to the CsPbBr₃ PNC surface via

their carboxylic and amine groups. It is notable that protective polymer shells have also been created around PNCs via hydrophobic interactions between native alkyl small organic ligands and amphiphilic block copolymers on PNC surfaces, dispensing with the need for chemical bonding.^[102]

End-group functionalization has also been utilized to craft strongly surface bound polymeric ligands. Amine, thiol, carboxyl and phosphate groups have all been found to strongly bind to PNCs and have been widely studied for end-group functionalization.^[103] Inorganic polymers, (e.g., thiol or amine functionalized polyhedral oligomeric silsesquioxane) have been observed to attach to PNCs via strong metal–S bonding or ionic interaction between the ammonium cation and PNCs.^[104] The water-triggered hydrolysis of the capped inorganic polymers results in the formation of a dense SiO₂ shell on the PNC surface.

As noted above, the “grafting from” approach involves initiating polymerization from the PNC surface. It has been reported that under UV light irradiation, the dissociation of the Pb–Br bond on the surface of CsPbBr₃ PNCs produces free radicals, which can be used to initiate the polymerization of styrene monomers.^[35] These polymer chains are directly and covalently bound to the surface of CsPbBr₃ PNCs through a Pb–C bond with high grafting density. Continuous UV light irradiation during polymerization has been found to dramatically increase the PLQY of CsPbBr₃ PNCs due to the increasing thickness and the protection rendered from the grafted PS shell. Moreover, the molecular weight of the grafted PS chains can be precisely controlled by altering reaction time.

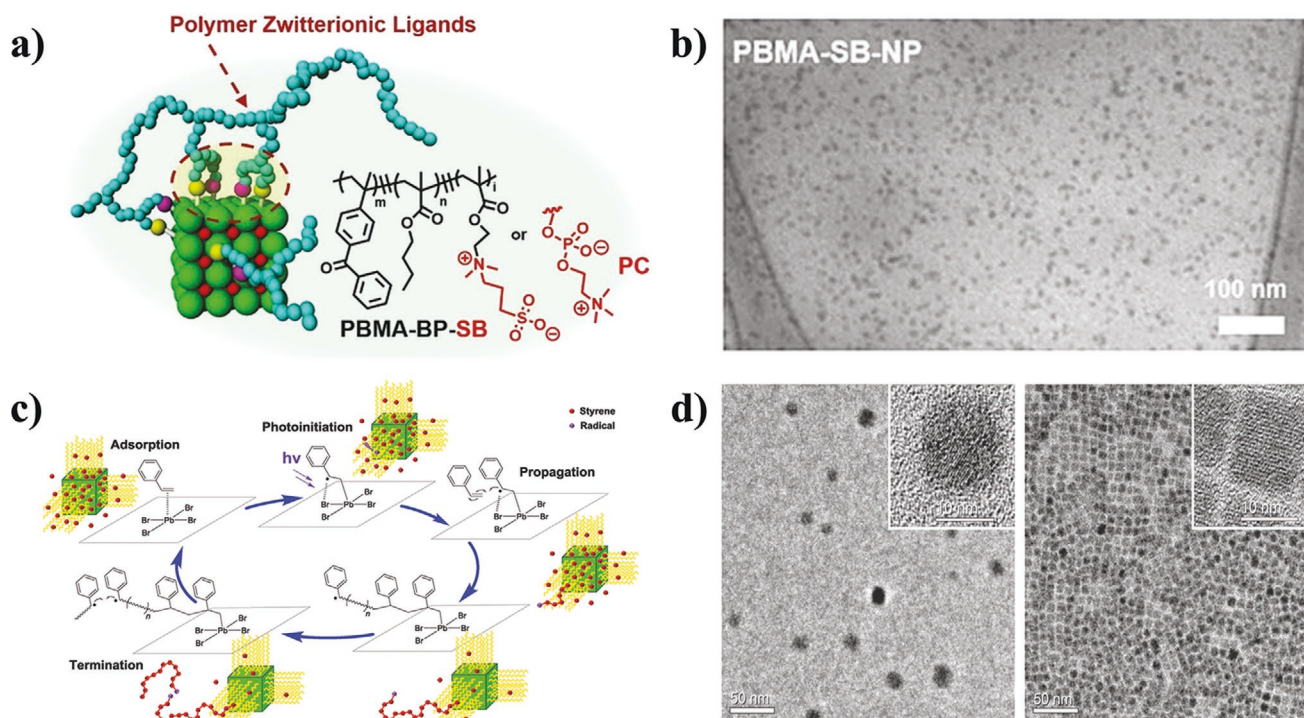


Figure 3. a) Illustration of multi-point anchoring of polymer zwitterions on a PNC surface, intended to impart NC stability and dispersion in polymer matrices. b) TEM images of PNCs with polymer zwitterions capped on surface. a,b) Adapted with permission.^[24a] Copyright 2020, Wiley-VCH. c) Proposed reaction mechanism of the perovskite photoactivated polymerization of styrene. d) TEM and HRTEM images of perovskite–polystyrene nanocomposite (left) and unreacted close-packed perovskite nanocrystals (right). c,d) Adapted with permission.^[35] Copyright 2018, Wiley-VCH.

2.2. Physical Mixing PNCs with Polymer

2.2.1. Physical Embedding Perovskite NCs into Polymer Matrix

PNCs have been physical blended with a wide range of polymer solutions, including poly(methyl methacrylate) (PMMA),^[14a] PS,^[29,36] poly(styrene-ethylene-butylene-styrene) (SEBS),^[29] and poly(lauryl methacrylate) (PLMA),^[29] to yield nanocomposites with enhanced stability and processability for optoelectronic devices. Many of these nanocomposites are crafted using a controlled solvent evaporation approach which has been demonstrated to result in poor control over film uniformity.^[105] Nanocomposite films with uniform size, thickness, and morphology were, however, produced through an optimized spin coating process.^[106] Therefore, physical blending has been recognized as a facile and promising approach for the large-scale production of perovskite NCs/polymer nanocomposites.

The “swelling-shrinking” technique is another physical blending strategy that has been used to produce PNC/polymer nanocomposites by capitalizing on the solubility differences of polymers in specific solvents.^[37] Polymer matrices are well-known to swell or shrink in specific solvents, depending on a variety of thermodynamic parameters. As shown in **Figure 4a**, PNC/polymer nanocomposites were conveniently obtained by mixing fully dissolved CsPbBr₃ PNCs with a polymer matrix (i.e., PS) in a good solvent for the polymer (i.e., toluene). Subsequently, the addition of a poor solvent (i.e., hexane) led to polymer shrinkage. The loading density of CsPbBr₃ PNCs was readily tuned by manipulating the mass or volume ratio

between the CsPbBr₃ PNCs and polymer matrices. This approach enabled the production of PNC/polymer nanocomposites under ambient conditions without inert gas protection in a relatively short timescale. Moreover, this approach eliminates the severe, disadvantageous phase separation that is normally seen in the spin-coating and controlled solvent drying approaches, which maintains the photoluminescence of CsPbBr₃ PNCs in the nanocomposites under UV light irradiation (**Figure 2b**). Polymers that have been used in this approach, include PS, polycarbonate (PC), acrylonitrile butadiene styrene (ABS),^[107] ethyl cellulose,^[74] cellulose acetate (CA), poly(vinyl chloride) (PVC), PMMA,^[107] and a superhydrophobic copolymer (i.e., poly(divinylbenzene)) that can be seen in **Figure 4c,d**.^[79]

Electrospinning, a widely applied technique for microfiber fabrication, has also been used to make PNC/polymer nanocomposites.^[108] Recently, CsPbBr₃ PNCs have been dispersed in PMMA and poly(vinylpyrrolidone) (PVP) microfibers by electrospinning at a variety of flow rates, applied voltages and needle-to-collector distances.^[58a] The CsPbBr₃ PNCs were found to be evenly distributed on the as-prepared microfibers and retained most of their optical properties.

2.2.2. Synthesis of PNCs via In Situ Conversion of Precursors in the Presence of Polymer Matrices

Physically embedding premade PNCs into polymer matrixes inevitably exposes PNCs to solvents and environments during

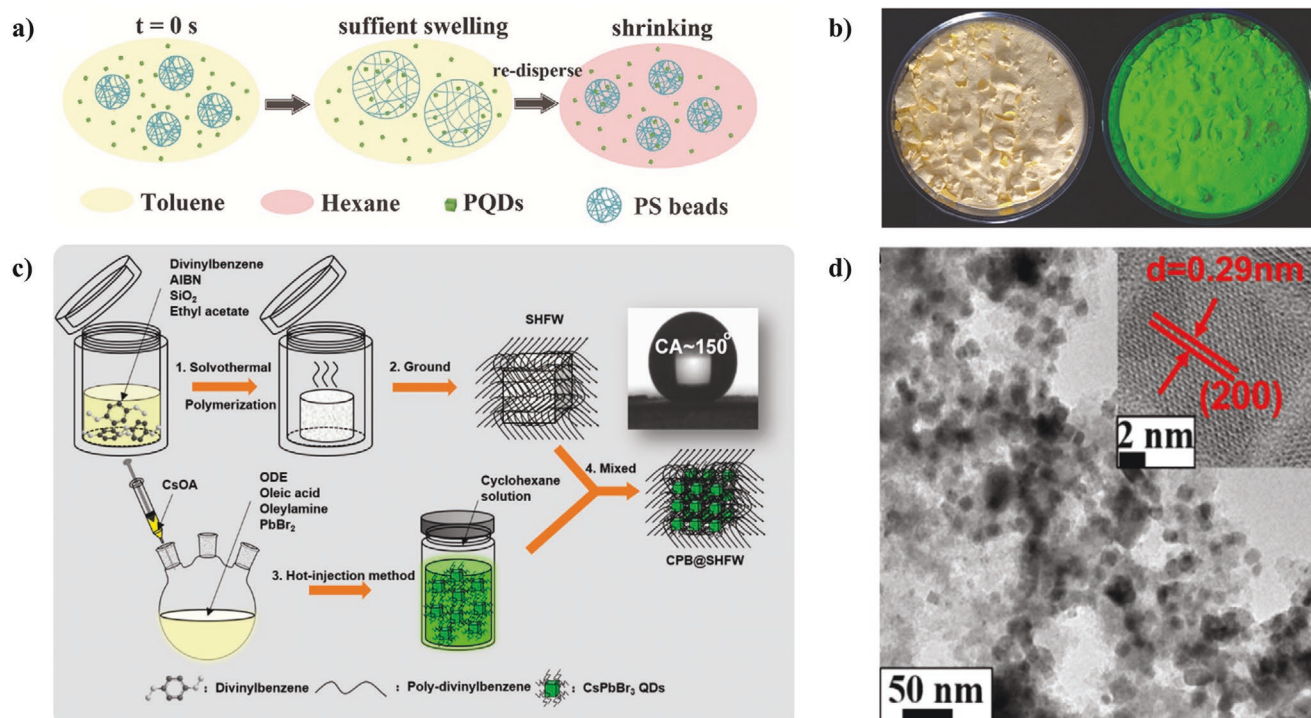


Figure 4. a) Schematic illustration of the preparation process of PNCs@PS composite spheres via swelling–shrinking strategy. b) Photographs of large-scale production under normal room light (left) and UV light (right). a,b) Adapted with permission.^[37] Copyright 2017, Wiley-VCH. c) Schematic illustration for preparation of CsPbBr₃ PNCs embedded superhydrophobic porous organic polymer (i.e., poly(divinylbenzene)) framework (CPB@SHFW) composites. d) TEM image of CPB@SHFW composite. c,d) Adapted with permission.^[79] Copyright 2019, American Chemical Society.

processing that may progressively deteriorate the crystal structure prior to receiving protection from polymer matrix. Incompatibility between the original surface-capped organic ligands on PNCs and specific polymer matrixes may also inhibit the formation of high-quality, uniform nanocomposite without phase separation. In this regard, many approaches have been developed to achieve in situ synthesis of PNCs within a polymer matrix.

For example, in situ synthesis of PNC/polymer nanocomposite films has been realized by controlled solvent evaporation via separating the crystallization of the poly(vinylidene fluoride) (PVDF) matrix and methyl ammonium lead halide (MAPbX₃) organic metal halide PNCs.^[51] The strong interaction between the ammonium cation in the precursor (i.e., MAX) with the fluoride of PVDF was found to favor permeation of the perovskite precursor into PVDF matrix and lead to uniform size and distribution of MAPbX₃ PNCs. In a typical experiment, a mixture of perovskite precursor and PVDF was first dissolved in DMF, and then drop cast onto a removable glass substrate. The spun coated substrate was then subject to two-staged controlled solvent evaporation. In the first stage of solvent drying, DMF was quickly and partially removed by vacuum, which led to the crystallization of the PVDF matrix and the formation of a colorless, transparent thin film. Residual DMF within PVDF matrix was found to inhibit the simultaneous crystallization of MAPbX₃ PNCs and thus retain the uniform distribution of perovskite precursors.^[51] In stage two, slow solvent drying of the residual DMF in ambient conditions gradually changed the colorless film into a green-emitting nanocomposite via the formation of MAPbX₃ PNCs. PVDF stands as a particularly promising polymer matrix because of its outstanding piezoelectric, thermal, and mechanical properties, as well as its hydrophobic stability.^[109] The high transparency and PLQY of these nanocomposites suggested the formation of uniformly distributed, nanoscale perovskite crystals without phase separation, making them promising candidates for LEDs.^[51]

By varying the types of polymer matrixes, this strategy can be readily extended to many commercialized polymers, such as PVP,^[60] PEO,^[47] and polydimethylsiloxane (PDMS).^[23b] For example, MAPbX₃ PNCs were grown in a porous PDMS template to produce PNC/polymer nanocomposites.^[23b]

The “swelling-shrinking” approach can also be utilized for the in situ conversion of precursors into PNCs within a polymer matrix (Figure 5a).^[38] By blending perovskite precursors instead of PNCs, perovskite crystal degradation can be avoided, thereby expanding the library of usable solvents and polymer matrixes. Typically, perovskite precursors were first mixed with selected polymers in DMF to form a homogeneous solution. Subsequently, the solution was dropped onto specific substrates to yield thin film nanocomposites without the addition of a poor solvent. The evaporation of DMF induced fast crystallization of MAPbBr₃ PNCs within the shrunk polymer matrixes. The formed PNCs possessed sizes ranging from 10 to over 100 nm in a depth-dependent size distribution (Figure 5b). Polymers with good solubility in DMF can be employed for this approach, including PS, PC, ABS, and poly(ethylene vinyl acetate) (PEVA).^[44,80]

The incorporation of perovskite precursors with polymers also enables the electrospinning of luminous fiber-shaped nanocomposites. Semicrystalline and hydrophobic polyacrylonitrile (PAN) has been found to offer good protection to MAPbX₃ PNCs against moisture.^[50] PAN was simultaneously and coaxially electrospun with perovskite precursors in DMF, thereby facilitating the in situ crystallization of MAPbX₃ PNCs within PAN after evaporating DMF.^[50] The morphology and photophysical properties of the MAPbX₃ PNCs inside the fibers was effectively tailored by manipulating the composition and stoichiometry of perovskite precursors, polymer concentration, and solvent compositions and concentrations. Color tunability, PLQY, and stability of the fiber-shaped nanocomposites were further tuned by introducing synthetic polymer additives into the PAN DMF solution.^[50] This approach has also been utilized with polymers other than PAN (such as PS,^[42] PVA,^[39] and PVP,^[61]) to fabricate PNC/polymer nanocomposites.

Notably, large-scale, continuous production of CsPbBr₃ PNCs/PMMA fiber nanocomposites was achieved at room temperature and without generating toxic waste by using a combination of electrospinning and microfluidic reactors.^[57] The stability, color purity, and optical properties of the resultant microfibers are comparable to the other facile approaches discussed above, making this method particularly promising for the mass production of PNCs-based nanocomposites.

Inkjet printing of perovskite precursor solutions onto patterned polymer matrixes has also emerged as a method to fabricate PNCs patterns for modern photonic and optoelectronic devices.^[43] As shown in Figure 5c, this strategy eliminates the use of polymer containing ink and directly crystallizes MAPbBr₃ PNCs within patterned polymer substrates. Notably, because the solvent is evaporated, this method dispenses with the need to consider the differences in solvent compatibility between the perovskite precursors and polymers. A diverse set of polymers, including PDMS,^[110] PVC,^[45] PMMA, PS, PAN, PVDF, and CA,^[43] have been utilized.

Polymer films with high-resolution perovskite patterns have been created using size exclusion lithography, which capitalizes on the in situ crystallization of PNCs during photopolymerization.^[84] In this method, perovskite precursors were first mixed with a photoinitiator and polar monomers (e.g., tri(propylene glycol) diacrylate (TPGDA), pentaerythritol triacrylate (PETA), and trimethylolpropane ethoxylate triacrylate (ETPTA)) in solution. Portions of the mixture were subsequently exposed to UV light, which induced the polymerization of polar monomers which dramatically decreased the solubility of perovskite precursors, resulting in spatially controlled crystallization of FAPbX₃ PNCs. The nanocomposite patterns synthesized from this approach exhibit high PLQY, broad color tunability, and tailorable flexibility. Similarly, by tuning the intensity and time that the laser irradiates a substrate, reversible CsPbBr₃ PNC patterns were created via laser-assisted crystallization.^[111] The recoverable perovskite patterns originate from the in situ crystallization and erasing of CsPbBr₃ PNCs via femtosecond laser irradiation and thermal treatment and exhibit switchable PL and good recyclability.^[112]

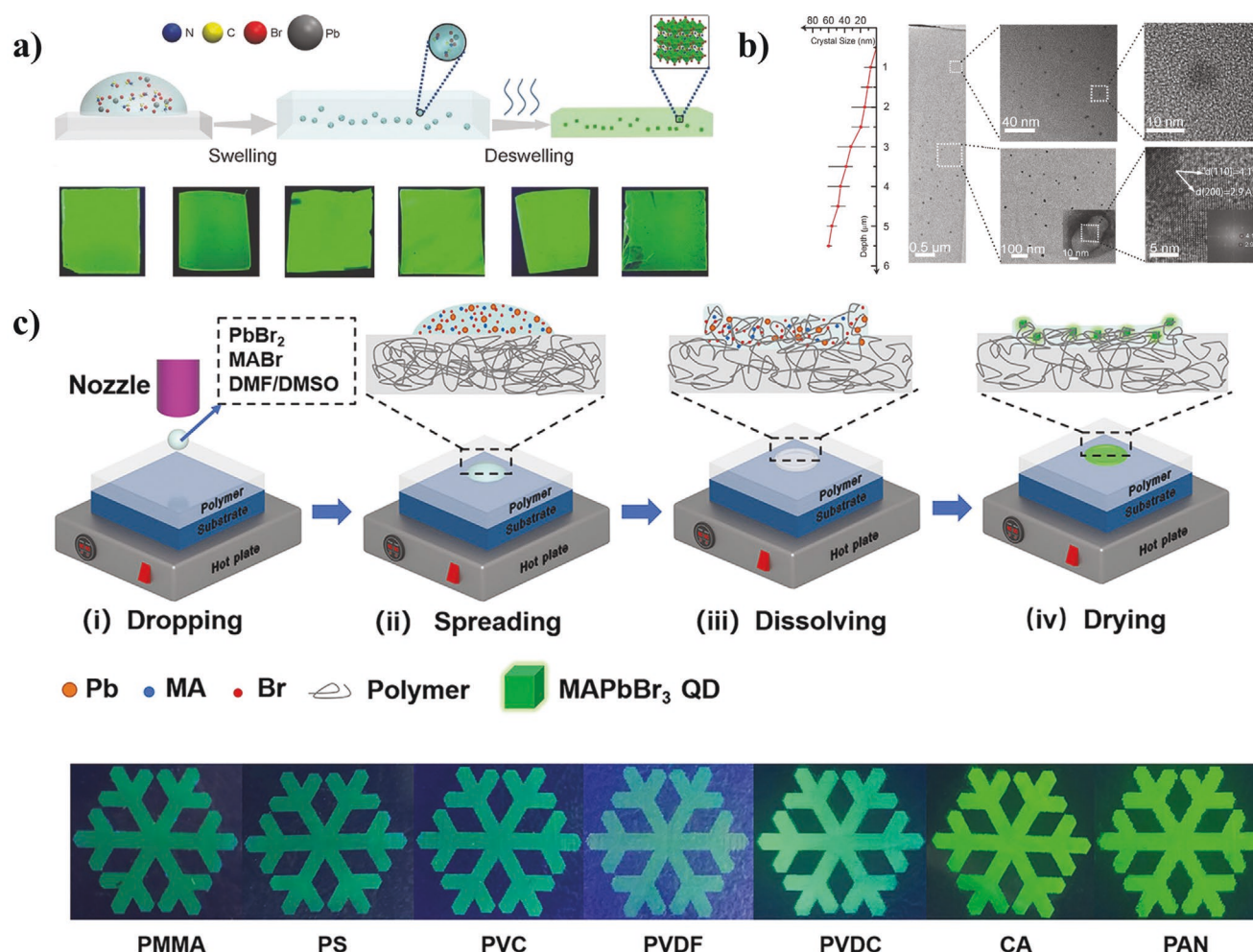


Figure 5. a) Scheme of the MAPbBr₃-polymer composite film formation process through swelling-deswelling (top) and images of the luminescent composite samples prepared by spin coating under UV excitation (365 nm) (bottom). Samples from left to right are MAPbBr₃-PS, MAPbBr₃-PC, MAPbBr₃-ABS, MAPbBr₃-CA, MAPbBr₃-PVC, and MAPbBr₃-PMMA, respectively. b) Size distribution of MAPbBr₃ NCs along with depth from top surface (left), and cross-section TEM and HRTEM images of the MAPbBr₃@PS films indicate a depth-dependent size effect of PNCs (right). a,b) Adapted with permission.^[38] Copyright 2016, Wiley-VCH. c) Schematic diagram of the in situ inkjet printing (ISIP) strategy (top) and optical images (bottom) of printed PNCs patterns on different polymer substrate under UV light irradiation. c) Adapted with permission.^[43] Copyright 2019, Wiley-VCH.

3. Properties of PNCs and PNC/Polymer Nanocomposites

3.1. Optical Properties of PNCs and PNC/Polymer Nanocomposites

3.1.1. Electronic Band Structure of PNCs

The bandgap energy of PNCs can easily be tailored by altering the relative composition of the A, B, and X components and by reducing the size of the PNC below its Bohr radius.^[3,14a] The bandgap tunability originates from the electronic structure of metal halide perovskites. Studies have shown that in lead halide perovskites, the conduction band is mainly formed from antibonding Pb 6p orbitals, as illustrated in Figure 6b.^[13] On the other hand, the valence band has been found to be primarily composed of the antibonding orbitals

from the hybridization of the Pb 6s and halide (Cl, Br, I, or their hybrid) p orbitals.^[113] Altering the halide composition of perovskites has been shown to shift the valence band edge, but result in little change to the conduction band edge. This can be seen in the shifts of the emission and absorption onset wavelength of cesium lead halide (CsPbX₃) PNCs, which can be easily tuned from 410 nm (X = Cl) to 512 nm (X = Br) to 685 nm (X = I) (Figure 6c). The replacement of Pb²⁺ in the B-site of perovskite with other cations (e.g., Sn²⁺) has also been found to alter the optical properties of PNCs because of the difference in electronegativity between Pb²⁺ and the substituted ions.^[114] Though the A-site cation has not been found to directly affect the bandgap in terms of density of states, variation of the A-site cation size can directly tilt the angle of the Pb-halide bonds and the concomitant distortion of the crystal lattice has been observed to alter band structure.^[115]

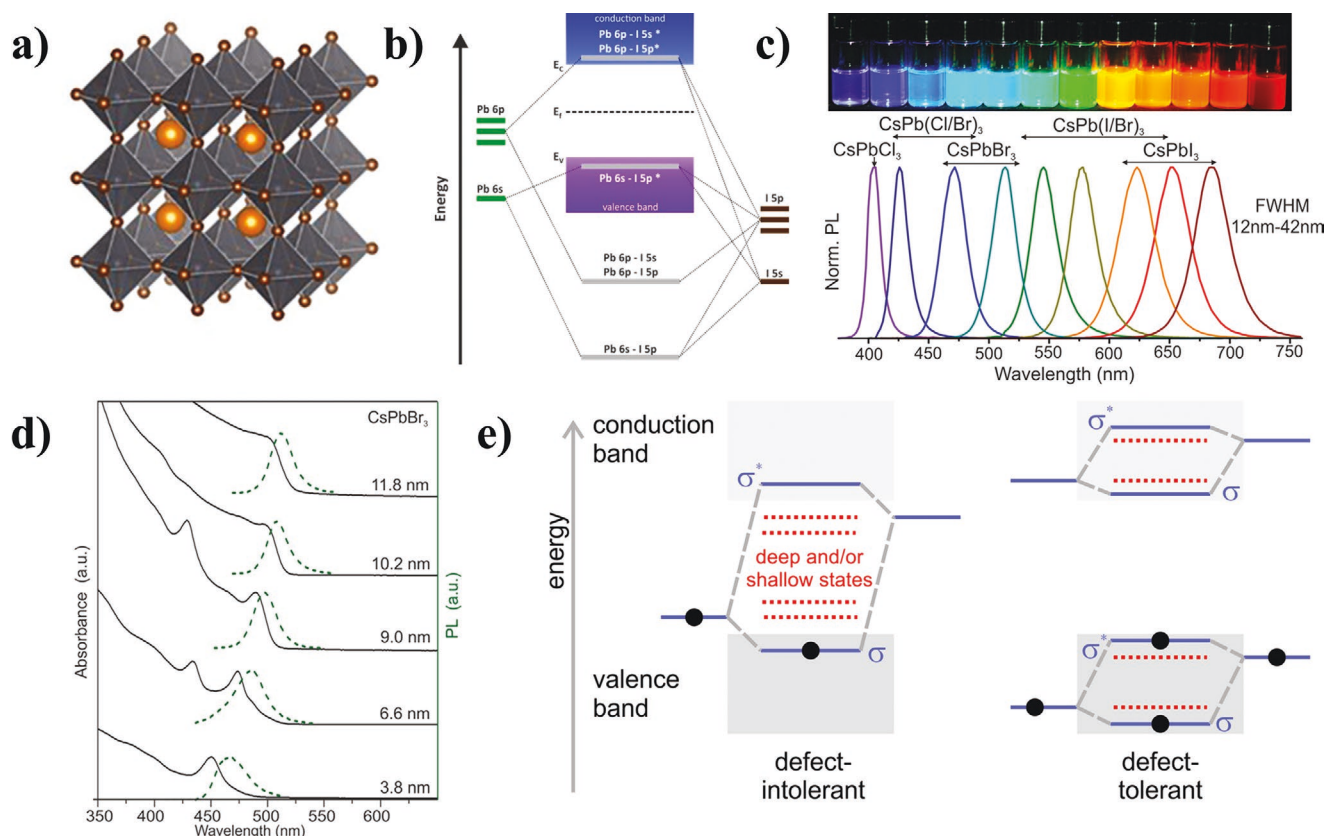


Figure 6. a) Schematic representation of cubic-phase ABX_3 metal halide crystal structures. b) Formation of energetic bands in a lead iodide perovskite material through the hybridization of lead and iodide orbitals. a,b) Adapted with permission.^[13] Copyright 2019, American Chemical Society. c) Colloidal $CsPbX_3$ PNCs ($X = Cl, Br, I$) exhibit size- and composition-tunable bandgap energies covering the entire visible spectral region with narrow and bright emission, top: colloidal solutions in toluene under UV lamp ($\lambda = 365$ nm); bottom: representative PL spectra ($\lambda_{exc} = 400$ nm for all but 350 nm for $CsPbCl_3$ samples). d) Quantum-size effects in the absorption and emission spectra of 5–12 nm $CsPbBr_3$ NCs. c,d) Adapted with permission.^[14a] Copyright 2015, American Chemical Society. e) Schematic of two limiting cases of the band-structure in semiconductors: conventional (defect-intolerant, left) and ideal hypothetical (defect-tolerant, right). Bonding and antibonding orbitals are identified as σ and σ^* , respectively. e) Adapted with permission.^[121] Copyright 2016, American Chemical Society.

3.1.2. Quantum Confinement Effect of PNCs

PNCs have been demonstrated to exhibit size-dependent absorption and emission due to the quantum confinement effect.^[14a,116] Typically, the wave functions of charge carriers in PNCs become confined when one or more dimensions of the PNCs are shrunk below the Bohr radius of their excitons,^[116,117] thereby confining charge carriers and blueshifting absorption onset energy. The exciton Bohr diameter in metal halide perovskite have been observed to be extremely small (e.g., 5 nm for $CsPbCl_3$, 7 nm for $CsPbBr_3$, and 12 nm for $CsPbI_3$).^[14a] By tailoring their size from 3 to 6 nm, the absorption and emission wavelengths of $CsPbBr_3$ PNCs were altered from 450 and 454 to 500 and 503 nm, respectively due to quantum confinement (Figure 6d).^[118]

3.1.3. Defect Tolerance of PNCs

Metal halide PNCs have demonstrated higher defect tolerance than conventional semiconducting QDs.^[119] Their ability to retain pristine electronic band structure in the presence of

a high concentration of defects is attributed to their unique electronic band structure in which bonding–antibonding interactions exist within their conduction and valence bands.^[120] Energy level splitting caused by strong spin–orbital coupling effects favorably broadens the conduction bands and increases the possibility of defect states located within conduction bands (Figure 6e).^[121] Density functional theory (DFT) calculations have corroborated that vacancies, interstitial atoms, and surface states do not induce defect states within perovskites' bandgap.^[122] Notably, because of their defect-tolerant nature, PNCs possess outstanding optical properties without the need for surface passivation, high purity, high temperature, or equipment-intensive vacuum synthesis, all of which are critical for conventional QDs.

3.1.4. Optical Properties of PNC/Polymer Nanocomposite

PNCs exhibit unique spectral tunability and high PLQY due to their advantageous electronic structure, strong quantum confinement effect, and intrinsic high defect tolerance, as described above. However, PNCs suffer from moisture-triggered

photodegradation and thermal and solvent instability, which deleteriously affect their structural integrity, compromise their PLQY, reduce their long-term stability in ambient conditions, and ultimately blueshift and quench their PL emission.^[123] In this context, the preparation of PNC/polymer nanocomposites stands as an attractive method to passivate the PNCs and retain high PLQY in otherwise harsh environments.

PC, PS, PMMA, and many other polymers have been reported to passivate the surface of PNCs and contribute to the enhanced PLQY observed in nanocomposites.^[38,124] The incorporation of a hygroscopic polymer (i.e., PEO) into perovskite materials has been found to boost PLQY by passivating the surface due to the chemical interaction between the oxygen in PEO and the undercoordinated defects sites on perovskite surface.^[49,125] It has been reported that films formed by spin-coating a mixture of PEO and CsPbBr₃ NCs (mixed in solution at a 0.065:1 weight ratio) exhibit a PLQY as high as 60% (one order of magnitude higher than that of neat CsPbBr₃ film (7%)), while the PL peak is unchanged (≈ 521 nm). Moreover, the average PL lifetime of CsPbBr₃ PNC/PEO film is also longer than that of neat perovskite (i.e., 86 vs 16 ns).^[49] Another oxygen-containing functional group, namely, maleic anhydride, in PMAO has been observed to interact with the PNCs via van der Waals interactions, thus passivating surface defects and improving PLQY.^[68] For instance, CsPbBr₃ PNC/PAMO nanocomposites possess a PLQY of 88.8% and PL lifetime of 54.5 ns, which are higher than that of pristine CsPbBr₃ NC (i.e., PLQY of 75.9% and PL lifetime of 36.89 ns).^[68] Moreover, polymers with nitrogen-containing functional groups have demonstrated an ability to strongly bind with PNCs via coordination of the nitrogen atoms with the undercoordinated lead atoms of PNC, thereby

eliminating the deleterious effects from surface defects.^[126] For example, amino-rich polymers (e.g., poly(ethylenimine) (PEI)), have been reported to compensate the unsaturated bonds on the CsPbBr₃ PNCs surface, increase the PLQY of PNC/polymer nanocomposite from $\approx 35\%$ to over 50% (Figure 7b), and prolong the lifetime of PL from 9.6 to 29.4 ns (Figure 7c).^[85] Other nitrogen-containing functional polymers (e.g., P2VP,^[76] polyimide (PI),^[87] poly(2-(dimethylamino)ethylmethacrylate) (PDMAEMA),^[88] etc.) have also been found to form a multidentate capping shell that closely tethers to the surface of the PNCs and results in enhanced surface passivation via a similar mechanism.

Many other functional groups have also been demonstrated to effectively passivate the surface of PNCs via a chemical interaction with their surface defects, including phosphorous-containing groups,^[103b,127] carboxylic acid,^[128] sulfur-containing groups,^[129] and aromatic groups.^[130] Recently, the rational design and thermal polymerization of phosphorous-containing copolymer, poly-diphenylvinylphosphine-styrene (PDPEP-co-PS), during in situ synthesis of CsPbBr₃ PNCs confers multiple unique properties to as-prepared PNC/polymer nanocomposites.^[75] The phosphorous atoms in DPEP segment of PDPEP have been found to reduce surface traps of CsPbBr₃ PNCs and increase the solubility of lead precursors via a strong coordination interaction with Pb²⁺ ions. Moreover, the long hydrophobic PS chains were observed to provide a space skeleton for the in situ synthesis of CsPbBr₃ PNCs and prevent moisture from contacting the CsPbBr₃ PNCs, thereby rendering nanocomposites with a PLQY of 90%.

Nonlinear block copolymer nanoreactors have also been used to tune the optical properties of PNCs.^[17a,83,97] The size and

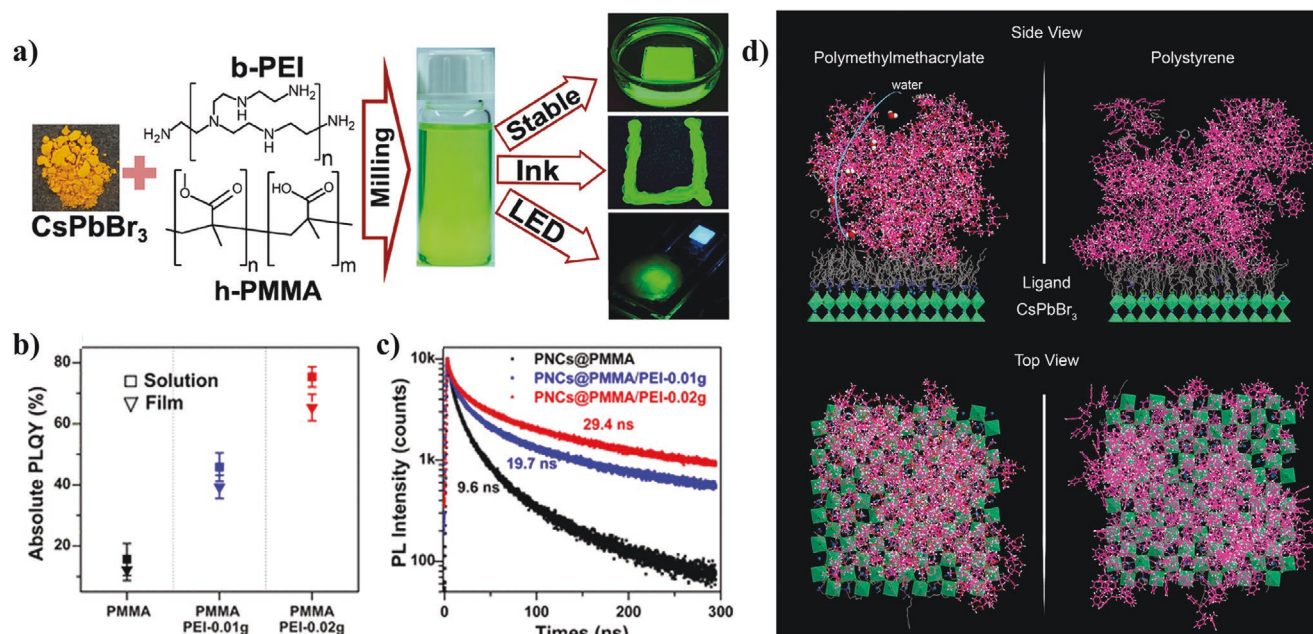


Figure 7. a) Hybridizing CsPbBr₃ PNCs with PMMA and PEI via a ball milling method to fabricate stable LED with solution-processable ink. b) PLQY values of PNCs with increasing PEI content. c) Time-resolved PL spectra of PNCs with increasing PEI content. a–c) Adapted with permission.^[85] Copyright 2019, American Chemical Society. d) Molecular mechanics simulations for the NC ligand–polymer interaction in the case of PMMA and PS. Side and top view images show that a denser surface coverage can be obtained with PS rather than PMMA. d) Adapted with permission.^[131] Copyright 2019, American Chemical Society.

composition of PNCs can be dictated by the molecular weight of the nonlinear block copolymers and the composition of precursors, thereby leading to tunable PL emission wavelength over the entire visible range with narrow full-width-at-half-maximum. It has been shown that the composition, hydrophobicity, and molecular packing density of the capping polymers on PNCs affect their structural integrity and PL behavior when exposed to moisture and oxygen (Figure 7d).^[131] In particular, PS has exhibited denser molecular packing and higher hydrophobicity than PMMA and SEBS, which affords a stable optical spectra from the PNCs and suppression PL blueshifting.^[29] The above studies suggested that the fabrication of PNC/polymer nanocomposite facilitates superior surface passivation, control over size, morphology and composition, protection against moisture, heat and air, enhanced PLQY, and a wide range of spectral tunability.

When PNCs are capped with poly(ethylene glycol) (PEG) homopolymers, the van der Waals interactions between hydrophilic PEG blocks in nonpolar solvents (i.e., chloroform) allow for the formation of highly ordered assemblies of CsPbBr₃ PNCs, including bundled pearl necklaces, lamellar, and nanorice assemblies.^[132] The self-assembled structures of CsPbBr₃ PNCs can be manipulated by controlling the concentration of PEG, which results in tunable inter-NC spacing, thereby altering the strength of inter-NC electronic coupling. As a result, the strong inter-NC electronic coupling of PNCs in the self-assembled ordered structure contributes a ≈ 240 meV bathochromic shift of the lowest energy absorption peak of CsPbBr₃ PNCs compared to pristine CsPbBr₃ PNCs.

On the other hand, individual CsPbBr₃ PNCs capped with polymers containing 1-alkynyl acid groups can readily self-assemble into 3D supercrystals under UV irradiation through the photo-induced alkynyl homocoupling reaction.^[89] By varying the carbon chain length of the surface-capped polymer, different morphologies of supercrystals, such as cuboid and spindle, can be obtained during the UV-induced assembling process. Due to enhanced crystallinity and surface passivation, the perovskite supercrystals manifest a 1000-fold PL intensity improvement and prolonged PL lifetime compared to that of pristine PNCs.^[89] Therefore, the above studies suggested that the fabrication of PNC/polymer nanocomposites facilitates superior surface passivation, control over size, morphology, composition, protection against moisture, heat, and air, enhanced PLQY, and a wide range of spectral tunability.

3.2. Optoelectronic and Electronic Properties of Perovskites and PNC/Polymer Nanocomposites

3.2.1. Charge Carrier Dynamics of Perovskites

Optically excited charge carriers in perovskite materials are either freely diffused or excitonically bound, mainly determined by the exciton binding energy, carrier density, and temperature.^[133] The generation, transport, and recombination of charge carriers depends significantly on the composition, crystal structure, size, and defects of perovskites.^[134] Free charge carriers move with diffusion coefficients ($D_{n,p}$) in the

absence of external fields, and drift with mobility ($\mu_{n,p}$) in a nonzero electric field related through the Einstein relation

$$\mu_{n,p} = eD_{n,p}/k_B T \quad (1)$$

where e is the absolute value of electron charge, k_B is the Boltzmann constant and T is the temperature. $D_{n,p}$ and $\mu_{n,p}$ are related to the electronic band structure of perovskite through the carriers' effective mass (m^{eff}) which is correlated to spin-orbital coupling, chemical composition, and crystal size.^[133,134] The $D_{n,p}$ and $\mu_{n,p}$ in perovskites have been proven to be modest compared with other high-quality semiconductors due to scattering by the presence of defects and lattice vibrations.^[134,135] Before recombination, charge carriers have been found to exhibit an average recombination life time (τ) determined by the radiative and nonradiative recombination rates, which are correlated to the carrier density, trap density, and many other factors.^[134] τ and $\mu_{n,p}$ are correlated to the diffusion length (L_D) of charge carriers via following equation

$$L_D = \left(\frac{k_B T \mu_{n,p} \tau}{e} \right)^{1/2} = (D_{n,p} \tau)^{1/2} \quad (2)$$

where high $\mu_{n,p}$ and long τ proportionally increase the L_D . The long L_D in perovskites has been found to contribute to their efficient charge transport in photovoltaic applications.^[133]

The charge carrier recombination dynamics of perovskites are governed by monomolecular, bimolecular, and Auger recombination via following rate equation^[133]

$$-\frac{dn}{dt} = k_1 n + k_2 n^2 + k_3 n^3 \quad (3)$$

where k_1 , k_2 , k_3 are the rate constants of monomolecular, bimolecular, and Auger recombination, respectively, and n is the carrier concentration. These recombination pathways collectively determine the τ and affect the L_D .^[133] The monomolecular recombination of charge carriers, also known as trap-assisted recombination, is largely governed by the energy, density, and distributions of trap states, and is highly influenced by the purity and crystallinity of perovskites.^[136] The monomolecular recombination rate is proportional to the trap density within perovskites.^[136a,b] On the other hand, the bimolecular recombination in perovskites is primarily determined by the electronic band structure, and thus the chemical composition of perovskites. Compositional engineering of perovskites has been shown to alter their spin-orbital coupling and electronic band structure, which can enable efficient spatial separation of charge carriers, extremely low bimolecular recombination, and long L_D exceeding one micron in polycrystalline perovskite films.^[136b] The last pathway of charge recombination, Auger recombination, is usually dominant at high charge carrier concentration and manifests as a phase-specific characteristic, which is prevalent in the orthorhombic phase at low temperature and rare in tetragonal and cubic phases at high temperature.^[136a] The high charge-collection efficiency and open-circuit voltage in perovskite-based photovoltaics has been attributed to low trap densities and recombination rates, and prolonged τ .^[137]

3.2.2. Effects of Polymer on the Charge Carrier Dynamics of PNCs in PNC/Polymer Nanocomposites

To date, many different polymeric materials have been incorporated with perovskites to achieve enhanced optoelectronic performance by promoting charge transport via electronic band alignment,^[138] directing perovskite crystallization,^[139] and passivating surface defects.^[125a,140] For example, the introduction of polythiophene into perovskite solar cells has been shown to mitigate energy losses and enhance charge carrier transport via interaction between the lone pair electrons in sulfur and Pb^{2+} in perovskites. This interaction is proven to passivate surface defect states, reduce electron–hole recombination within perovskites, and result in a high open-circuit voltage over 1.3 V.^[141]

As noted in Section 3.1.4, incorporating polymers with PNCs can, on some occasions, reduce defect density by surface passivation, thereby leading to a higher PLQY of the PNC/polymer nanocomposite compared to that of the pristine PNCs. In addition to increasing PLQY, the polymer induced surface passivation of PNCs alters the energy and dynamics of charge carriers. For instance, chemically anchoring PEI to CsPbBr_3 NPLs during in situ synthesis has been found to concurrently prolong average PL lifetimes (i.e., increases from 20.6 to 47.4 ns), decrease exciton elimination rate, and narrow energy level distribution of charge carriers in the PNC/polymer nanocomposite.^[86] Therefore, CsPbBr_3 NPL/PEL nanocomposite-based LEDs manifest low trap densities and a peak brightness of 631 cd m^{-2} at 8.4 V for electroluminescence.^[86]

Creating a nanocomposite composed of MAPbBr_3 PNC and V-18 has been demonstrated to increase Auger recombination lifetime (i.e., from 104 to 143 ps) via decreasing surface defect density.^[64] As a result, the MAPbBr_3 PNC/V-18 nanocomposite renders a 75% enhancement of PLQY (from 32% of pure PNC to 56% of nanocomposite) and a more than 30% enhancement of average PL lifetimes over that of pure PNCs.^[64] The as-prepared nanocomposite thin film LEDs exhibits a shifted conduction band energy level (from -6.9 to -6.8 eV), suggesting a reduced energy band offset between the nanocomposite thin film and electron transport layer (ETL), efficient charge injection, and good electroluminescent performance with a low turn-on voltage (i.e., $\approx 3 \text{ V}$) of the nanocomposite-based LEDs.^[64] In addition to chemical anchoring approaches,^[68] simply physically mixing PNCs with polymer (e.g., PEO,^[49] PEI,^[85] PI^[87]) has also been shown to provide similar surface passivation and altering of PNC's charge carrier dynamics.^[70]

3.2.3. Dielectric, Ferroelectric, and Piezoelectric Properties of Perovskites

A dielectric is a nonconducting substance that undergoes polarization under an applied electric field. Polar molecules with permanent electric dipole moments occupying the A-site of perovskite crystals have been observed to induce possible disordered orientation and polarization of perovskites.^[142] The response of a dielectric material to an applied electric field is determined by its conductivity and permittivity.^[109] In

PNC/polymer nanocomposites, the presence of heterogeneous interfaces has been found to render interfacial or Maxwell–Wagner–Sillars polarization under light illumination which induces an abrupt variation of the total dielectric constant.^[143] High concentration and dense distribution of PNCs in polymer matrixes have been observed to narrow and solidify the distance and dipole polarization between PNCs, and thus increase the dielectric constant leading to higher polarization.^[53,55]

Metal halide perovskites have been observed to alter their spontaneous polarization direction under specific applied electric fields (also known as ferroelectric properties) due to the presence of polar molecules in the A-site and the non-centrosymmetric structure resulting from distortion of BX_6 octahedron.^[109] In MAPbI_3 metal halide perovskites, spontaneous polarization can be caused by the breaking of crystal symmetry that arises from the reorientation of MA^+ cations in the A-site which distort the PbI_6 octahedron.^[144] The presence of ferroelectric polarization has been found to produce an additional polarization electric field in perovskites that can affect charge separation and collection and bend of electronic bands, thereby endowing current–voltage hysteresis which influences the recombination rate of charge carriers and alters performance of perovskite optoelectronics.^[145]

External mechanical fields have been shown to alter the orientation of dipole moments produce electrical fields. Metal halide perovskites with an absence of centrosymmetry in their crystal structure have been used to generate electric potential under applied mechanical stress through the piezoelectric effect.^[109] The piezoelectricity coefficient represents the ability of specific material to scavenge and convert mechanical energy into electrical energy and correlates that proportionally with the dielectric constant and polarization. The piezoelectric coefficient of metal halide PNCs has been found to increase dramatically under light illumination and applied external electric fields, which can be attributed to the formation of large photo-induced dipole moments via reorientation of the A-site cation.^[146] Figure 8a,b shows the butterfly-shaped amplitude loop ($A(E)$) and rectangular-shaped hysteresis loop of FAPbBr_3 PNCs in phase angle $[\varphi(E)]$, with a bias voltage of $\pm 3 \text{ V}$, respectively. The phase angle loop shows a 180° difference which indicates that polarization can be switched to upward or downward directions by an external electric field, confirming the existence of ferroelectric-like behavior in the FAPbBr_3 NCs.^[55]

Recently, piezoelectric nanogenerators made of PNCs and PDMS have shown great potential toward the large-scale production of piezoelectric energy harvesters due to their ease of fabrication, cost effectiveness, mechanic robustness, and outstanding performance (Figure 8g–i).^[55] The nanocomposites of PNCs and PVDF have attracted considerable attention for the construction of piezoelectric generators due to the intrinsic piezoelectric properties of both PVDF and perovskites. As discussed above, PVDF additionally exhibits outstanding thermal, mechanical, and hydrophobic properties, as well as the ability to passivate the surface of the perovskite. PVDF/PNCs nanocomposites enable the fabrication of piezoelectric nanogenerators with a high piezoelectric charge coefficient, which will be discussed in detail in the following section.^[147]

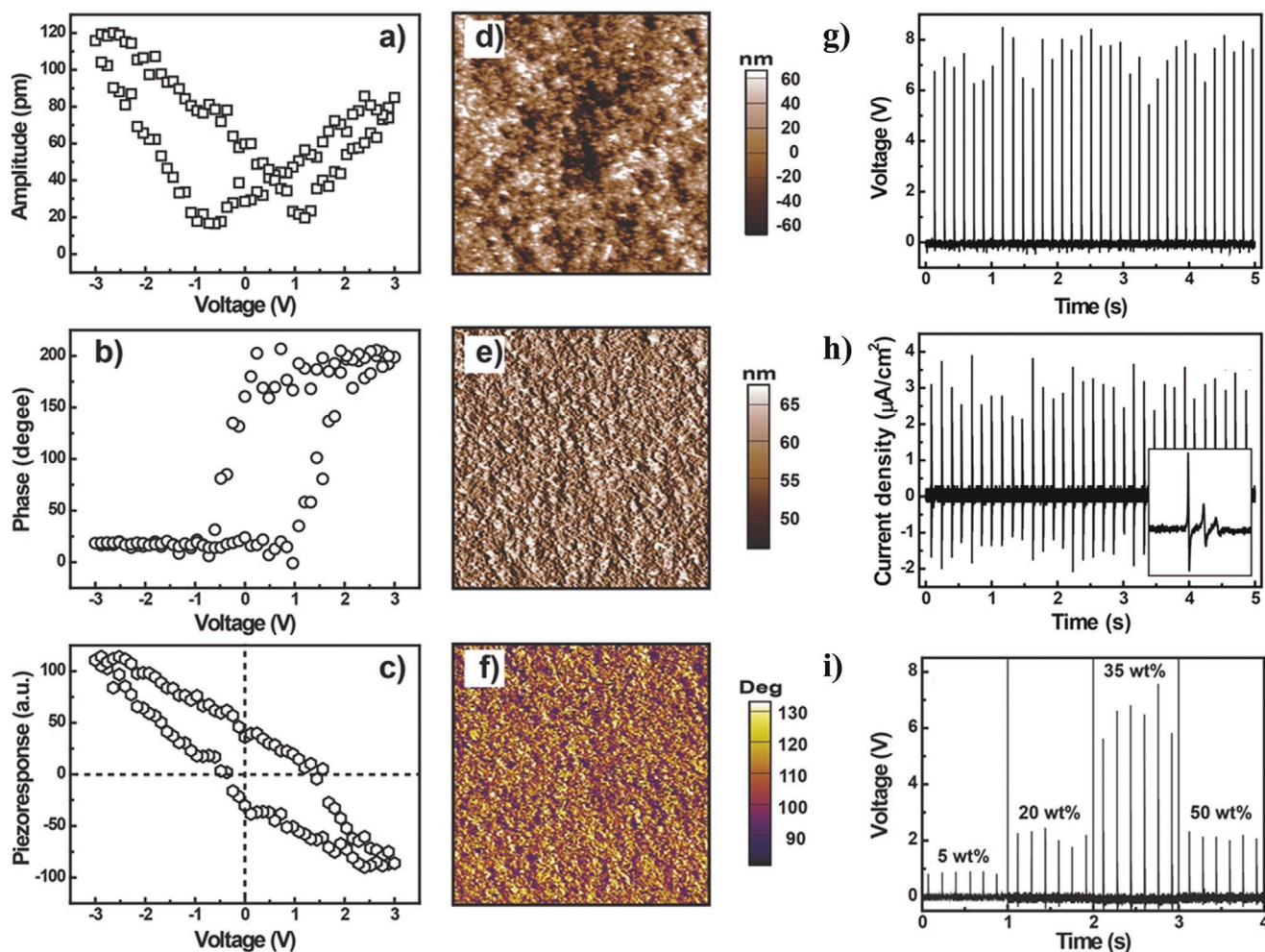


Figure 8. a) Amplitude “butterfly” loop ($A(E)$). b) Phase hysteresis loop ($\phi(E)$) obtained with a direct current (DC) voltage of 1 V. c) The piezoresponse hysteresis loop, $PR(E)$, which is calculated and plotted using the equation $PR(E) = A(E)\cos[\phi(E)]$. d–f) Topography, amplitude, and phase images of the FAPbBr₃ PNCs, respectively. g) Output voltage and h) current density from FAPbBr₃ PNCs/PDMS nanocomposite nanogenerator induced by periodically vertical compression. i) Output voltage from nanogenerators with different FAPbBr₃ PNCs concentration. a–i) Adapted with permission.^[55] Copyright 2016, Wiley-VCH.

3.3. Stretchability Properties of PNC/Polymer Nanocomposites

Perovskites intrinsically possess a highly brittle, salt-like crystal structure and extremely low cohesion energy, and thus suffer from limited fracture resistance and high mechanical fragility.^[148] The fracture resistance of perovskite depends heavily on the density and distribution of defects as the presence of defects promote the propagation of crack tip with less resistance. Studies have shown that the inherent fragility of perovskites cannot be overcome by simply reducing defects.^[149] In this regard, external reinforcement by polymers with advantageous mechanical properties (e.g., PVDF) have been investigated.^[51] A large mismatch of thermal expansion coefficient between perovskites and external reinforcement materials (e.g., polymer matrix) has been found to lead to lattice strain under elevated temperature, and thus accelerate ion migration and crystal degradation, which significantly reduce stability and reliability.^[150] Encapsulating perovskites in polymer matrixes with matched thermal expansion coefficients and favorable

mechanical properties could provide an avenue to improve stability and reliability of the PNC/polymer nanocomposites.^[151] Incorporating perovskite within low elastic moduli PEVA has been found to allow for sufficient plastic deformation to dissipate strain or external mechanical energy under varied temperatures, which increased fracture energy from 0.2 to around 0.8 J m^{-2} .^[151a] Solar cells that incorporated PEVA retained over 90% of initial PCE at elevated temperatures and multiple cycles of bending.

In NCs/polymer nanocomposites, specific spatial organization of NCs within the polymer matrix has been found to affect polymer–NC interactions and significantly enhance the structural and mechanical properties, such as elastic modulus, yield stress, and creep durability.^[152] As an example, the incorporation of MAPbBr₃ PNCs into the conjugated polymer poly(3-hexylthiophene-2,5-diyl) (P3HT) has been shown to increase the P3HT crystalline domain size and crystallinity.^[65] The mechanical flexibility, high transparency within the visible light spectrum, and tunable electronic properties of polymers allow

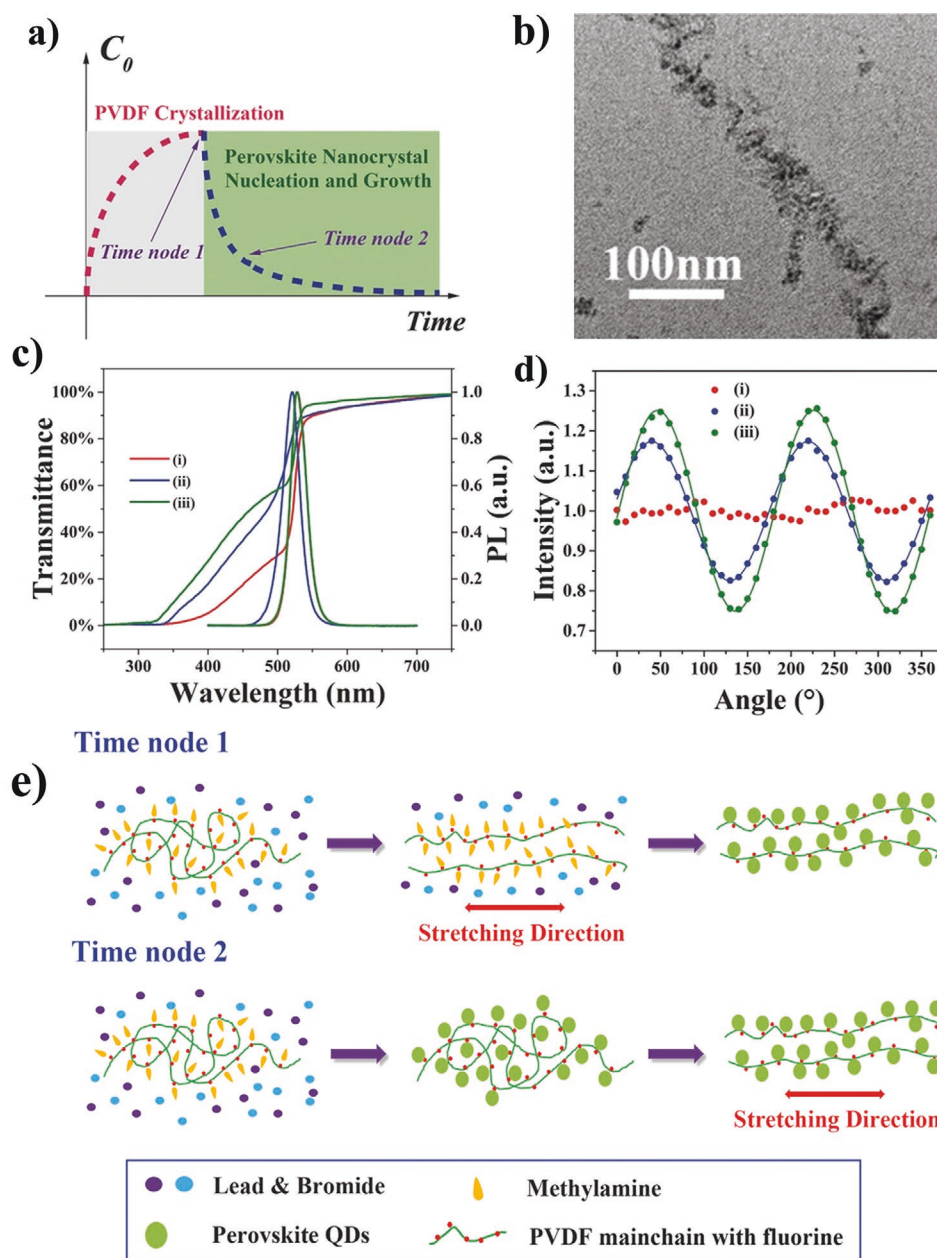


Figure 9. a) Schematic diagram of the stages for stretching MAPbX₃ PNCs/PVDF nanocomposite films. b) TEM image of a MAPbX₃ PNCs/PVDF nanocomposite film stretched at time node 2. c) Transmittance and PL spectra and d) the polarization measurements of the MAPbX₃ PNCs/PVDF nanocomposite films (the mass fraction of perovskite precursors is 8%): i) films without stretching; ii) films stretched at time node 1; iii) films stretched at time node 2. e) Illustration of formation mechanism of perovskite "NCs-aligned wires" embedded in the composite films stretched at time nodes 1 and 2. a–e) Adapted with permission.^[52] Copyright 2017, Wiley-VCH.

their utilization in PNC/polymer nanocomposite-based stretchable optoelectronics.^[153] As shown in **Figure 9a–e**, the stretchable PVDF matrix in MAPbX₃ PNC/polymer nanocomposites enabled the alignment of MAPbX₃ PNCs along the stretching direction and established dielectric confinement of the optical electric field and exciton–exciton interactions, which resulted in isotropic light absorption and polarized PL emission.^[52] It is notable that flexible PEVA and PI are commonly used to introduce stretchability to PNC/polymer nanocomposite.^[80,154] CsPbBr₃ PNC/PEVA nanocomposites were found to retain

photoluminescent ability under UV irradiation when stretched to 350% of its original length.^[80] The addition of PEVA was also observed to render extremely high bending stability, as evidenced but its superior durability against mechanical bending from 0° to 180° for over 1000 cycles.^[80] MAPbBr₃ PNCs were embedded in intrinsically stretchable PEO matrixes to craft perovskite LEDs that capitalize on PEO as a microscale elastic connector for the rigid and brittle perovskite NCs and to render stretchability to the composite emissive layer.^[34a] The as-prepared stretchable LEDs withstood 40% uniaxial strain without

any degradation in the turn-on voltage and displayed a 18.5% improvement in maximum electroluminescent efficiency over unstrained LEDs.^[34a] Further engineering of the mechanical properties of polymer matrixes endows additional enhancement to the durability and stretchability of optoelectronic devices.^[155]

3.4. Stability of PNCs in PNC/Polymer Nanocomposite

PNCs suffer from instabilities toward moisture, oxygen, light, and heat due to their ionic crystal nature and large surface energy.^[90b] The intrinsic instability of PNCs triggers the degradation of their optoelectronic properties which significantly affects their practical applications. In this regard, many strategies have been developed to enhance their long-term stability, such as co-doping or hybridizing with other cations,^[119] surface passivation with small molecule organic compounds via postsynthesis ligand exchange or during in situ synthesis,^[156] and incorporation of polymers.^[124,157] However, co-doping or hybridizing other cations into PNCs has been found to enable only limited modification to crystal structure and stability improvement.^[158] Adding small molecule organic compounds during in situ synthesis can lead to poor control over the crystallinity and morphology of PNCs, and postsynthesis modification inevitably exposes PNCs to other solvents that potentially result in their degradation.^[159]

As noted above, polymers carry many advantageous properties, such as easy processability, light weight, mechanical flexibility, and low cost.^[124] In PNC/polymer nanocomposites, the incorporation of polymers has been shown to concurrently passivate the surface of PNCs, form a physical barrier between PNCs and harsh environments, and enhance dispersity and compatibility in organic solvents for solution-based processing. As shown in **Figure 10a–c**, poly(isobutylene-*alt*-maleic anhydride) (PIMA), a synthetic polymer, has been modified to introduce PEG, amine, and sulfobetaine zwitterion groups on its backbone or side chains that can strongly interact with the anions and cations of CsPbBr₃ PNCs.^[69] The multidentate zwitterion-modified PIMA was found to endow improved dispersion and stability of CsPbBr₃ PNCs in polar solvents and enhance optical properties. These improvements were ascribed to the surface passivation and protection of the CsPbBr₃ PNCs from the high-affinity coordination and the dense packing of the polymer chains (**Figure 10d**). The CsPbBr₃ PNCs capped with zwitterion-modified PIMA retained over 90% of initial PL intensity in polar solvents (e.g., ethanol) for over 8 months (**Figure 10e**). Other synthetic and commercially available polymers (e.g., P2VP,^[76] PMAO,^[67] PEO,^[49] and PEG^[125b]) have also been shown to provide similar surface passivation and stability improvement of PNCs.^[24a,124]

A key challenge for PNC stability is the dynamic nature of ligand attachment. As discussed previously, the use of nonlinear block copolymers as nanoreactors during in situ synthesis of PNCs has been shown to yield uniform PNCs covalently ligated with permanent polymer shells.^[17a,83,97] The covalently tethered polymer shells have been found to endow the PNCs with excellent stability against moisture, oxygen, heat and UV light. Excellent dispersity and aggregation-free long-term colloidal stability was achieved for PS-capped PNCs because of PS's excellent solubility in nonpolar solvents. After the introduction

of water, however, the hydrophobic polymers collapsed to form a dense shell around the CsPbBr₃ PNCs and functioned as a barrier to effectively prevent water and oxygen from reaching and degrading the PNCs.^[17a,97] Increasing the length of polymer chains ligated on the surface of CsPbBr₃ PNCs has been found to impart a thicker barrier that more effectively inhibits degradation from external stimuli (e.g., moisture, heat, UV light) (**Figure 11**).^[17a]

In addition, the stabilities of PNCs can be further improved by judiciously designing dual-shelled protection. PNCs with a protective inner inorganic shell (e.g., SiO₂) and an outer polymeric shell (e.g., PS or PEO) have been successfully synthesized, as previously discussed.^[83] Additionally, PEO-capped MAPbBr₃ PNCs synthesized using star-like P4VP-*b*-PAA-*b*-PEO nanoreactors exhibited surface hydrophilicity and an unfavorable interaction with hydrophobic, nonpolar organic solvents (e.g., hexane). The ability to use hexane as a destabilizing solvent for purifying PEO-capped PNCs eliminates the need to use polar or protic solvents during purification which are inevitable and indispensable for PNCs capped with small organic molecular capping ligands. As such, the potential degradation of PNCs by the polar or protic solvents can be minimized and the structural integrity of the PNCs is retained. Interestingly, dual-shelled MAPbBr₃ PNCs concurrently protected by an inorganic SiO₂ shell and organic PEO shell have been demonstrated to display an array of remarkably enhanced stabilities, reduced surface defect density, and improved optical properties.^[83] The thin films prepared by spin coating dual-shelled PNC retained 80% remnant PL after 14-days of storage under 80% humidity and 72% remnant PL after 14-days of continuous illumination ($\lambda = 470$ nm). The PL of oleylamine- and oleic acid- co-capped MAPbBr₃ PNCs (control sample) dropped to nearly 0 at relative humidity of 75% after 12 h.^[83]

Physically mixing PNCs with polymer matrix has also been shown to enhance various stabilities.^[36,66,92,125a,160] For instance, MAPbX₃ or CsPbX₃ PNCs/PVDF nanocomposites possess aggregation-free dispersion of PNCs and excellent stability after immersion in water for 400 h or illumination with UV light for 400 h.^[51,54] The stabilities of PNCs in nanocomposites have been found to be related to the water resistance and oxygen diffusion rate of the polymer matrix (e.g., PS, PMMA, SEBS).^[29] This was verified in a study where PNCs were capped with a variety of polymers, including PS, PMMA, PLMA, and SEBS. The PS-capped PNCs demonstrated the greatest enhancement of stability in water and under ambient conditions (i.e., no change in emission spectrum before and after 60 days of water immersion), which was attributed to the fact that of all polymers in the set, PS possessed the highest water resistance, lowest oxygen diffusion rate, and densest molecular packing at the PNC surface. Compositional and/or structural engineering to maximize water resistance and minimize the oxygen diffusion rate of polymers has been identified as an effective strategy to select matrixes that will enhance the stability of PNCs in nanocomposites.^[37,131] Physically mixing CsPbBr₃ PNCs with poly(divinylbenzene-*block*-ethyl acetate) (PDVB-*b*-PEA) has been found to form a superhydrophobic nanocomposite that can increase the water stability of CsPbBr₃ PNCs for several months.^[79] Moreover, for the “swelling–shrinking” strategy it has been reported that the enhancement of water and thermal

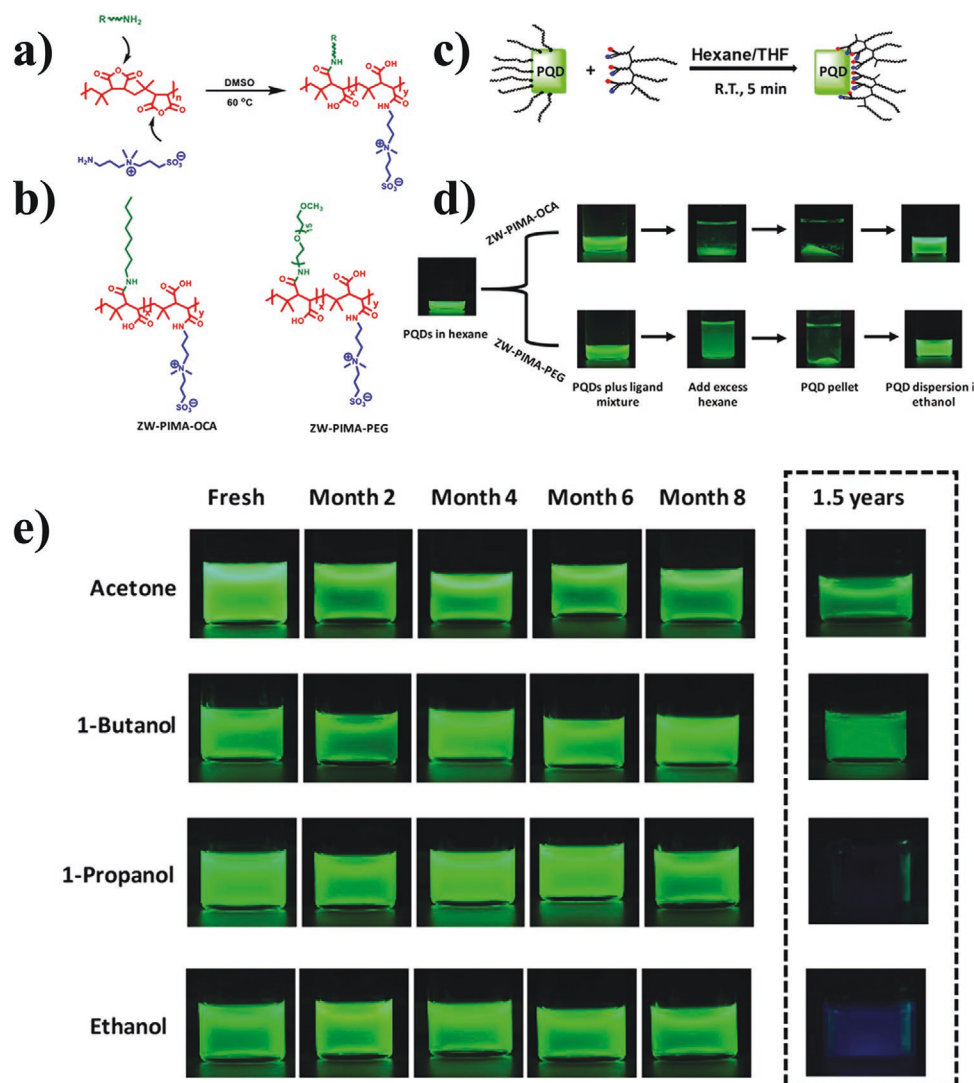


Figure 10. a) Schematic representation of the one-step nucleophilic addition reaction used to prepare the multidentate zwitterion (ZW) modified polymers starting with PIMA precursor. b) Structures of two representative ligands are shown: ZW-PIMA-OCA and ZW-PIMA-PEG. c) Schematic representation of the ligand exchange process. d) Fluorescence images (λ_{exc} = 365 nm) of perovskite NCs during the ligand exchange steps with ZW-PIMA-OCA (top) or ZW-PIMA-PEG (bottom). e) Fluorescence images of ZW-PIMA-OCA-capped perovskite NCs dispersions in different polar solvents, UV excitation at 365 nm and collected every month for a total period of 8 months; images from the same dispersions after 1.5 years of storage are also shown. a–e) Adapted with permission.^[69] Copyright 2020, American Chemical Society.

stabilities of PNCs is proportional to a variety of properties of the polymer matrixes, including size, swelling ability in specific solvents, glass transition temperature, and water resistance.^[38] For example, MAPbBr₃ PNCs/PC nanocomposites have been shown to possess better thermal stability than MAPbBr₃ PNCs/PS nanocomposite due to PC's relatively higher glass transition temperature (140 °C for PC and 100 °C for PS).^[38]

It is interesting to note that the introduction of PVP into perovskite precursor solutions has been found to increase viscosity via interactions between the pyrrolidone groups of PVP and the PNCs during and after in situ synthesis.^[161] This finding was used to facilitate the utilization of inkjet printing techniques for fabricating patterned PNCs/polymer nanocomposites without the coffee-ring effect, which enables control over size and spatial distribution.^[161] The homogeneity

and compatibility of the patterned PNCs on substrates was enhanced by replacing PVP with a mixture of PEA and PVC (polymers that possess favorable mechanical and chemical properties for inkjet printing), and the resulting nanocomposites displayed outstanding optical properties with enhanced resistance to abrasion, air, water, light irradiation, and various polar solvents.^[45] This method stands as an attractive candidate for potential large-scale and low-cost manufacturing of nanocomposites for optoelectronic applications.

4. Application of PNC/Polymer Nanocomposite

As discussed above, PNC/polymer nanocomposites combine the superior properties of perovskites and unique advantages

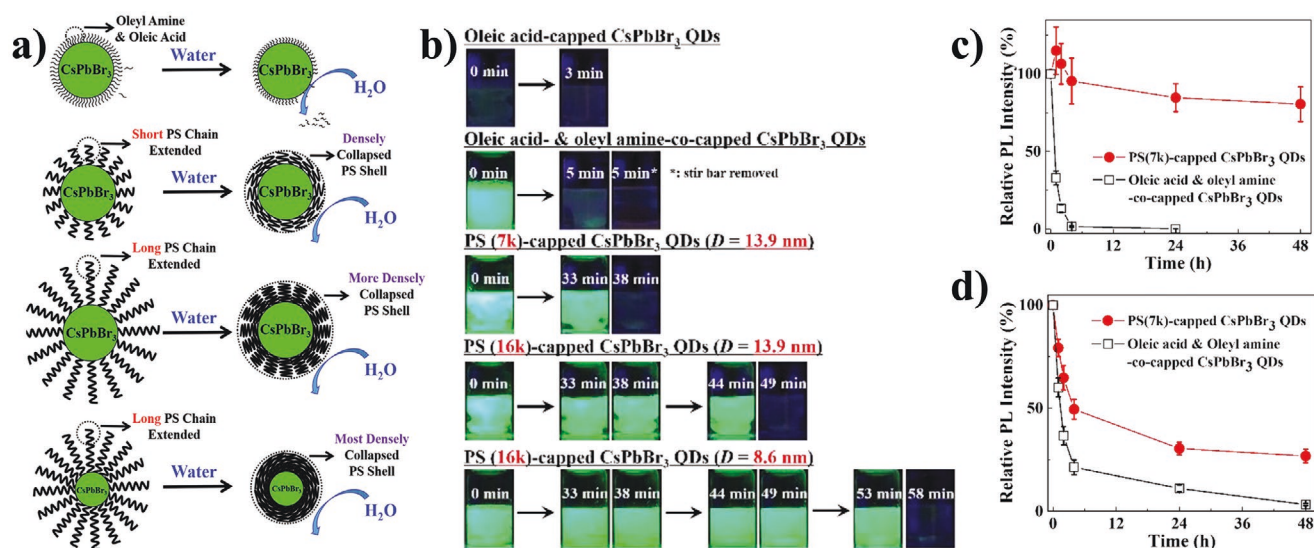


Figure 11. a) Illustration of PS-capped PNCs with varied NC sizes and PS chain lengths. PS capping resulted in markedly improved colloidal and moisture stabilities compared to conventional small molecular organic ligands-capped perovskite NCs (top). b) Representative digital images depicting the water stability of CsPbBr₃ PNCs under UV excitation. The far-right image of each row was taken immediately after the sharp and complete disappearance of PL emission. c) Relative PL of PS(7k)-capped CsPbBr₃ PNCs in toluene solution after heating at 80 °C for up to 48 h. d) Relative PL of PS(7k)-capped CsPbBr₃ PNCs in toluene solution after irradiating with UV-light ($\lambda = 365$ nm) for up to 48 h. a–d) Adapted with permission.^[17a] Copyright 2019, Wiley-VCH.

of polymers, which result in enhanced performance and additional functionalities for many applications. In this section, representative applications of metal halide PNC/polymer nanocomposites will be summarized.

4.1. LEDs

Metal halide perovskites have gained extensive attention for applications in LEDs over the past few years due to their tunable emitting wavelength from visible to near-infrared, large carrier mobility, narrow band emission, sharp optical absorption onset with absorption coefficient (α) larger than 10^4 cm⁻¹ near the band edge, and low nonradiative recombination rates.^[11,14a,17a,162] As shown in **Figure 12a**, a typical perovskite LED (PeLED) consists of an intrinsic active layer in a double-heterojunction structure with an ETL and a hole transport layer. Under forward bias, charge carriers are injected into the luminescent active layer and recombine radiatively, emitting light in all directions.^[162d]

Even though PeLEDs carry many advantageous properties over conventional colloidal quantum dot LED (QLED) and organic LED (OLED), there are obstacles to their mass production and commercialization. For example, they lack long-term stability toward external environment stimulus, such as moisture and heat. In this regard, PNC/polymer nanocomposites can effectively protect PNCs from the chemical and structural degradation triggered by external environment stimuli. Combining PNCs with polymers also benefits their optoelectronic properties and device performance because of the reduced surface defect density, reduced nonradiative current losses, and uniform distribution of NCs within polymer matrix.^[105,163] Furthermore, PNC/polymer nanocomposites

enable additional properties (e.g., mechanical property, flexibility, stretchability, processability, etc.) in as-prepared LED devices, which are inherited from polymers. As discussed in Section 2.2, the most widely used method to form the PNC/polymer nanocomposites for LED devices is through physical mixing, i.e., embedding PNCs within polymers,^[36,79,105,160b,164] and in situ conversion of perovskite precursors to NCs in the presence of polymer matrixes.^[38,47,51,163] Recently, a superhydrophobic CsPbBr₃ PNCs/polymer composite (IPQDs@SHFW) was formed via mixing PNCs with a superhydrophobic porous organic polymer framework (SHFW).^[79] The uniform distribution of PNCs within the polymer framework prevented fluorescence quenching of PNCs in the solid agglomeration state and CsPbBr₃@SHFW powder exhibited a high PLQY up to 60%. More importantly, the nanocomposite powder displayed unchanged large water contact angle (150°) and a well-maintained PLQY (i.e., 54%, which is 91% of initial PLQY) after being immersed in water for 31 days (Figure 12b). Chemical approaches can also be employed to produce PNC/polymer nanocomposites for LED applications. For instance, by using star-shaped amphiphilic block copolymer PAA-*b*-PS as nanoreactors, as-synthesized CsPbBr₃ NCs can be endowed with permanently affixed hydrophobic PS chains on the surface.^[17a,82,83,97] Low water and gas penetration rates and the good thermal stability of the PS resulted in PNC/polymer nanocomposites with impressive stability against water, air, and heat exposure. As a result, a white light emitting diode (WLED) fabricated from PS-capped CsPbBr₃ NCs maintained excellent stability after being stored in ambient conditions for 400 days and displayed significantly enhanced thermal stability in a thermal cycling test (ranging from 25 to 100 °C), retaining 96% of original PL compared with only 45% for oleic acid- and oleylamine-capped CsPbBr₃ NCs.^[17a] It is worth mentioning

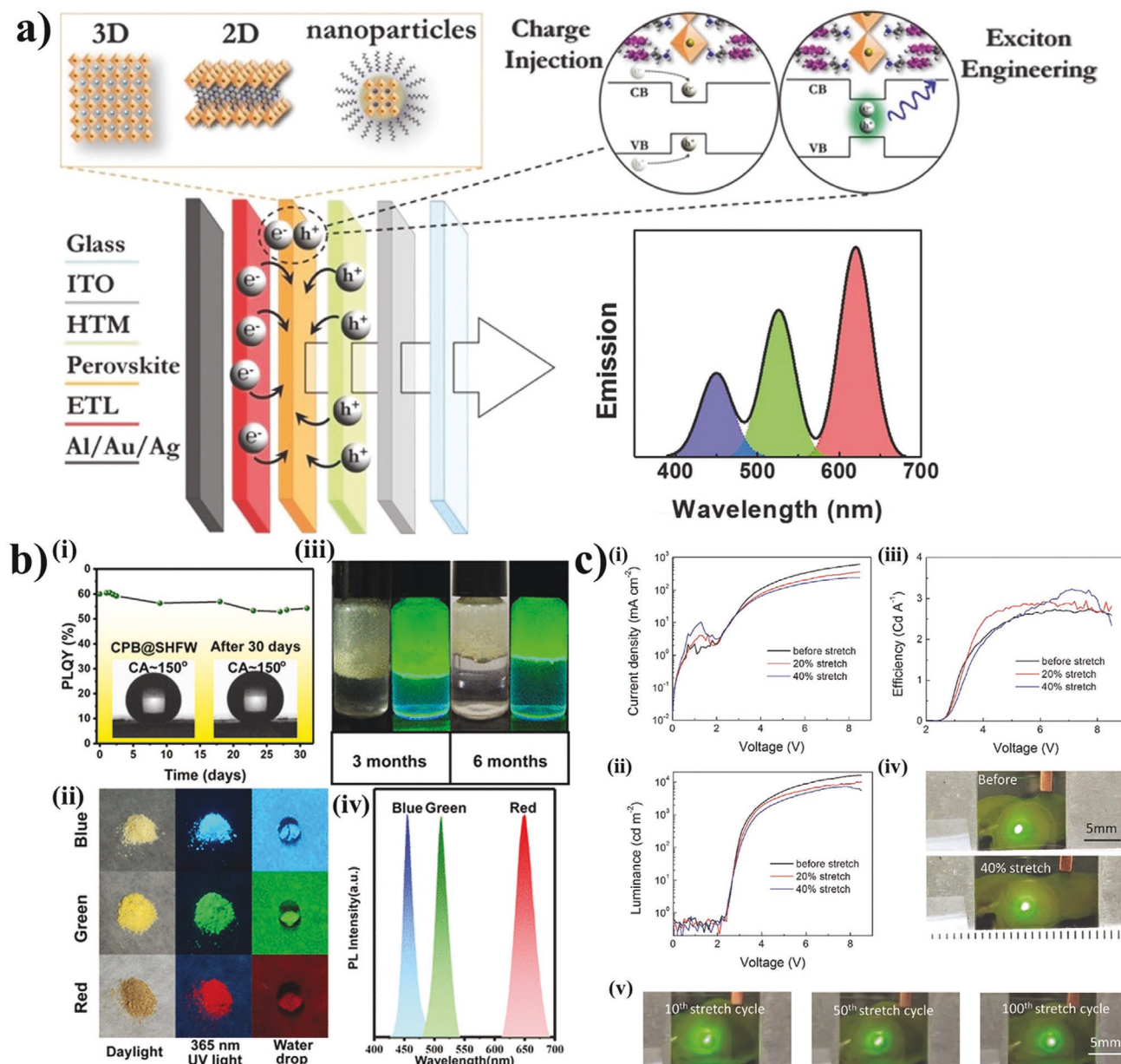


Figure 12. a) Schematic representation of PeLED devices. a) Adapted with permission.^[165] Copyright 2016, Wiley-VCH. b) i) PLQY of CPB@SHFW composite powders as a function of time in water (inset: the contact angle images before and after being immersed in water for 31 days). ii) Photographs of CPB@SHFW composite powders immersed in water for 3 months and 6 months under white light and 365 nm UV light, respectively. iii) Photographs of blue-, green-, and red-emitting IPQDs@SHFW composite powders, and the images of water drops on the composite films under white light and 365 nm UV light, respectively. iv) PL spectra of the IPQDs@SHFW composite powders. b) Adapted with permission.^[79] Copyright 2019, American Chemical Society. c) i) Current-density–voltage, ii) luminance–voltage, and iii) current-efficiency–voltage characteristics of the stretchable perovskite LEDs before and after stretching to 20% and 40% strain. iv) Photos of a LED under a 4 V bias before (top) and after (bottom) stretching to 40% strain. v) Photos of another LED at 4 V after the 10th, 50th, and 100th stretching cycle at strain of 0–40%. c) Adapted with permission.^[34a] Copyright 2017, Wiley-VCH.

that CsPbBr₃ and CsPbBr_{1.2}I_{1.8} PNCs have been utilized as photoinitiators for the in situ polymerization of PS and PMMA matrixes that physically encapsulate the PNCs.^[35] The resulting nanocomposites showed enhanced stability after immersion in water for 24 h and showed only a slight drop in PLQY from 44% to 36%. In addition to the enhanced environmental stability, PeLED made from PNC/polymer nanocomposites can

be flexible and stretchable due to the soft and elastic nature of many polymers. Figure 12c demonstrates a mechanically robust and highly stretchable green LED composed of a transparent PEO/poly(3,4-ethylenedioxythiophene) polystyrene sulfonate (PEDOT:PSS) anode, a MAPbBr₃/PEO nanocomposite emitting layer, and an eutectic indium–gallium cathode on a PDMS substrate that can be reversibly stretched to up 40% strain after

100 testing cycles.^[34a] Device efficiency was even observed to slightly increase at 40% strain (3.2 cd A^{-1}) compared with the as prepared nonstretched device (2.7 cd A^{-1}). This improvement was due possibly to a more balanced electron/hole recombination due to the thinner emission layer in the stretched device.

4.2. Lasers

After the first demonstration of optically pumped room-temperature amplified spontaneous emission (ASE) and lasing in 2014, perovskite lasers using a broad range of cavities have been developed, including Fabry–Pérot cavities,^[166] distributed feedback (DFB),^[167] spherical resonators,^[168] microplatelets,^[169] nanowires,^[170] and natural photonic crystal corrugations.^[171] However, the thermal and moisture instability of perovskites greatly hinders their potential in long-term, practical laser applications. In this context, PNC/polymer nanocomposites provide promising alternatives to overcome this challenge. Recently, stable two-photon-pumped random lasing, with excitation wavelength centered at 1064 nm and a threshold at around 1.1 mJ cm^{-2} , was achieved in an FAPbBr₃ PNC/PEO

nanocomposite thin film (Figure 13a).^[48] The as-prepared device showed significantly improved optical stability compared with a FAPbBr₃ thin film laser. When exposed to ambient atmosphere, FAPbBr₃ thin films showed a dramatic decrease in their PL intensity (i.e., decreases to 16% of original intensity) after 10 000 s, while the lasing emission of the nanocomposites remained 90% of its original value. The enhancement in stability resulted from the protection of PEO that isolated the PNCs from moist air, leading to the potential in continuous-wave pumping lasers. Laser emission was achieved in an MAPb(Br_xCl_(1-x))₃ ($x = 0.1$ or 0.4) PNC/poly(fluorine-co-divinylbenzene) conjugated polymer particle (CPP) nanocomposite via energy transfer from the perovskite to the self-assembled CPP photonic crystal, as depicted in Figure 13b.^[70] The small PNCs concurrently functioned as an encapsulating matrix to assist the ordering of large CPPs ($d = 1 \mu\text{m}$) particles, and as a donor to facilitate laser emission after energy transfer from the pumped perovskite to the organic semiconductor. The lower lasing threshold (13 mJ cm^{-2}) in the $x = 0.1$ nanocomposite compared to a 16 mJ cm^{-2} threshold in CPPs indicated a very efficient energy transfer from perovskite to the CPPs. By integrating the superior optoelectrical properties of perovskites

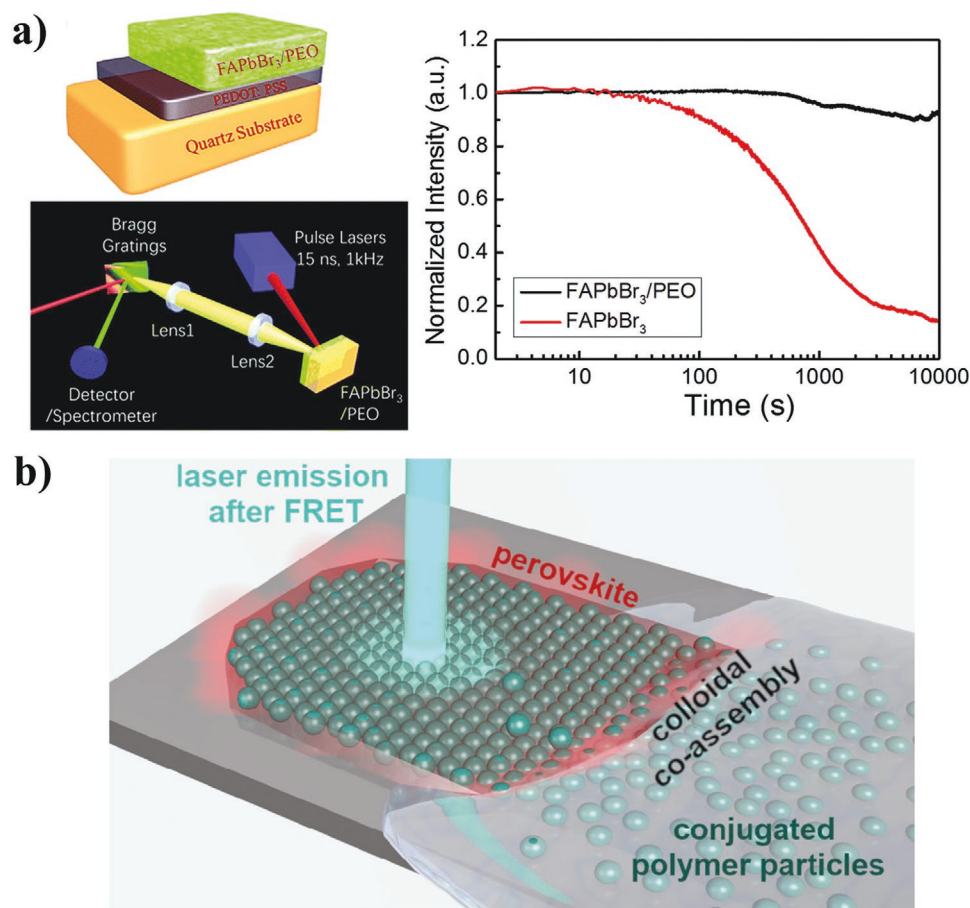


Figure 13. a) A schematic diagram of the prepared FAPbBr₃/PEO based random lasing device (upper left). Illustration of experimental setup of two-photon-pumped random lasing test (bottom left) and stability of random lasing emission intensity of FAPbBr₃/PEO and the two-photon-pumped photoluminescence of FAPbBr₃ perovskite thin films (right). a) Adapted with permission.^[48] Copyright 2018, The Royal Society of Chemistry. b) A schematic diagram of laser emission after energy transfer in PNCs/CPP nanocomposites. b) Adapted with permission.^[70] Copyright 2019, American Chemical Society.

and the excellent optical properties of conjugated polymers, the great potential for solution-processed electrically pumped solid-state lasers was demonstrated.^[70]

4.3. Scintillators and X-ray Detectors

Scintillators are based on materials that are capable of absorbing high-energy X-ray photons and converting the absorbed energy into low-energy photons in visible spectrum. They find a wide range of applications in radiation exposure monitoring, security inspection, and medial radiography.^[172] Conventional scintillator materials are constituted of heavy atoms, synthesized by high-temperature crystallization, and have a hardly tunable radioluminescence in visible spectrum.^[173] Metal halide PNCs with readily tunable PL across the entire visible spectrum have been found to possess large X-ray stopping ability and the capacity to transform X-ray photons into low-energy photons, which suggests their unprecedented potential for use as scintillators.^[174]

Embedding scintillating materials into polymer matrixes to fabricate plastic scintillators has emerged as an affordable alternative to conventional single-crystal all-inorganic scintillators

that normally require time-consuming, high-temperature, and high-cost crystallization.^[175] The key features of fabricating polymer scintillators with high performance and sensitivity are efficient scintillation, high interaction probability with X-rays, limited self-absorption, and loss-free waveguiding. To this end, CsPbBr₃ PNCs and a perylene-based organic dye have been incorporated into a PMMA matrix to fabricate highly sensitive plastic scintillators (**Figure 14a**).^[58b] A physical mixture of highly luminescent CsPbBr₃ PNCs, PMMA, and perylene dye was first made in a nonpolar solvent and then slowly evaporated to craft bubble- and crack-free nanocomposites. In this plastic scintillator, PMMA was selected for its favorable mechanical properties, solution processability, compatibility with the perylene-based organic dye, ability to spatially disperse perovskite NCs without aggregation, and protect CsPbBr₃ PNCs from environmental stimuli. As shown in Figure 14b,c, the CsPbBr₃ PNCs served as a high-atom-number (high-Z) sensitizers to convert high-energy X-ray photons to low-energy charge carriers that were then transferred to the perylene dye for efficient luminescence with a large Stokes shift (60 nm) and low self-absorption (only about 15%). It is noteworthy that the ratio between CsPbBr₃ PNCs and perylene dye and their loading amounts dictated scintillation performance, which after optimization was

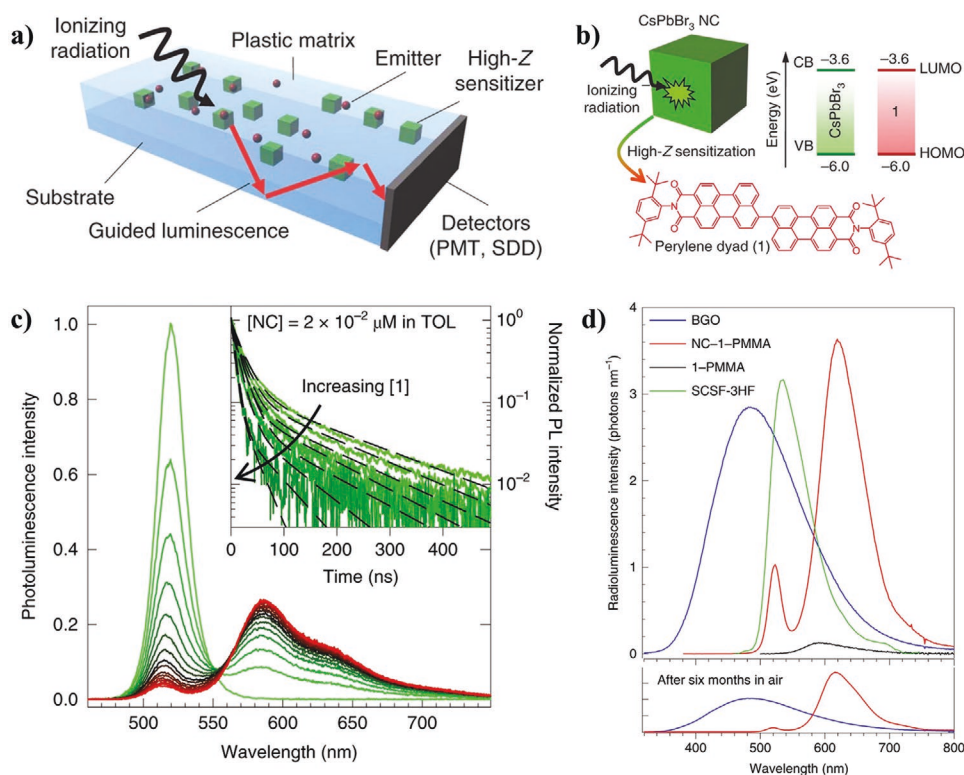


Figure 14. a) Schematic depiction of a high-Z sensitized plastic scintillator. b) Sketch of a CsPbBr₃ PNC sensitizing the perylene dye. The energy levels of the two systems are also shown to highlight the resonance between the respective frontier levels, which is important to prevent charge separation between the two species leading to slow indirect exciton decay or efficiency losses by exciton splitting. CB, conduction band; VB, valence band. c) Photoluminescence spectra of toluene (TOL) solution of CsPbBr₃ PNCs with increasing concentration of perylene dye ([1], from zero, green curve, to 4.8×10^{-6} M, red curve) under selective NC excitation at $\lambda_{\text{ex}} = 400$ nm. Inset: respective photoluminescence decay traces for perylene dye ([1]) from zero to 2.2×10^{-6} M together with the fitting curves (dashed black lines) to double exponential functions. d) Radioluminescence spectra of two PMMA nanocomposites containing either pure 1 (0.15 wt%, black line) or a binary mixture of perylene dye ([1]) and CsPbBr₃ PNCs (0.15 and 2.0 wt%, respectively, red line) under X-ray irradiation (30 kV, 20 mA). The radioluminescence spectra of a high quality commercial bismuth germanate (BGO) crystal (blue line) and of a plastic scintillator (SCSF-3HF, green line), collected in the same excitation and collection geometry. Bottom panel, radioluminescence spectra of the same sample after storage in air for six months compared to the same BGO crystal, showing comparable performance to the as-made nanocomposite. a–d) Adapted with permission.^[58b] Copyright 2020, The Authors, published by Springer Nature.

found to be comparable to commercially available scintillators (Figure 14d).

Different from scintillators, X-ray detectors convert absorbed high-energy X-ray photons into charge carriers to generate electrical signals for imaging with better spatial resolution.^[176] High sensitivity is of paramount importance for medical applications of X-ray detectors as it reduces the exposure of the body to high doses of X-rays that may cause potential health problems. PNC's ability to efficiently generate charge carriers, low cost, and ease of fabrication have led to their implementation as a promising candidate for X-ray detection.^[58c] Recently, CsPbBr₃ PNCs were embedded into a PMMA matrix to crafting an X-ray detector.^[58c] Due to their shorter average PL lifetime and stronger emission, CsPbBr₃ PNCs encapsulated with PMMA render higher spatial resolution (9.8 vs 6.2 lp mm⁻¹, at modulation transfer function = 0.2), faster response time (200 ns vs 1200 ns), and comparable stability under X-ray irradiation over X-ray irradiation of 40 Gyairs⁻¹ compared to commercialized gadolinium oxysulfide (GOS) X-ray detectors. Interestingly, CsPbBr₃ PNCs have been deposited on a flexible PET substrate via a low-cost inkjet printing process to yield flexible X-ray detectors with homogeneously distributed PNCs and high sensitivity.^[71]

4.4. Bioimaging and Biosensors

Inorganic QDs also hold appealing potential as imaging markers, biosensing probes, and optical coding agents for applications in bioimaging and biosensor.^[177] However, conventional inorganic QDs possess a relatively broad full width at half maximum of emission and low PLQY if no protective shell is present, which limits their use in bioimaging.^[178] In this context, PNCs with a narrow and readily tunable emission over the entire visible spectrum have emerged as promising

alternatives.^[40,179] As shown in Figure 15, CsPbX₃ PNC/PS nanocomposites allow for the fabrication of water-resistant samples that exhibit tunable luminescence. Additionally, the incorporation of PNCs into a polymer matrix decreases the probability of release of toxic heavy metal atoms into environment, which would obviously be detrimental to bio applications. The PL peak position and intensity of the nanocomposites were easily tailored by adjusting the composition and loading amount of CsPbX₃ PNCs. Notably, mixing nanocomposites of different emission wavelengths showed no overlapping in cells. The CsPbX₃ PNC/polymer nanocomposites were found to be capable of diffusing into living cells and serving as multiplexed luminescent probes to individually tag around 10 million cells for bioassay displays.

Hydrophilic polymers, such as PEG and PVP, have also been utilized to cap PNCs to enhance water resistance, water solubility, and biocompatibility, yielding PNC/polymer nanocomposites that can be used as luminescent probes in cell imaging.^[46,62] Tethering PNCs with amphiphilic block copolymers has been found to further enhance the compatibility of PNCs in aqueous media and lower the cytotoxicity of nanocomposites, while retaining the structural integrity and high PL stability of PNCs. For example, 90% of human cervical epithelial carcinoma cells were observed to survive in concentrations of PS-*b*-PEO capped CsPbX₃ PNCs below 30 µg mL⁻¹.^[81] The PLQY of nanocomposite aqueous solution decreased by only 23% (from 43% to 33%) after 7 months of storage. When high molecular weight PS was used, the PL of the nanocomposite aqueous solution, which had been stored in ambient environment for one month, remained nearly unchanged until 70 °C. Furthermore, the external polymer encapsulation prevents the ion exchanges from environment. The PL of PNCs in living cells, has also been found to remain very stable under continuous UV light irradiation for over an hour.^[81] Furthermore,

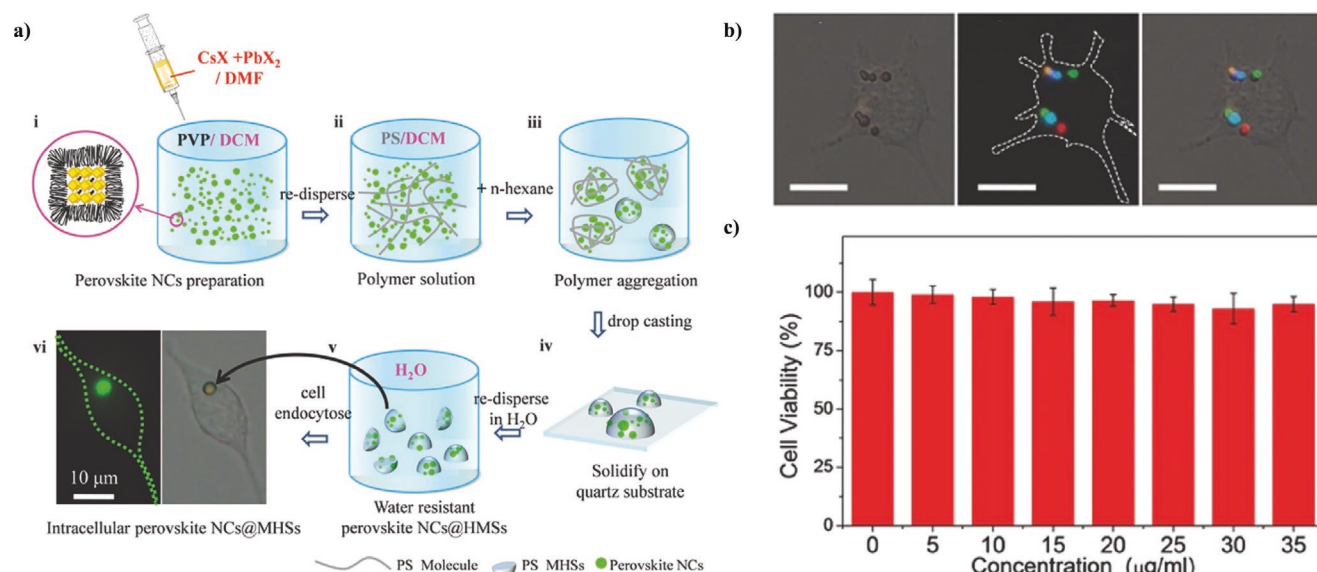


Figure 15. a) Schematic diagram of intracellular CsPbX₃ PNCs@PS microhemispheres (MHSS) fabrication process. b) Bright-field (left) and fluorescence (middle) images of live cell incubated with mixed NCs@MHSS. The fluorescence images are taken under 325–375 nm irradiation. Right: overlaid picture of left and middle. The scale bars are 20 µm. c) Viability of RAW 264.7 cells at various CsPbBr₃ concentrations in NCs@MHSS. a–c) Adapted with permission.^[40] Copyright 2017, Wiley-VCH.

the incorporation of antibodies to as-prepared nanocomposites enabled their binding to breast tumor-derived exosomes which allowed for the ability to track tumor type and stage, and monitor cancer treatment response.^[125b]

4.5. Photocatalysis

Photocatalysis has been regarded as an efficient strategy for solar energy capture and has found many important applications including water splitting, CO₂ reduction, chemical transformations, and remediation of organic pollutants.^[180] Chemical reactions driven by photocatalysis typically follow three individual processes, that is, generation of charge carriers by photon absorption, charge carriers separation, and migration to reactive sites on the surface of photocatalyst, and chemical oxidation and reduction at the surface of photocatalyst.^[181] Owing to their large optical absorption coefficient, efficient charge separation, and tunable electronic band structure, metal halide PNCs represent promising candidates for photocatalysis.^[182] For example, Ag doping of Cs₃Bi₂Br₉ perovskite was found to significantly alter its crystal structure and optoelectronic properties which led to over 100-fold enhancement in

its photocatalytic hydrogen evolution reaction.^[182b] Hybridizing graphene oxide with CsPbBr₃ PNCs was observed to enhance electron extraction and transport, resulting in a 25.5% increase in electron consumption, a reduction rate of 23.7 μmol g⁻¹ h⁻¹, and a selectivity over 99.3%.^[183]

It is interesting to note that CsPbI₃ PNCs have been found to exert sufficient photocatalytic activity to promoting polymerization of 2,2',5',2''-ter-3,4-ethylenedioxythiophene (TerEDOT) under visible light illumination while preserving their desirable cubic crystal structure.^[72] As shown in **Figure 16**, under illumination photoexcited charge carriers (i.e., holes and electrons) were continuously generated in CsPbI₃ PNCs and then transferred to either hole acceptors (TerEDOT) and electron acceptors (1,4-benzoquinone or molecular oxygen), respectively. The oxidized TerEDOT subsequently underwent polymerization to form conjugated PEDOT situated on the PNC surface (Figure 16c), thereby providing a novel strategy to create PNC/polymer nanocomposites. Moreover, tuning the composition of PNCs has been shown to render different electronic band structures and activation wavelengths that can be utilized to facilitate photoinduced electron/energy transfer-reversible addition-fragmentation chain transfer polymerization (PET-RAFT) under a broad range of irradiation wavelengths in nonpolar solvents.^[184]

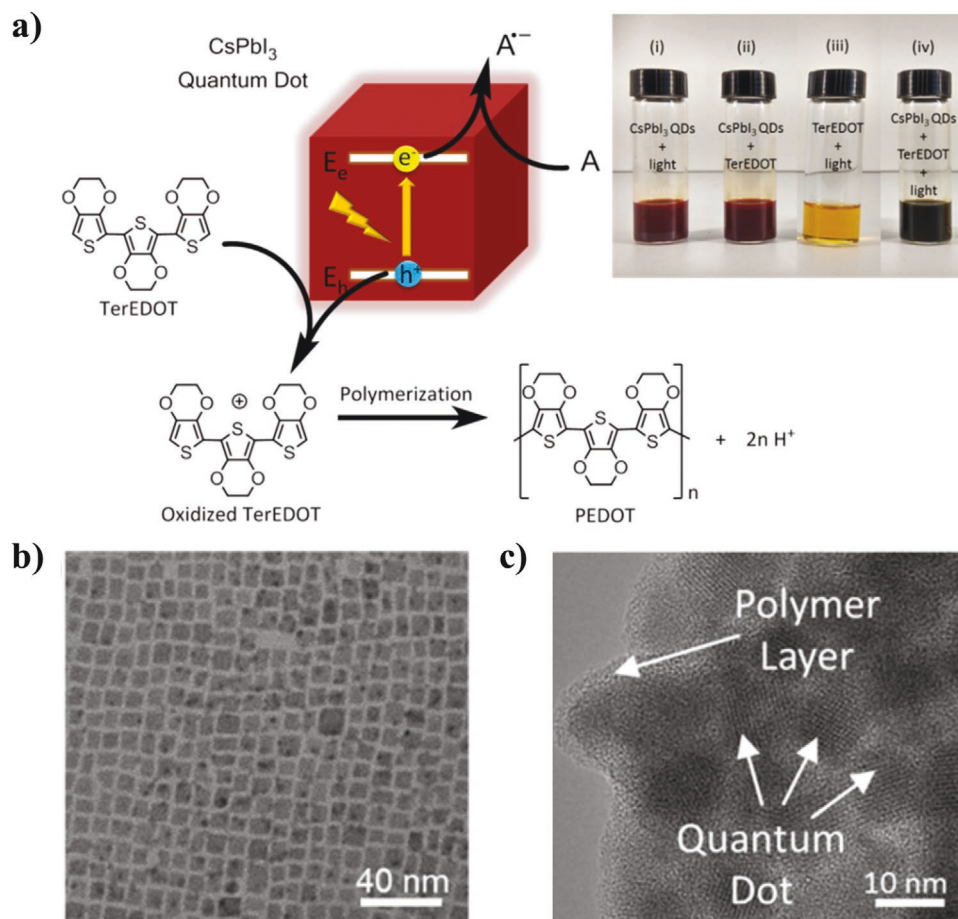


Figure 16. a) Illustration of the proposed mechanism for photocatalytic polymerization of TerEDOT over CsPbI₃ PNCs under visible light illumination. b) TEM image of CsPbI₃ PNCs. c) TEM image of CsPbI₃ PNCs encapsulated by PEDOT. a–c) Adapted with permission.^[72a] Copyright 2017, American Chemical Society.

Specifically, CsPbX₃ PNCs have served as a photocatalyst in PET-RAFT to generate photoexcited charge carriers and activate typical RAFT agents for the polymerization of a series of monomers, including methyl acrylate, butyl acrylate, 2,2,2-trifluoroethyl acrylate, and methyl methacrylate. Excellent control over the conversion, molecular weight, molecular weight distribution, and chain-end fidelity can be realized via this strategy with light irradiation from the UV to the NIR region as a result of the tunable electronic band structure of CsPbX₃ PNCs. As discussed above, styrene monomers have been polymerized with controllable molecular weight and conversion and grafted from the surface of PNCs under UV light irradiation.^[35]

It is worth noting that the PNC/polymer nanocomposites are also applied in photocatalysis with enhanced performance and stability over pristine PNCs. For example, MAPbBr₃ PNC/conjugated polymer PEDOT: PSS displayed drastically enhanced hole transportation due to its favorable band alignment, thereby rendering efficient charge separation and an increased reaction rate of the hydrogen evolution reaction from 6 to 65 $\mu\text{mol h}^{-1}$ in aqueous solution.^[31] In another study, MAPbBr₃ PNCs were encapsulated in poly(norepinephrine) (PNE) via in situ polymerization and retained their structural integrity in chloroform due to a thin protective PNE layer coated on their surface.^[73] The MAPbBr₃ PNC/PNE nanocomposite possessed drastically better stability than pristine MAPbBr₃ PNCs which showed a significant increase in PbBr₂ content after three cycles of photocatalytic activities. The addition of PNE was also shown to enhancing the light-harvesting ability of nanocomposite because PNE itself possesses the capability of absorbing visible light, generate photoexcited charge carriers, and efficiently transport and separating charge carriers. The reaction rate of photocatalytic degradation of malachite green has been found to be greatly improved by using the MAPbBr₃ PNC/PNE photocatalyst.^[73]

4.6. Piezoelectric Nanogenerators (PENG)

PENG are a class of device that scavenge mechanical energy in ambient conditions and convert it into usable electrical energy by capitalizing on piezoelectric materials.^[185] The hybridization of metal halide PNCs with outstanding piezoelectric properties, cost effectiveness, and ease of fabrication, and polymers with stretchable, solution-processable, and stable attributes has led to the practical implantation and versatile utilization of PENGs in flexible, wearable, and biocompatible electronic devices.^[109] A nanocomposite of mechanically robust PDMS and FAPbBr₃ NCs was created via mechanical mixing. The FAPbBr₃ PNC/PDMS nanocomposite was then deposited onto a stretchable, electrode-coated PET substrate to craft a PENG. The as-prepared PENG delivered a maximum output voltage of 8.5 V and current density of 3.8 $\mu\text{A cm}^{-2}$ under periodic vertical compression and release operations. Notably, this output was capable of charging a capacitor and illuminating a commercial red LED.^[55]

However, phase separation and aggregation of PNCs in the PDMS matrix restricted further performance improvement of the as-prepared nanocomposite PENG due to the highly viscous nature of PDMS and the limited interaction between PNCs and PDMS. In this context, a PVDF matrix was selected

as a promising alternative because of its intrinsic piezoelectric properties, remarkable flexibility, and ability to interact with PNCs, thus conferring uniform spatial distribution of PNCs (Figure 17a).^[51,147,186] Figure 17b depicts the working mechanism of a PENG.^[53] The initial stage showed no charge accumulation on the electrode surfaces of PENG. The generated piezoelectric potentials in the PVDF matrix enabled the formation of macro-dipoles in MAPbI₃ when applying an external force and resulted in the accumulation of charges with opposite polarity at the MAPbI₃-PVDF interfaces and surfaces.^[53] Subsequently, the decreased charge density of the top and bottom electrodes allowed for the flow of charges from the bottom to the top, producing a positive signal. During the release process, the relaxation of the MAPbI₃-PVDF matrix increased the charge density on both electrodes, leading to a flow of charges from the top to bottom, generating a negative output signal.^[53] As such, the utilization of the piezoelectric polymer PVDF as a matrix and homogeneous distribution of MAPbBr₃ PNCs was found to synergistically improve the outputs of the as-prepared PENG with a voltage of 45.6 V and current density of 4.7 $\mu\text{A cm}^{-2}$ (Figure 17c).^[53]

5. Conclusions and Perspectives

We have summarized the recent progress in synthesis, properties, and applications of metal halide PNC/polymer nanocomposites. First, several methods to craft PNC/polymer nanocomposites were introduced. The intriguing optical, optoelectronic, electronic, mechanical, and chemical properties of PNCs and PNC/polymer nanocomposites were then scrutinized. Subsequently, a wide range of relevant applications for PNC/polymer nanocomposites were provided.

The synthetic routes for PNC/polymer nanocomposites are categorized into two main groups: 1) where polymers are chemically anchored onto PNCs and 2) where polymers and PNCs physically mixed. For chemical approaches, the in situ synthesis of PNCs in the presence of polymerizable and polymer capping agents was first discussed. Second, in situ synthesis of PNCs inside polymer nanoreactors (e.g., micelles formed by linear or star-shaped multiarm block copolymers) was introduced. The coordination interaction between functional groups (e.g., -COOH in PAA and pyridine group in P2VP and P4VP) and metal moieties of PNC precursors has been shown to facilitate nucleation and growth of PNCs within the compartment occupied by corresponding polymer blocks. Third, postsynthesis anchoring of polymers onto PNCs via “graft from” and “graft on” approaches was summarized. PNC/polymer nanocomposite production via physical mixing, either by embedding synthesized PNCs into polymer matrices or in situ growth of PNCs within polymeric materials^[29,37,38,47,51,60] was then discussed. The intrinsic lightweight, cost effectiveness, and solution processability of most polymers allow for facile processing of PNC/polymer nanocomposites through a set of well-established large-scale manufacturing techniques such as electrospinning, inkjet printing, and size exclusion lithography.^[38,43,57,84,110] It is also worth noting that among the above mentioned methods, only the nanoreactor approach was shown to provide precise control over the size and architecture of PNCs.

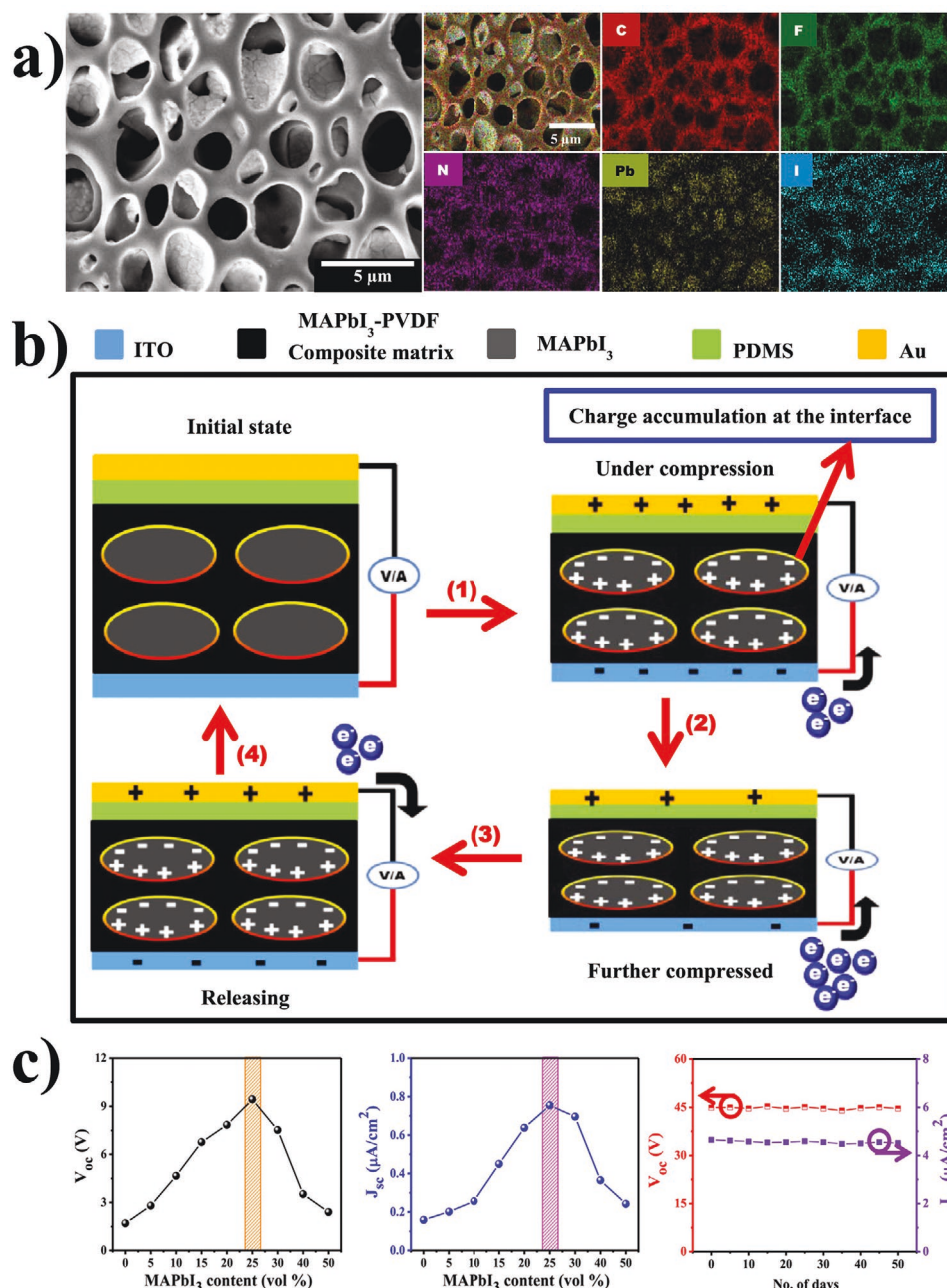


Figure 17. a) Scanning electron microscopy–energy-dispersive X-ray spectroscopy (SEM–EDS) mapping images of spin-coated 25 vol% MAPbI₃/PVDF nanocomposite film on fluorine-doped tin oxide (FTO) substrate. b) Schematic diagram of the MAPbI₃/PVDF-nanocomposite-based piezoelectric nanogenerator working mechanism. c) Output voltage (V_{oc}) (left) and current density (J_{sc}) (middle) as a function of MAPbI₃ PNCs volume fraction; Right: the stability test results of 25 vol% of MAPbI₃/PVDF piezoelectric nanogenerator under an applied force of 50 N and corresponding V_{oc} and J_{sc} . a–c) Adapted with permission.^[53] Copyright 2018, Elsevier.

In the next section, the intriguing properties of PNCs and PNC/polymer nanocomposites were reviewed in detail. First, the optical properties of PNCs, including their electronic band structure, quantum confinement effect, and defect tolerance were summarized. The ability to use both size and composition of PNCs to tune such intriguing properties was highlighted. Second, the optoelectronic properties (i.e., the charge carrier dynamics) and electronic properties (i.e., dielectric, ferroelectric, and piezoelectric properties) of PNCs and

PNC/polymer nanocomposites were detailed. Furthermore, the mechanical stretchability of PNC/polymer nanocomposites was introduced. Thermal expansion coefficient matching between PNCs and polymers, and spatial organization of PNCs within a polymer matrix were emphasized as two key factors that affect the stretchability of their nanocomposites. Additionally, the enhanced stability from polymer encapsulation of PNCs in PNC/polymer nanocomposites was noted. Finally, a broad array of applications of PNC/polymer nanocomposites

were highlighted, including LEDs, lasers, scintillators and X-ray detectors, bioimaging and biosensing, photocatalysis, and PENGs.

Though PNC/polymer nanocomposites possess a variety of excellent properties and a wide range of applications, a few challenges still hinder their commercialization. First, the long-term stability of PNCs and PNC/polymer nanocomposites is a critical issue. To overcome this, enhanced intrinsic structural integrity of PNCs is needed. Several strategies have been explored to achieve this goal: 1) Engineering the composition of PNCs to tailor the tolerance factor and enhance the formation energy via selecting ions with a favorable radius and/or doping of additional components.^[119,187] 2) Deliberately selecting low-polarity solvents and antisolvents in synthesis and purification of PNCs to avoid the formation of surface defects.^[124] 3) Rational design and synthesis utilizing ligands with specific functional groups, for instance, zwitterions, which strongly bind to the surface of PNCs and can eliminate the detachment of dangling ligands.^[90b]

Synthesizing PNC/polymer nanocomposites with more advanced polymeric ligands is a promising strategy to further improve stabilities against multiple environmental factors and durability of nanocomposite-based devices. A particularly intriguing option to achieve this is to capitalize on polymeric zwitterionic ligands with multiple anchoring groups and long hydrocarbon chains. The introduction of zwitterionic polymers has already been shown to increase the stability of CsPbBr₃ PNC/polymer nanocomposites in polar solvents to over 1.5 years,^[69] and passivate and disperse PNCs in as-prepared nanocomposite thin films.^[24a] One challenge to this strategy, however, is that the synthesis of zwitterionic polymer ligands normally requires multiple steps and results in relatively limited yields. Therefore, the development of easily synthesized zwitterionic polymer ligands is needed to widely incorporate them with PNCs to render enhanced protection and surface passivation.

Moreover, preparing PNC/polymer nanocomposites with crosslinked polymers offers another promising alternative. The crosslinked polymer matrix outside PNCs can boost environmental stability by providing a dense protective layer that inhibits the diffusion of moisture and polar solvents to reach PNC surface. This can be seen in the extraordinary stability of MAPbBr₃ PNC/polymer nanocomposites in harsh environments (e.g., 85 °C and 85% relative humidity^[188]).^[37] Additionally, crosslinked polymer matrixes can limit ion migration in PNCs. Furthermore, selecting crosslinking monomers with functional groups that can effectively passivate PNC surfaces (e.g., 1-alkynyl acid) has been demonstrated to enhance PL emission intensity of CsPbBr₃ PNCs.^[89] Thus, because of their ability to enhance stability and passivate surfaces, crosslinked polymer matrixes merit further exploration for use in PNC/polymer nanocomposites. In addition, the structural integrity of PNCs can be enhanced by encapsulation in inorganic matrixes or other organic materials (i.e., metal organic frameworks (MOFs)) with high water resistance and low oxygen diffusion rate.^[189] Moreover, the development of PNC/polymer nanocomposites with self-healing capabilities has been proven to enhance the stability and retain the structural integrity of perovskite/polymer composites.^[190]

The unsatisfactory conductivity of PNC/polymer nanocomposites represents another challenge. In perovskite thin films, the incorporation of conductive conjugated polymers (e.g., PEDOT and P3HT) has been shown to enhance stability,^[191] passivate surfaces,^[192] and improve inherent conductivity.^[141,193] The optoelectronic performance of nanocomposite-based devices can be improved by rationally engineering the side chains of conjugated polymers to optimize their conductivity, solubility, processability, bandgap energies, and energy levels which in turn minimize phase segregation of PNCs and promote efficient charge separation and transport by optimizing the energy level alignment between conjugated polymers and perovskites.^[194] However, PNC/conjugated polymer nanocomposites have been rarely reported and explored. Systematic investigation of PNC/conjugated polymer nanocomposites with respect to their synthetic methods, stability, optoelectronic properties, and processability is an intriguing area of opportunity for future studies. Tunable lifetime and separation of charge carriers in PNC/polymer nanocomposites can also benefit the applications beyond optoelectronics, for example, in photocatalysis where efficient charge carrier separation is also required.^[180]

Another area ripe for future study is in deciphering the concrete mechanisms of how polymers interact with PNCs. For example, what functional groups of polymers passivate trap states of perovskites and how polymers affect the termination and surface energy of PNCs are still not clear and should be studied. Additionally, how chain packing and composition of polymers affect water and oxygen diffusion and a polymers' overall contribution to electronic band structure and stability needs to be elucidated. In this context, a suite of surface analysis techniques, including vibrational spectroscopy, nuclear magnetic resonance spectroscopy, X-ray photoelectron spectroscopy, and small-angle neutron scattering technique may be needed to clarify the interactions between polymers and the PNCs.^[13,195] To optimize nanocomposites for optoelectronic applications, an in-depth understanding of the influence of polymers on charge carrier dynamics and PL decay kinetics is of key importance. Time-resolved PL, transient absorption, and time-resolved fluorescence quenching spectroscopies are some critical techniques to precisely measuring exciton behaviors, PL lifetime, exciton diffusion length, and mobility of charge carriers that will allow for the exploration of structure-optoelectronic properties correlation of PNC/polymer nanocomposites.^[196] Furthermore, computational simulation techniques could be a powerful tool to facilitate the understanding of polymer-PNC interactions and the development of PNC/polymer nanocomposites with enhanced properties. Density functional theory and molecular dynamics have been applied in studying surface defects,^[197] interaction between perovskite surfaces and coordinating molecules^[140] and external environment,^[198] and the charge carrier dynamics of PNCs. Yet, such modeling strategies have rarely been applied in the study of PNC/polymer nanocomposites and may represent an important area for future research.

Last, lead toxicity also inhibits the successful commercialization PNC/polymer nanocomposites. The presence of lead in PNCs raises obvious toxicity concerns for the introduction of these materials into consumer devices.^[15b] Therefore, it

is of profound interest to develop lead-free PNCs (LFPNCs). So far, Sn^{II} , Sn^{IV} , Sb^{III} , Bi^{III} , Pd^{IV} , Cu^{II} , In^{III} , and Ag^{I} have been employed to replace Pb and yield less- and nontoxic LFPNCs.^[15b,199] However, a clear understanding of crystal structure, synthetic methods, and a correlation between properties, composition, structure, and morphologies of LFPNCs remains to be achieved. Further development of reliable LFPNCs is needed to stimulate progress in research of LFPNC/polymer nanocomposites.

Research in PNC/polymer nanocomposites has undergone a rapid evolution in the recent years. Yet, several interesting research areas remain as potential directions for future studies. First, the integration of stimuli-responsive polymers with PNCs may afford additional functionalities and significantly broaden the applications of perovskite materials. Many polymers possess fascinating stimuli-responsive properties that can be triggered by light of a specific wavelength (e.g., poly(7-methylacryloyloxy-4-methylcoumarin) (PMAMC)^[96a]), pH (e.g., P4VP^[200]) and temperature (e.g., poly(*N*-isopropylacrylamide) (PNIPAM)^[201]) variations. These polymers have been incorporated with conventional QDs and noble metal NCs for a wide range of applications in drug delivery, bioimaging, and biosensing.^[96a,201,202] For instance, PMAMC-capped Au nanoparticles display light-enabled reversible self-assembly due to the photo-responsive nature of coumarin containing PMAMC. These samples possess remarkable potential as smart guest molecule nanocarriers.^[96a] Following the example of these nanocrystals, stimuli-responsive polymers could be introduced to PNCs for achieving a diverse assortment of properties.

An additional area for further exploration is the higher-order structure and hierarchical structure of PNC/nanocomposites, especially those of samples prepared via nanoreactors and with polymers chemically anchored. Polymer-directed self-assembly of traditional NCs into higher-order structures and hierarchical superstructures has been extensively investigated.^[203] Self-assembled NCs possess unique properties due to the close proximity and packing of the NC building blocks and can be easily scaled for mass manufacturing. For example, shifting Au nanorod assemblies from side-by-side to end-to-end arrangements has been demonstrated to enable tunable plasmonic resonance in both longitudinal and transverse directions.^[204] As noted above, using PEG homopolymers as surface capping ligands resulted in the assembly of CsPbBr_3 PNCs and a shift of absorption peak toward lower energy due to interparticle coupling.^[132] In addition to homopolymers, block copolymers are well known to phase separate into well-defined, thermodynamically stable mesostructures with different morphologies and precise domain sizes.^[205] To date, block copolymers have not yet been utilized to direct the self-assembly of PNCs. Compared to homopolymers, the incorporation of block copolymers will improve the structural integrity of NC ordered structures because one block acts as a stabilizing agent to improve the dispersity of NCs, while the other block promotes the segregation of ligands.^[203b] Furthermore, the readily tunable sequence, composition, and molecular weight of each block provide additional functionalities and parameters to manipulate the interactions and self-assembly of NCs.^[203b,206] Therefore, utilizing surface-capped polymers to guide the assembly of PNCs of various sizes and shapes into predictable structures

may provide opportunities to scrutinize the interaction between adjacent NCs and their influence on the optical and electronic properties of the resulting self-assembled nanostructures.^[132]

PNC/polymer nanocomposites have already demonstrated tremendous potential, and the continued progress being made in synthesis, fundamental understanding in composition–structure–property relation, and applications suggests that further improvements are not far on the horizon. We hope that this review spurs interest in for in depth study of PNC/polymer nanocomposites and helps realize significant developments for this exciting material.

Acknowledgements

S.L., M.Z., and G.M.B. contributed equally to this work. This work was supported by the NSF (CMMI 1914713; CBET 1803495; DMR 1903990; ECCS1914562) and AFOSR (FA9550-19-1-0317).

Conflict of Interest

The authors declare no conflict of interest.

Keywords

materials and devices, metal halide perovskites, nanocomposites, nanocrystals, optoelectronics, polymers

Received: August 29, 2020

Revised: February 18, 2021

Published online:

- [1] a) A. Poglitsch, D. Weber, *J. Chem. Phys.* **1987**, *87*, 6373; b) O. Yaffe, Y. Guo, L. Z. Tan, D. A. Egger, T. Hull, C. C. Stoumpos, F. Zheng, T. F. Heinz, L. Kronik, M. G. Kanatzidis, *Phys. Rev. Lett.* **2017**, *118*, 136001; c) L. Mao, C. C. Stoumpos, M. G. Kanatzidis, *J. Am. Chem. Soc.* **2018**, *141*, 1171; d) J. Even, L. Pedesseau, C. Katan, *J. Phys. Chem. C* **2014**, *118*, 11566.
- [2] M. Liu, M. B. Johnston, H. J. Snaith, *Nature* **2013**, *501*, 395.
- [3] J. H. Noh, S. H. Im, J. H. Heo, T. N. Mandal, S. I. Seok, *Nano Lett.* **2013**, *13*, 1764.
- [4] C. Law, L. Miseikis, S. Dimitrov, P. Shakya-Tuladhar, X. Li, P. R. Barnes, J. Durrant, B. C. O'Regan, *Adv. Mater.* **2014**, *26*, 6268.
- [5] K. W. Tan, D. T. Moore, M. Saliba, H. Sai, L. A. Estroff, T. Hanrath, H. J. Snaith, U. Wiesner, *ACS Nano* **2014**, *8*, 4730.
- [6] Q. Dong, Y. Fang, Y. Shao, P. Mulligan, J. Qiu, L. Cao, J. Huang, *Science* **2015**, *347*, 967.
- [7] T. Zhang, M. Yang, Y. Zhao, K. Zhu, *Nano Lett.* **2015**, *15*, 3959.
- [8] F. X. Xie, D. Zhang, H. Su, X. Ren, K. S. Wong, M. Grätzel, W. C. Choy, *ACS Nano* **2015**, *9*, 639.
- [9] Y. Deng, E. Peng, Y. Shao, Z. Xiao, Q. Dong, J. Huang, *Energy Environ. Sci.* **2015**, *8*, 1544.
- [10] D. Luo, R. Su, W. Zhang, Q. Gong, R. Zhu, *Nat. Rev. Mater.* **2019**, *5*, 44.
- [11] L. N. Quan, B. P. Rand, R. H. Friend, S. G. Mhaisalkar, T.-W. Lee, E. H. Sargent, *Chem. Rev.* **2019**, *119*, 7444.
- [12] S. D. Stranks, H. J. Snaith, *Nat. Nanotechnol.* **2015**, *10*, 391.
- [13] J. Shamsi, A. S. Urban, M. Imran, L. De Trizio, L. Manna, *Chem. Rev.* **2019**, *119*, 3296.

- [14] a) L. Protesescu, S. Yakunin, M. I. Bodnarchuk, F. Krieg, R. Caputo, C. H. Hendon, R. X. Yang, A. Walsh, M. V. Kovalenko, *Nano Lett.* **2015**, 15, 3692; b) P. Tyagi, S. M. Arveson, W. A. Tisdale, *J. Phys. Chem. Lett.* **2015**, 6, 1911.
- [15] a) L. C. Schmidt, A. Pertegás, S. González-Carrero, O. Malinkiewicz, S. Agouram, G. Minguez Espallargas, H. J. Bolink, R. E. Galian, J. Pérez-Prieto, *J. Am. Chem. Soc.* **2014**, 136, 850; b) Q. Fan, G. V. Biesold-McGee, J. Ma, Q. Xu, S. Pan, J. Peng, Z. Lin, *Angew. Chem., Int. Ed.* **2020**, 59, 1030.
- [16] H. C. Wang, Z. Bao, H. Y. Tsai, A. C. Tang, R. S. Liu, *Small* **2018**, 14, 1702433.
- [17] a) Y. J. Yoon, Y. Chang, S. Zhang, M. Zhang, S. Pan, Y. He, C. H. Lin, S. Yu, Y. Chen, Z. Wang, Y. Ding, J. Jung, N. Thadhani, V. V. Tsukruk, Z. Kang, Z. Lin, *Adv. Mater.* **2019**, 31, 1901602; b) M. C. Weidman, M. Seitz, S. D. Stranks, W. A. Tisdale, *ACS Nano* **2016**, 10, 7830; c) J. Shamsi, Z. Dang, P. Bianchini, C. Canale, F. Di Stasio, R. Brescia, M. Prato, L. Manna, *J. Am. Chem. Soc.* **2016**, 138, 7240; d) D. Zhang, S. W. Eaton, Y. Yu, L. Dou, P. Yang, *J. Am. Chem. Soc.* **2015**, 137, 9230.
- [18] a) Q. A. Akkerman, V. D'Innocenzo, S. Accornero, A. Scarpellini, A. Petrozza, M. Prato, L. Manna, *J. Am. Chem. Soc.* **2015**, 137, 10276; b) G. E. Eperon, C. E. Beck, H. J. Snaith, *Mater. Horiz.* **2016**, 3, 63.
- [19] G. Grancini, M. K. Nazeeruddin, *Nat. Rev. Mater.* **2019**, 4, 4.
- [20] a) H. Tsai, W. Nie, J.-C. Blancon, C. C. Stoumpos, R. Asadpour, B. Harutyunyan, A. J. Neukirch, R. Verduzco, J. J. Crochet, S. Tretiak, *Nature* **2016**, 536, 312; b) D. H. Cao, C. C. Stoumpos, O. K. Farha, J. T. Hupp, M. G. Kanatzidis, *J. Am. Chem. Soc.* **2015**, 137, 7843.
- [21] C. Wang, Y. Zhang, A. Wang, Q. Wang, H. Tang, W. Shen, Z. Li, Z. Deng, *Chem. Mater.* **2017**, 29, 2157.
- [22] a) T. A. Berhe, W.-N. Su, C.-H. Chen, C.-J. Pan, J.-H. Cheng, H.-M. Chen, M.-C. Tsai, L.-Y. Chen, A. A. Dubale, B.-J. Hwang, *Energy Environ. Sci.* **2016**, 9, 323; b) T. Leijtens, G. E. Eperon, N. K. Noel, S. N. Habisreutinger, A. Petrozza, H. J. Snaith, *Adv. Energy Mater.* **2015**, 5, 1500963.
- [23] a) F. P. G. de Arquer, X. Gong, R. P. Sabatini, M. Liu, G.-H. Kim, B. R. Sutherland, O. Voznyy, J. Xu, Y. Pang, S. Hoogland, D. Sinton, E. Sargent, *Nat. Commun.* **2017**, 8, 14757; b) W. Cha, H.-J. Kim, S. Lee, J. Kim, *J. Mater. Chem. C* **2017**, 5, 6667.
- [24] a) H. Kim, N. Hight-Huf, J. H. Kang, P. Bisnoff, S. Sundararajan, T. Thompson, M. Barnes, R. C. Hayward, T. Emrick, *Angew. Chem., Int. Ed.* **2020**, 59, 10802; b) B. Jeong, H. Han, H. H. Kim, W. K. Choi, Y. J. Park, C. Park, *ACS Nano* **2020**, 14, 1645; c) J. He, Z. He, A. Towers, T. Zhan, H. Chen, L. Zhou, C. Zhang, R. Chen, T. Sun, A. J. Gesquiere, *Nanoscale Adv.* **2020**, 2, 2034; d) T. Zhu, Y. Yang, L. Zheng, L. Liu, M. L. Becker, X. Gong, *Adv. Funct. Mater.* **2020**, 30, 1909487.
- [25] Q. Shan, J. Song, Y. Zou, J. Li, L. Xu, J. Xue, Y. Dong, B. Han, J. Chen, H. Zeng, *Small* **2017**, 13, 1701770.
- [26] D. Yang, X. Li, H. Zeng, *Adv. Mater. Interfaces* **2018**, 5, 1701662.
- [27] N. Tomczak, D. Jańczewski, M. Han, G. J. Vancso, *Prog. Polym. Sci.* **2009**, 34, 393.
- [28] E. Glogowski, R. Tangirala, T. P. Russell, T. Emrick, *J. Polym. Sci., Part A: Polym. Chem.* **2006**, 44, 5076.
- [29] S. N. Raja, Y. Bekenstein, M. A. Koc, S. Fischer, D. Zhang, L. Lin, R. O. Ritchie, P. Yang, A. P. Alivisatos, *ACS Appl. Mater. Interfaces* **2016**, 8, 35523.
- [30] M. Righetto, D. Meggiolaro, A. Rizzo, R. Sorrentino, Z. He, G. Meneghesso, T. C. Sum, T. Gatti, F. Lamberti, *Prog. Mater. Sci.* **2020**, 110, 100639.
- [31] H. Wang, X. Wang, R. Chen, H. Zhang, X. Wang, J. Wang, J. Zhang, L. Mu, K. Wu, F. Fan, *ACS Energy Lett.* **2018**, 4, 40.
- [32] J. Yuan, X. Ling, D. Yang, F. Li, S. Zhou, J. Shi, Y. Qian, J. Hu, Y. Sun, Y. Yang, *Joule* **2018**, 2, 2450.
- [33] X. Chen, C. Sun, Y. Liu, L. Yu, K. Zhang, A. M. Asiri, H. M. Marwani, H. Tan, Y. Ai, X. Wang, *Chem. Eng. J.* **2020**, 379, 122360.
- [34] a) S. G. R. Bade, X. Shan, P. T. Hoang, J. Li, T. Geske, L. Cai, Q. Pei, C. Wang, Z. Yu, *Adv. Mater.* **2017**, 29, 1607053; b) Y. Zhao, J. Wei, H. Li, Y. Yan, W. Zhou, D. Yu, Q. Zhao, *Nat. Commun.* **2016**, 7, 10228.
- [35] Y. C. Wong, J. De Andrew Ng, Z. K. Tan, *Adv. Mater.* **2018**, 30, 1800774.
- [36] S. Pathak, N. Sakai, F. Wisnivesky Rocca Rivarola, S. D. Stranks, J. Liu, G. E. Eperon, C. Ducati, K. Wojciechowski, J. T. Griffiths, A. A. Haghighirad, A. Pellaroque, R. H. Friend, H. J. Snaith, *Chem. Mater.* **2015**, 27, 8066.
- [37] Y. Wei, X. Deng, Z. Xie, X. Cai, S. Liang, P. a. Ma, Z. Hou, Z. Cheng, J. Lin, *Adv. Funct. Mater.* **2017**, 27, 1703535.
- [38] Y. Wang, J. He, H. Chen, J. Chen, R. Zhu, P. Ma, A. Towers, Y. Lin, A. J. Gesquiere, S. T. Wu, Y. Dong, *Adv. Mater.* **2016**, 28, 10710.
- [39] H. Liao, S. Guo, S. Cao, L. Wang, F. Gao, Z. Yang, J. Zheng, W. Yang, *Adv. Opt. Mater.* **2018**, 6, 1800346.
- [40] H. Zhang, X. Wang, Q. Liao, Z. Xu, H. Li, L. Zheng, H. Fu, *Adv. Funct. Mater.* **2017**, 27, 1604382.
- [41] H. Kim, S. So, A. Ribbe, Y. Liu, W. Hu, V. V. Duzhko, R. C. Hayward, T. Emrick, *Chem. Commun.* **2019**, 55, 1833.
- [42] Y. Wang, Z. Zhu, J. Huang, J. Cai, J. Zhu, X. Yang, J. Shen, H. Jiang, C. Li, *J. Phys. Chem. Lett.* **2016**, 7, 4253.
- [43] L. Shi, L. Meng, F. Jiang, Y. Ge, F. Li, X. g. Wu, H. Zhong, *Adv. Funct. Mater.* **2019**, 29, 1903648.
- [44] J. He, H. Chen, H. Chen, Y. Wang, S.-T. Wu, Y. Dong, *Opt. Express* **2017**, 25, 12915.
- [45] S. Jia, G. Li, P. Liu, R. Cai, H. Tang, B. Xu, Z. Wang, Z. Wu, K. Wang, X. W. Sun, *Adv. Funct. Mater.* **2020**, 30, 1910817.
- [46] Q.-B. Yan, N. Bao, S.-N. Ding, *J. Mater. Chem. B* **2019**, 7, 4153.
- [47] J. Li, S. G. R. Bade, X. Shan, Z. Yu, *Adv. Mater.* **2015**, 27, 5196.
- [48] L. Xu, Y. Meng, C. Xu, P. Chen, *RSC Adv.* **2018**, 8, 36910.
- [49] Y. Ling, Y. Tian, X. Wang, J. C. Wang, J. M. Knox, F. Perez-Orive, Y. Du, L. Tan, K. Hanson, B. Ma, H. Gao, *Adv. Mater.* **2016**, 28, 8983.
- [50] P. C. Tsai, J. Y. Chen, E. Ercan, C. C. Chueh, S. H. Tung, W. C. Chen, *Small* **2018**, 14, 1704379.
- [51] Q. Zhou, Z. Bai, W. g. Lu, Y. Wang, B. Zou, H. Zhong, *Adv. Mater.* **2016**, 28, 9163.
- [52] W. G. Lu, X. G. Wu, S. Huang, L. Wang, Q. Zhou, B. Zou, H. Zhong, Y. Wang, *Adv. Opt. Mater.* **2017**, 5, 1700594.
- [53] V. Jella, S. Ippili, J.-H. Eom, J. Choi, S.-G. Yoon, *Nano Energy* **2018**, 53, 46.
- [54] P. Liang, P. Zhang, A. Pan, K. Yan, Y. Zhu, M. Yang, L. He, *ACS Appl. Mater. Interfaces* **2019**, 11, 22786.
- [55] R. Ding, H. Liu, X. Zhang, J. Xiao, R. Kishor, H. Sun, B. Zhu, G. Chen, F. Gao, X. Feng, *Adv. Funct. Mater.* **2016**, 26, 7708.
- [56] A. Pan, J. Wang, M. J. Jurov, M. Jia, Y. Liu, Y. Wu, Y. Zhang, L. He, Y. Liu, *Chem. Mater.* **2018**, 30, 2771.
- [57] K. Ma, X.-Y. Du, Y.-W. Zhang, S. Chen, *J. Mater. Chem. C* **2017**, 5, 9398.
- [58] a) P. G. Papagiorgis, A. Manoli, A. Alexiou, P. Karacosta, X. Karagiorgis, G. Papaparaskeva, M. Bodnarchuk, M. V. Kovalenko, T. Krasia, G. Itskos, *Front. Chem.* **2019**, 7, 87; b) M. Gandini, I. Villa, M. Beretta, C. Gotti, M. Imran, F. Carulli, E. Fantuzzi, M. Sassi, M. Zaffalon, C. Brofferio, L. Manna, L. Beverina, A. Vedda, M. Fasoli, L. Gironi, S. Brovelli, *Nat. Nanotechnol.* **2020**, 15, 462; c) J. H. Heo, D. H. Shin, J. K. Park, D. H. Kim, S. J. Lee, S. H. Im, *Adv. Mater.* **2018**, 30, 1801743.
- [59] J. Tong, J. Wu, W. Shen, Y. Zhang, Y. Liu, T. Zhang, S. Nie, Z. Deng, *ACS Appl. Mater. Interfaces* **2019**, 11, 9317.
- [60] L. Zhang, X. Yang, Q. Jiang, P. Wang, Z. Yin, X. Zhang, H. Tan, Y. M. Yang, M. Wei, B. R. Sutherland, E. H. Sargent, *Nat. Commun.* **2017**, 8, 15640.

- [61] J. Hai, H. Li, Y. Zhao, F. Chen, Y. Peng, B. Wang, *Chem. Commun.* **2017**, 53, 5400.
- [62] M. J. Tan, D. Ravichandran, H. L. Ang, E. W. Y. Ong, C. Q. X. Lim, G. M. Kam, A. P. Kumar, Z. K. Tan, *Adv. Healthcare Mater.* **2019**, 8, 1900859.
- [63] L. Rao, Y. Tang, C. Yan, J. Li, G. Zhong, K. Tang, B. Yu, Z. Li, J. Z. Zhang, *J. Mater. Chem. C* **2018**, 6, 5375.
- [64] H. Sun, Z. Yang, M. Wei, W. Sun, X. Li, S. Ye, Y. Zhao, H. Tan, E. L. Kynaston, T. B. Schon, H. Yan, Z.-H. Lu, G. A. Ozin, E. H. Sargent, D. S. Seferos, *Adv. Mater.* **2017**, 29, 1701153.
- [65] A. Privitera, M. Righetto, M. De Bastiani, F. Carraro, M. Rancan, L. Armelao, G. Granozzi, R. Bozio, L. Franco, *J. Phys. Chem. Lett.* **2017**, 8, 5981.
- [66] M. Meyns, M. Perálvarez, A. Heuer-Jungemann, W. Hertog, M. Ibáñez, R. Nafria, A. Genç, J. Arbiol, M. V. Kovalenko, J. Carreras, A. Cabot, A. G. Kanaras, *ACS Appl. Mater. Interfaces* **2016**, 8, 19579.
- [67] D. Baranov, G. Caputo, L. Goldoni, Z. Dang, R. Scarfiello, L. De Trizio, A. Portone, F. Fabbri, A. Camposeo, D. Pisignano, L. Manna, *Chem. Sci.* **2020**, 11, 3986.
- [68] H. Wu, S. Wang, F. Cao, J. Zhou, Q. Wu, H. Wang, X. Li, L. Yin, X. Yang, *Chem. Mater.* **2019**, 31, 1936.
- [69] S. Wang, L. Du, Z. Jin, Y. Xin, H. Mattoussi, *J. Am. Chem. Soc.* **2020**, 142, 12669.
- [70] A. Mikosch, S. Ciftci, G. Tainter, R. Shivanna, B. Haehnle, F. Deschler, A. J. Kuehne, *Chem. Mater.* **2019**, 31, 2590.
- [71] J. Liu, B. Shabbir, C. Wang, T. Wan, Q. Ou, P. Yu, A. Tadich, X. Jiao, D. Chu, D. Qi, *Adv. Mater.* **2019**, 31, 1901644.
- [72] a) K. Chen, X. Deng, G. Dodekatos, H. Tüysüz, *J. Am. Chem. Soc.* **2017**, 139, 12267; b) Y. Li, Q. Shu, Q. Du, Y. Dai, S. Zhao, J. Zhang, L. Li, K. Chen, *ACS Appl. Mater. Interfaces* **2019**, 12, 451.
- [73] Y. Wang, L. Luo, Z. Wang, B. Tawiah, C. Liu, J. H. Xin, B. Fei, W.-Y. Wong, *ACS Appl. Mater. Interfaces* **2020**, 12, 27578.
- [74] Y. H. Song, J. S. Yoo, B. K. Kang, S. H. Choi, E. K. Ji, H. S. Jung, D. H. Yoon, *Nanoscale* **2016**, 8, 19523.
- [75] W. Yang, L. Fei, F. Gao, W. Liu, H. Xu, L. Yang, Y. Liu, *Chem. Eng. J.* **2020**, 387, 124180.
- [76] S. Hou, Y. Guo, Y. Tang, Q. Quan, *ACS Appl. Mater. Interfaces* **2017**, 9, 18417.
- [77] V. A. Hintermayr, C. Lampe, M. Löw, J. Roemer, W. Vanderlinden, M. Gramlich, A. X. Böhm, C. Sattler, B. Nickel, T. Lohmüller, A. S. Urban, *Nano Lett.* **2019**, 19, 4928.
- [78] L. Hui, C. Beswick, A. Getachew, H. Heilbrunner, K. Liang, G. Hanta, R. Arbi, M. Munir, H. Dawood, N. I. Goktas, *ACS Appl. Nano Mater.* **2019**, 2, 4121.
- [79] T. Xuan, J. Huang, H. Liu, S. Lou, L. Cao, W. Gan, R.-S. Liu, J. Wang, *Chem. Mater.* **2019**, 31, 1042.
- [80] Y. Li, Y. Lv, Z. Guo, L. Dong, J. Zheng, C. Chai, N. Chen, Y. Lu, C. Chen, *ACS Appl. Mater. Interfaces* **2018**, 10, 15888.
- [81] S. Yang, F. Zhang, J. Tai, Y. Li, Y. Yang, H. Wang, J. Zhang, Z. Xie, B. Xu, H. Zhong, *Nanoscale* **2018**, 10, 5820.
- [82] S. Pan, Y. Chen, Z. Wang, Y.-W. Harn, J. Yu, A. Wang, M. J. Smith, Z. Li, V. V. Tsukruk, J. Peng, Z. Lin, *Nano Energy* **2020**, 77, 105043.
- [83] Y. He, Y. J. Yoon, Y. W. Harn, G. V. Biesold-McGee, S. Liang, C. H. Lin, V. V. Tsukruk, N. Thadhani, Z. Kang, Z. Lin, *Sci. Adv.* **2019**, 5, eaax4424.
- [84] D. N. Minh, S. Eom, L. A. T. Nguyen, J. Kim, J. H. Sim, C. Seo, J. Nam, S. Lee, S. Suk, J. Kim, *Adv. Mater.* **2018**, 30, 1802555.
- [85] G. Jiang, C. Guhrenz, A. Kirch, L. Sonntag, C. Bauer, X. Fan, J. Wang, S. Reineke, N. Gaponik, A. Eychmüller, *ACS Nano* **2019**, 13, 10386.
- [86] W. Yin, M. Li, W. Dong, Z. Luo, Y. Li, J. Qian, J. Zhang, W. Zhang, Y. Zhang, S. V. Kershaw, X. Zhang, W. Zheng, A. L. Rogach, *ACS Energy Lett.* **2021**, 6, 477.
- [87] J. Zhang, P. Jiang, Y. Wang, X. Liu, J. Ma, G. Tu, *ACS Appl. Mater. Interfaces* **2019**, 12, 3080.
- [88] A. Pan, L. Yan, X. Ma, Y. Wu, Y. Zhang, G. Zhou, L. He, *J. Alloys Compd.* **2020**, 844, 156102.
- [89] H. Li, X. Liu, Q. Ying, C. Wang, W. Jia, X. Xing, L. Yin, Z. Lu, K. Zhang, Y. Pan, Z. Shi, L. Huang, D. Jia, *Angew. Chem., Int. Ed.* **2020**, 59, 17207.
- [90] a) J. De Roo, M. Ibáñez, P. Geiregat, G. Nedelcu, W. Walravens, J. Maes, J. C. Martins, I. Van Driessche, M. V. Kovalenko, Z. Hens, *ACS Nano* **2016**, 10, 2071; b) Q. A. Akkerman, G. Raino, M. V. Kovalenko, L. Manna, *Nat. Mater.* **2018**, 17, 394.
- [91] D. Ling, M. J. Hackett, T. Hyeon, *Nano Today* **2014**, 9, 457.
- [92] F. Zhang, H. Zhong, C. Chen, X.-g. Wu, X. Hu, H. Huang, J. Han, B. Zou, Y. Dong, *ACS Nano* **2015**, 9, 4533.
- [93] S. Förster, M. Antonietti, *Adv. Mater.* **1998**, 10, 195.
- [94] X. Pang, L. Zhao, W. Han, X. Xin, Z. Lin, *Nat. Nanotechnol.* **2013**, 8, 426.
- [95] a) W. L. Leong, P. S. Lee, A. Lohani, Y. M. Lam, T. Chen, S. Zhang, A. Dodabalapur, S. G. Mhaisalkar, *Adv. Mater.* **2008**, 20, 2325; b) S. Darling, *Prog. Polym. Sci.* **2007**, 32, 1152; c) X. Pang, L. Zhao, M. Akinc, J. K. Kim, Z. Lin, *Macromolecules* **2011**, 44, 3746.
- [96] a) Y. Chen, Z. Wang, Y. He, Y. J. Yoon, J. Jung, G. Zhang, Z. Lin, *Proc. Natl. Acad. Sci. USA* **2018**, 115, E1391; b) M. Massignani, C. LoPresti, A. Blanz, J. Madsen, S. P. Armes, A. L. Lewis, G. Battaglia, *Small* **2009**, 5, 2424.
- [97] Y. Liu, Z. Wang, S. Liang, Z. Li, M. Zhang, H. Li, Z. Lin, *Nano Lett.* **2019**, 19, 9019.
- [98] a) P. E. Chen, N. C. Anderson, Z. M. Norman, J. S. Owen, *J. Am. Chem. Soc.* **2017**, 139, 3227; b) J. S. Owen, J. Park, P.-E. Trudeau, A. P. Alivisatos, *J. Am. Chem. Soc.* **2008**, 130, 12279.
- [99] D. N. Dirin, S. Dreyfuss, M. I. Bodnarchuk, G. Nedelcu, P. Papagiorgis, G. Itkos, M. V. Kovalenko, *J. Am. Chem. Soc.* **2014**, 136, 6550.
- [100] L. M. Wheeler, E. M. Sanehira, A. R. Marshall, P. Schulz, M. Suri, N. C. Anderson, J. A. Christians, D. Nordlund, D. Sokaras, T. Kroll, *J. Am. Chem. Soc.* **2018**, 140, 10504.
- [101] J. Li, L. Xu, T. Wang, J. Song, J. Chen, J. Xue, Y. Dong, B. Cai, Q. Shan, B. Han, *Adv. Mater.* **2017**, 29, 1603885.
- [102] S. M. Lee, H. Jung, W. I. Park, Y. Lee, E. Koo, J. Bang, *ChemistrySelect* **2018**, 3, 11320.
- [103] a) F. Krieg, S. T. Ochsenbein, S. Yakunin, S. Ten Brinck, P. Aellen, A. Süess, B. Clerc, D. Guggisberg, O. Nazarenko, Y. Shynkarenko, *ACS Energy Lett.* **2018**, 3, 641; b) T. Xuan, X. Yang, S. Lou, J. Huang, Y. Liu, J. Yu, H. Li, K.-L. Wong, C. Wang, J. Wang, *Nanoscale* **2017**, 9, 15286.
- [104] a) S. Li, D. Lei, W. Ren, X. Guo, S. Wu, Y. Zhu, A. L. Rogach, M. Chhowalla, A. K.-Y. Jen, *Nat. Commun.* **2020**, 11, 1192; b) H. Huang, B. Chen, Z. Wang, T. F. Hung, A. S. Susha, H. Zhong, A. L. Rogach, *Chem. Sci.* **2016**, 7, 5699; c) B. Luo, Y. C. Pu, S. A. Lindley, Y. Yang, L. Lu, Y. Li, X. Li, J. Z. Zhang, *Angew. Chem., Int. Ed.* **2016**, 55, 8864.
- [105] G. Li, Z.-K. Tan, D. Di, M. L. Lai, J. Jiang, J. H.-W. Lim, R. H. Friend, N. C. Greenham, *Nano Lett.* **2015**, 15, 2640.
- [106] L. Zhao, Y.-W. Yeh, N. L. Tran, F. Wu, Z. Xiao, R. A. Kerner, Y. L. Lin, G. D. Scholes, N. Yao, B. P. Rand, *ACS Nano* **2017**, 11, 3957.
- [107] S. Chang, Z. Bai, H. Zhong, *Adv. Opt. Mater.* **2018**, 6, 1800380.
- [108] E. Kang, G. S. Jeong, Y. Choi, K. H. Lee, A. Khademhosseini, S.-H. Lee, *Nat. Mater.* **2011**, 10, 877.
- [109] V. Jella, S. Ippili, J.-H. Eom, S. Pammi, J.-S. Jung, V.-D. Tran, V. H. Nguyen, A. Kirakosyan, S. Yun, D. Kim, *Nano Energy* **2019**, 57, 74.
- [110] Z. Gu, Z. Huang, X. Hu, Y. Wang, L. Li, M. Li, Y. Song, *ACS Appl. Mater. Interfaces* **2020**, 12, 22157.
- [111] X. Huang, Q. Guo, D. Yang, X. Xiao, X. Liu, Z. Xia, F. Fan, J. Qiu, G. Dong, *Nat. Photonics* **2020**, 14, 82.
- [112] X. Huang, Q. Guo, S. Kang, T. Ouyang, Q. Chen, X. Liu, Z. Xia, Z. Yang, Q. Zhang, J. Qiu, *ACS Nano* **2020**, 14, 3150.

- [113] T. Umehayashi, K. Asai, T. Kondo, A. Nakao, *Phys. Rev. B* **2003**, 67, 155405.
- [114] T. C. Jellicoe, J. M. Richter, H. F. Glass, M. Tabachnyk, R. Brady, S. n. E. Dutton, A. Rao, R. H. Friend, D. Credgington, N. C. Greenham, *J. Am. Chem. Soc.* **2016**, 138, 2941.
- [115] a) A. Swarnkar, V. K. Ravi, A. Nag, *ACS Energy Lett.* **2017**, 2, 1089; b) S. Meloni, G. Palermo, N. Ashari-Astani, M. Grätzel, U. Rothlisberger, *J. Mater. Chem. A* **2016**, 4, 15997.
- [116] D. V. Talapin, J.-S. Lee, M. V. Kovalenko, E. V. Shevchenko, *Chem. Rev.* **2010**, 110, 389.
- [117] J. A. Sichert, Y. Tong, N. Mutz, M. Vollmer, S. Fischer, K. Z. Milowska, R. García Cortadella, B. Nickel, C. Cardenas-Daw, J. K. Stolarczyk, *Nano Lett.* **2015**, 15, 6521.
- [118] a) Y. Dong, T. Qiao, D. Kim, D. Parobek, D. Rossi, D. H. Son, *Nano Lett.* **2018**, 18, 3716; b) M. Imran, F. Di Stasio, Z. Dang, C. Canale, A. H. Khan, J. Shamsi, R. Brescia, M. Prato, L. Manna, *Chem. Mater.* **2016**, 28, 6450.
- [119] C.-H. Lu, G. V. Biesold-McGee, Y. Liu, Z. Kang, Z. Lin, *Chem. Soc. Rev.* **2020**, 49, 4953.
- [120] J. Kang, L.-W. Wang, *J. Phys. Chem. Lett.* **2017**, 8, 489.
- [121] D. N. Dirin, L. Protesescu, D. Trummer, I. V. Kochetygov, S. Yakunin, F. Krumeich, N. P. Stadie, M. V. Kovalenko, *Nano Lett.* **2016**, 16, 5866.
- [122] a) W.-J. Yin, T. Shi, Y. Yan, *Appl. Phys. Lett.* **2014**, 104, 063903; b) A. Buin, P. Pietsch, J. Xu, O. Voznyy, A. H. Ip, R. Comin, E. H. Sargent, *Nano Lett.* **2014**, 14, 6281; c) S. Ten Brinck, I. Infante, *ACS Energy Lett.* **2016**, 1, 1266.
- [123] a) G. Yuan, C. Ritchie, M. Ritter, S. Murphy, D. E. Gómez, P. Mulvaney, *J. Phys. Chem. C* **2017**, 122, 13407; b) H. Cho, Y. H. Kim, C. Wolf, H. D. Lee, T. W. Lee, *Adv. Mater.* **2018**, 30, 1704587; c) H. Huang, M. I. Bodnarchuk, S. V. Kershaw, M. V. Kovalenko, A. L. Rogach, *ACS Energy Lett.* **2017**, 2, 2071.
- [124] W. Lv, L. Li, M. Xu, J. Hong, X. Tang, L. Xu, Y. Wu, R. Zhu, R. Chen, W. Huang, *Adv. Mater.* **2019**, 31, 1900682.
- [125] a) M. Kim, S. G. Motti, R. Sorrentino, A. Petrozza, *Energy Environ. Sci.* **2018**, 11, 2609; b) A. Pramanik, K. Gates, S. Patibandla, D. Davis, S. Begum, R. Iftikhar, S. Alamgir, S. Paige, M. M. Porter, P. C. Ray, *ACS Appl. Bio Mater.* **2019**, 2, 5872.
- [126] S. Lee, J. H. Park, B. R. Lee, E. D. Jung, J. C. Yu, D. Di Nuzzo, R. H. Friend, M. H. Song, *J. Phys. Chem. Lett.* **2017**, 8, 1784.
- [127] F. Liu, Y. Zhang, C. Ding, S. Kobayashi, T. Izuishi, N. Nakazawa, T. Toyoda, T. Ohta, S. Hayase, T. Minemoto, *ACS Nano* **2017**, 11, 10373.
- [128] J. Pan, Y. Shang, J. Yin, M. De Bastiani, W. Peng, I. Dursun, L. Sinatra, A. M. El-Zohry, M. N. Hedhili, A.-H. Emwas, *J. Am. Chem. Soc.* **2017**, 140, 562.
- [129] H. Zhang, Y. Wu, C. Shen, E. Li, C. Yan, W. Zhang, H. Tian, L. Han, W. H. Zhu, *Adv. Energy Mater.* **2019**, 9, 1803573.
- [130] E. T. Vickers, T. A. Graham, A. H. Chowdhury, B. Bahrami, B. W. Dreskin, S. Lindley, S. B. Naghadeh, Q. Qiao, J. Z. Zhang, *ACS Energy Lett.* **2018**, 3, 2931.
- [131] G. Rainò, A. Landuyt, F. Krieg, C. Bernasconi, S. T. Ochsenbein, D. N. Dirin, M. I. Bodnarchuk, M. V. Kovalenko, *Nano Lett.* **2019**, 19, 3648.
- [132] Y. Yang, J. T. Lee, T. Liyanage, R. Sardar, *J. Am. Chem. Soc.* **2019**, 141, 1526.
- [133] L. Chouhan, S. Ghimire, C. Subrahmanyam, T. Miyasaka, V. Biju, *Chem. Soc. Rev.* **2020**, 49, 2869.
- [134] T. M. Brenner, D. A. Egger, L. Kronik, G. Hodes, D. Cahen, *Nat. Rev. Mater.* **2016**, 1, 15007.
- [135] a) R. E. Brandt, V. Stevanovic, D. S. Ginley, T. Buonassisi, *MRS Commun.* **2015**, 5, 265; b) S. M. Sze, K. K. Ng, *Physics of Semiconductor Devices*, John Wiley & Sons, Hoboken, NJ, USA **2006**; c) T. M. Brenner, D. A. Egger, A. M. Rappe, L. Kronik, G. Hodes, D. Cahen, *J. Phys. Chem. Lett.* **2015**, 6, 4754.
- [136] a) R. L. Milot, G. E. Eperon, H. J. Snaith, M. B. Johnston, L. M. Herz, *Adv. Funct. Mater.* **2015**, 25, 6218; b) C. Wehrenfennig, G. E. Eperon, M. B. Johnston, H. J. Snaith, L. M. Herz, *Adv. Mater.* **2014**, 26, 1584; c) N. K. Noel, S. D. Stranks, A. Abate, C. Wehrenfennig, S. Guarnera, A.-A. Haghighirad, A. Sadhanala, G. E. Eperon, S. K. Pathak, M. B. Johnston, *Energy Environ. Sci.* **2014**, 7, 3061.
- [137] W. Tress, N. Marinova, O. Inganäs, M. K. Nazeeruddin, S. M. Zakeeruddin, M. Graetzel, *Adv. Energy Mater.* **2015**, 5, 1400812.
- [138] a) A. Abrusci, S. D. Stranks, P. Docampo, H.-L. Yip, A. K.-Y. Jen, H. J. Snaith, *Nano Lett.* **2013**, 13, 3124; b) P. L. Qin, G. Yang, Z. w. Ren, S. H. Cheung, S. K. So, L. Chen, J. Hao, J. Hou, G. Li, *Adv. Mater.* **2018**, 30, 1706126.
- [139] D. Bi, C. Yi, J. Luo, J.-D. Décoppet, F. Zhang, S. M. Zakeeruddin, X. Li, A. Hagfeldt, M. Grätzel, *Nat. Energy* **2016**, 1, 16142.
- [140] T.-H. Han, J.-W. Lee, C. Choi, S. Tan, C. Lee, Y. Zhao, Z. Dai, N. De Marco, S.-J. Lee, S.-H. Bae, Y. Yuan, H. M. Lee, Y. Huang, Y. Yang, *Nat. Commun.* **2019**, 10, 520.
- [141] Q. Zeng, X. Zhang, X. Feng, S. Lu, Z. Chen, X. Yong, S. A. Redfern, H. Wei, H. Wang, H. Shen, *Adv. Mater.* **2018**, 30, 1705393.
- [142] A. M. Leguy, J. M. Frost, A. P. McMahon, V. G. Sakai, W. Kockelmann, C. Law, X. Li, F. Foglia, A. Walsh, B. C. O'Regan, J. Nelson, J. T. Cabral, P. R. F. Barnes, *Nat. Commun.* **2015**, 6, 7124.
- [143] a) K. Y. Lee, D. Kim, J. H. Lee, T. Y. Kim, M. K. Gupta, S. W. Kim, *Adv. Funct. Mater.* **2014**, 24, 37; b) E. J. Juarez-Perez, R. S. Sanchez, L. Badia, G. Garcia-Belmonte, Y. S. Kang, I. Mora-Sero, J. Bisquert, *J. Phys. Chem. Lett.* **2014**, 5, 2390.
- [144] J. M. Frost, K. T. Butler, F. Brivio, C. H. Hendon, M. Van Schilfgaarde, A. Walsh, *Nano Lett.* **2014**, 14, 2584.
- [145] a) B. Chen, M. Yang, S. Priya, K. Zhu, *J. Phys. Chem. Lett.* **2016**, 7, 905; b) L. Li, Z. Sun, P. Wang, W. Hu, S. Wang, C. Ji, M. Hong, J. Luo, *Angew. Chem., Int. Ed.* **2017**, 56, 12150.
- [146] a) S. Liu, F. Zheng, I. Grinberg, A. M. Rappe, *J. Phys. Chem. Lett.* **2016**, 7, 1460; b) Y.-M. You, W.-Q. Liao, D. Zhao, H.-Y. Ye, Y. Zhang, Q. Zhou, X. Niu, J. Wang, P.-F. Li, D.-W. Fu, *Science* **2017**, 357, 306.
- [147] R. Ding, X. Zhang, G. Chen, H. Wang, R. Kishor, J. Xiao, F. Gao, K. Zeng, X. Chen, X. W. Sun, *Nano Energy* **2017**, 37, 126.
- [148] a) N. Rolston, B. L. Watson, C. D. Bailie, M. D. McGehee, J. P. Bastos, R. Gehlhaar, J.-E. Kim, D. Vak, A. T. Mallajosyula, G. Gupta, *Extreme Mech. Lett.* **2016**, 9, 353; b) J. Yu, M. Wang, S. Lin, *ACS Nano* **2016**, 10, 11044.
- [149] N. Rolston, A. D. Printz, J. M. Tracy, H. C. Weerasinghe, D. Vak, L. J. Haur, A. Priyadarshi, N. Mathews, D. J. Slotcavage, M. D. McGehee, *Adv. Energy Mater.* **2018**, 8, 1702116.
- [150] J. Zhao, Y. Deng, H. Wei, X. Zheng, Z. Yu, Y. Shao, J. E. Shield, J. Huang, *Sci. Adv.* **2017**, 3, eaao5616.
- [151] a) R. Cheacharoen, N. Rolston, D. Harwood, K. A. Bush, R. H. Dauskardt, M. D. McGehee, *Energy Environ. Sci.* **2018**, 11, 144; b) N. Rolston, K. A. Bush, A. D. Printz, A. Gold-Parker, Y. Ding, M. F. Toney, M. D. McGehee, R. H. Dauskardt, *Adv. Energy Mater.* **2018**, 8, 1802139.
- [152] F. Ondreas, P. Lepcio, M. Zboncak, K. Zarybnicka, L. E. Govaert, J. Jancar, *Macromolecules* **2019**, 52, 6250.
- [153] a) X. Fan, W. Nie, H. Tsai, N. Wang, H. Huang, Y. Cheng, R. Wen, L. Ma, F. Yan, Y. Xia, *Adv. Sci.* **2019**, 6, 1900813; b) D. Yang, R. Yang, S. Priya, S. Liu, *Angew. Chem., Int. Ed.* **2019**, 58, 4466; c) D. Zhang, T. Huang, L. Duan, *Adv. Mater.* **2020**, 32, 1902391.
- [154] a) S.-B. Kang, H.-J. Kim, Y.-J. Noh, S.-I. Na, H.-K. Kim, *Nano Energy* **2015**, 11, 179; b) Z. Wu, P. Li, Y. Zhang, Z. Zheng, *Small Methods* **2018**, 2, 1800031.
- [155] Y.-C. Chiang, H.-C. Wu, H.-F. Wen, C.-C. Hung, C.-W. Hong, C.-C. Kuo, T. Higashihara, W.-C. Chen, *Macromolecules* **2019**, 52, 4396.
- [156] M. V. Kovalenko, L. Protesescu, M. I. Bodnarchuk, *Science* **2017**, 358, 745.

- [157] D. Yang, M. Cao, Q. Zhong, P. Li, X. Zhang, Q. Zhang, *J. Mater. Chem. C* **2019**, 7, 757.
- [158] F. Liu, J. Jiang, Y. Zhang, C. Ding, T. Toyoda, S. Hayase, R. Wang, S. Tao, Q. Shen, *Angew. Chem., Int. Ed.* **2020**, 59, 8421.
- [159] a) E. T. Vickers, E. E. Enlow, W. G. Delmas, A. C. DiBenedetto, A. H. Chowdhury, B. Bahrami, B. W. Dreskin, T. A. Graham, I. N. Hernandez, S. A. Carter, *ACS Energy Lett.* **2020**, 5, 817; b) Y. Dong, Y.-K. Wang, F. Yuan, A. Johnston, Y. Liu, D. Ma, M.-J. Choi, B. Chen, M. Chekini, S.-W. Baek, L. K. Sagar, J. Fan, Y. Hou, M. Wu, S. Lee, B. Sun, S. Hoogland, R. Quintero-Bermudez, H. Ebe, P. Todorovic, F. Dinic, P. Li, H. T. Kung, M. I. Saidaminov, E. Kumacheva, E. Spiecker, L.-S. Liao, O. Voznyy, Z.-H. Lu, E. H. Sargent, *Nat. Nanotechnol.* **2020**, 15, 668; c) M. I. Saleem, S. Yang, R. Zhi, M. Sulaman, P. V. Chandrasekar, Y. Jiang, Y. Tang, A. Batool, B. Zou, *Adv. Mater. Interfaces* **2020**, 7, 2000360.
- [160] a) Y. Xin, W. Shen, Z. Deng, J. Zhang, *ACS Appl. Mater. Interfaces* **2018**, 10, 28971; b) Y. Xin, H. Zhao, J. Zhang, *ACS Appl. Mater. Interfaces* **2018**, 10, 4971.
- [161] Y. Liu, F. Li, L. Qiu, K. Yang, Q. Li, X. Zheng, H. Hu, T. Guo, C. Wu, T. W. Kim, *ACS Nano* **2019**, 13, 2042.
- [162] a) Y. H. Kim, H. Cho, J. H. Heo, T. S. Kim, N. Myoung, C. L. Lee, S. H. Im, T. W. Lee, *Adv. Mater.* **2015**, 27, 1248; b) G. Nedelcu, L. Protesescu, S. Yakunin, M. I. Bodnarchuk, M. J. Grotevent, M. V. Kovalenko, *Nano Lett.* **2015**, 15, 5635; c) M. Cha, P. Da, J. Wang, W. Wang, Z. Chen, F. Xiu, G. Zheng, Z.-S. Wang, *J. Am. Chem. Soc.* **2016**, 138, 8581; d) B. R. Sutherland, E. H. Sargent, *Nat. Photonics* **2016**, 10, 295.
- [163] Y. Tian, C. Zhou, M. Worku, X. Wang, Y. Ling, H. Gao, Y. Zhou, Y. Miao, J. Guan, B. Ma, *Adv. Mater.* **2018**, 30, 1707093.
- [164] S. Wei, H. Zhu, J. Zhang, L. Wang, M. An, Y. Wang, X. Zhang, Y. Liu, *J. Alloys Compd.* **2019**, 789, 209.
- [165] S. A. Veldhuis, P. P. Boix, N. Yantara, M. Li, T. C. Sum, N. Mathews, S. G. Mhaisalkar, *Adv. Mater.* **2016**, 28, 6804.
- [166] F. Deschler, M. Price, S. Pathak, L. E. Klintberg, D.-D. Jarausch, R. Higler, S. Hüttner, T. Leijtens, S. D. Stranks, H. J. Snaith, M. Atatüre, R. T. Phillips, R. H. Friend, *J. Phys. Chem. Lett.* **2014**, 5, 1421.
- [167] a) J. Gong, Y. Wang, S. Liu, P. Zeng, X. Yang, R. Liang, Q. Ou, X. Wu, S. Zhang, *Opt. Express* **2017**, 25, A1154; b) H. Cha, S. Bae, H. Jung, M. J. Ko, H. Jeon, *Adv. Opt. Mater.* **2017**, 5, 1700545.
- [168] B. R. Sutherland, S. Hoogland, M. M. Adachi, C. T. Wong, E. H. Sargent, *ACS Nano* **2014**, 8, 10947.
- [169] Q. Zhang, S. T. Ha, X. Liu, T. C. Sum, Q. Xiong, *Nano Lett.* **2014**, 14, 5995.
- [170] J. Xing, X. F. Liu, Q. Zhang, S. T. Ha, Y. W. Yuan, C. Shen, T. C. Sum, Q. Xiong, *Nano Lett.* **2015**, 15, 4571.
- [171] G. Xing, M. H. Kumar, W. K. Chong, X. Liu, Y. Cai, H. Ding, M. Asta, M. Grätzel, S. Mhaisalkar, N. Mathews, *Adv. Mater.* **2016**, 28, 8191.
- [172] C. Dujardin, E. Auffray, E. Bourret-Courchesne, P. Dorenbos, P. Lecoq, M. Nikl, A. Vasil'Ev, A. Yoshikawa, R.-Y. Zhu, *IEEE Trans. Nucl. Sci.* **2018**, 65, 1977.
- [173] M. Nikl, A. Yoshikawa, *Adv. Opt. Mater.* **2015**, 3, 463.
- [174] a) Q. Chen, J. Wu, X. Ou, B. Huang, J. Almutlaq, A. A. Zhumekenov, X. Guan, S. Han, L. Liang, Z. Yi, *Nature* **2018**, 561, 88; b) Y. C. Kim, K. H. Kim, D.-Y. Son, D.-N. Jeong, J.-Y. Seo, Y. S. Choi, I. T. Han, S. Y. Lee, N.-G. Park, *Nature* **2017**, 550, 87; c) Y. Zhang, R. Sun, X. Ou, K. Fu, Q. Chen, Y. Ding, L.-J. Xu, L. Liu, Y. Han, A. V. Malko, *ACS Nano* **2019**, 13, 2520; d) B. Yang, L. Yin, G. Niu, J. H. Yuan, K. H. Xue, Z. Tan, X. S. Miao, M. Niu, X. Du, H. Song, *Adv. Mater.* **2019**, 31, 1904711; e) D. Yu, P. Wang, F. Cao, Y. Gu, J. Liu, Z. Han, B. Huang, Y. Zou, X. Xu, H. Zeng, *Nat. Commun.* **2020**, 11, 3395.
- [175] C. Liu, Z. Li, T. J. Hajagos, D. Kishpaugh, D. Y. Chen, Q. Pei, *ACS Nano* **2017**, 11, 6422.
- [176] R. T. Williams, W. W. Wolszczak, X. Yan, D. L. Carroll, *ACS Nano* **2020**, 14, 5161.
- [177] Y. Zhong, Z. Ma, S. Zhu, J. Yue, M. Zhang, A. L. Antaris, J. Yuan, R. Cui, H. Wan, Y. Zhou, W. Wang, N. F. Huang, J. Luo, Z. Hu, H. Dai, *Nat. Commun.* **2017**, 8, 737.
- [178] M. Humar, S. H. Yun, *Nat. Photonics* **2015**, 9, 572.
- [179] Y. Dong, X. Tang, Z. Zhang, J. Song, T. Niu, D. Shan, H. Zeng, *Matter* **2020**, 3, 273.
- [180] H. Huang, B. Pradhan, J. Hofkens, M. B. Roeffaers, J. A. Steele, *ACS Energy Lett.* **2020**, 5, 1107.
- [181] T. Hisatomi, J. Kubota, K. Domen, *Chem. Soc. Rev.* **2014**, 43, 7520.
- [182] a) Y. Wu, P. Wang, X. Zhu, Q. Zhang, Z. Wang, Y. Liu, G. Zou, Y. Dai, M. H. Whangbo, B. Huang, *Adv. Mater.* **2018**, 30, 1704342; b) M. Shi, G. Li, W. Tian, S. Jin, X. Tao, Y. Jiang, E. A. Pidko, R. Li, C. Li, *Adv. Mater.* **2020**, 32, 2002137; c) X. Zhu, Y. Lin, J. San Martin, Y. Sun, D. Zhu, Y. Yan, *Nat. Commun.* **2019**, 10, 2843; d) Q. Chen, Y. Dong, K. Li, W. Luo, C. Zhu, H. Guan, H. Wang, L. Wang, K. Deng, H. Zhou, *Angew. Chem., Int. Ed.* **2020**, 59, 12931; e) M. Hamdan, A. K. Chandiran, *Angew. Chem., Int. Ed.* **2020**, 59, 16033.
- [183] Y.-F. Xu, M.-Z. Yang, B.-X. Chen, X.-D. Wang, H.-Y. Chen, D.-B. Kuang, C.-Y. Su, *J. Am. Chem. Soc.* **2017**, 139, 5660.
- [184] Y. Zhu, Y. Liu, K. A. Miller, H. Zhu, E. Egap, *ACS Macro Lett.* **2020**, 9, 725.
- [185] Z. L. Wang, J. Song, *Science* **2006**, 312, 242.
- [186] a) A. Sultana, P. Sadhukhan, M. M. Alam, S. Das, T. R. Mridha, D. Mandal, *ACS Appl. Mater. Interfaces* **2018**, 10, 4121; b) A. Sultana, M. M. Alam, P. Sadhukhan, U. K. Ghorai, S. Das, T. R. Mridha, D. Mandal, *Nano Energy* **2018**, 49, 380.
- [187] M. Liu, Y. Chen, C.-S. Tan, R. Quintero-Bermudez, A. H. Proppe, R. Munir, H. Tan, O. Voznyy, B. Scheffel, G. Walters, *Nature* **2019**, 570, 96.
- [188] J. Jang, Y.-H. Kim, S. Park, D. Yoo, H. Cho, J. Jang, H. B. Jeong, H. Lee, J. M. Yuk, C. B. Park, D. Y. Jeon, Y.-H. Kim, B.-S. Bae, T.-W. Lee, *Adv. Mater.* **2021**, 33, 2005255.
- [189] J. Liu, Z. Yang, B. Ye, Z. Zhao, Y. Ruan, T. Guo, X. Yu, G. Chen, S. Xu, *J. Mater. Chem. C* **2019**, 7, 4934.
- [190] X. Li, F. Zhang, H. He, J. J. Berry, K. Zhu, T. Xu, *Nature* **2020**, 578, 555.
- [191] J. Zhang, G. Hodes, Z. Jin, S. Liu, *Angew. Chem., Int. Ed.* **2019**, 58, 15596.
- [192] Y. Hou, H. Zhang, W. Chen, S. Chen, C. O. R. Quiroz, H. Azimi, A. Osvet, G. J. Matt, E. Zeira, J. Seuring, *Adv. Energy Mater.* **2015**, 5, 1500543.
- [193] K. Hwang, Y. S. Jung, Y. J. Heo, F. H. Scholes, S. E. Watkins, J. Subbiah, D. J. Jones, D. Y. Kim, D. Vak, *Adv. Mater.* **2015**, 27, 1241.
- [194] a) J. Hou, O. Inganäs, R. H. Friend, F. Gao, *Nat. Mater.* **2018**, 17, 119; b) H. Yao, L. Ye, H. Zhang, S. Li, S. Zhang, J. Hou, *Chem. Rev.* **2016**, 116, 7397.
- [195] Z. Luo, D. Marson, Q. K. Ong, A. Loiudice, J. Kohlbrecher, A. Radulescu, A. Krause-Heuer, T. Darwish, S. Balog, R. Buonsanti, D. I. Svergun, P. Posocco, F. Stellacci, *Nat. Commun.* **2018**, 9, 1343.
- [196] a) N. Yaritha, H. Tahara, T. Ihara, T. Kawawaki, R. Sato, M. Saruyama, T. Teranishi, Y. Kanemitsu, *J. Phys. Chem. Lett.* **2017**, 8, 1413; b) G. R. Yettapu, D. Talukdar, S. Sarkar, A. Swarnkar, A. Nag, P. Ghosh, P. Mandal, *Nano Lett.* **2016**, 16, 4838.
- [197] R. Wang, J. Xue, K.-L. Wang, Z.-K. Wang, Y. Luo, D. Fenning, G. Xu, S. Nuryyeva, T. Huang, Y. Zhao, J. L. Yang, J. Zhu, M. Wang, S. Tan, I. Yavuz, K. N. Houk, Y. Yang, *Science* **2019**, 366, 1509.
- [198] a) D. Meggiolaro, E. Mosconi, F. De Angelis, *ACS Energy Lett.* **2018**, 3, 447; b) E. Mosconi, J. M. Aspiroz, F. De Angelis, *Chem. Mater.* **2015**, 27, 4885.
- [199] F. Giustino, H. J. Snaith, *ACS Energy Lett.* **2016**, 1, 1233.
- [200] X. Li, J. Zuo, Y. Guo, X. Yuan, *Macromolecules* **2004**, 37, 10042.

- [201] Y. Chen, Z. Wang, Y. W. Harn, S. Pan, Z. Li, S. Lin, J. Peng, G. Zhang, Z. Lin, *Angew. Chem., Int. Ed.* **2019**, *58*, 11910.
- [202] A. P. Blum, J. K. Kammeyer, A. M. Rush, C. E. Callmann, M. E. Hahn, N. C. Gianneschi, *J. Am. Chem. Soc.* **2015**, *137*, 2140.
- [203] a) H. Xu, Y. Xu, X. Pang, Y. He, J. Jung, H. Xia, Z. Lin, *Sci. Adv.* **2015**, *1*, e1500025; b) C. Yi, Y. Yang, B. Liu, J. He, Z. Nie, *Chem. Soc. Rev.* **2020**, *49*, 465.
- [204] Z. Nie, D. Fava, M. Rubinstein, E. Kumacheva, *J. Am. Chem. Soc.* **2008**, *130*, 3683.
- [205] T. N. Hoheisel, K. Hur, U. B. Wiesner, *Prog. Polym. Sci.* **2015**, *40*, 3.
- [206] a) X. Lin, S. Ye, C. Kong, K. Webb, C. Yi, S. Zhang, Q. Zhang, J. T. Fourkas, Z. Nie, *J. Am. Chem. Soc.* **2020**, *142*, 17282; b) C. Yi, Y. Yang, Z. Nie, *J. Am. Chem. Soc.* **2019**, *141*, 7917.



Shuang Liang is a Ph.D. student in Dr. Zhiqun Lin's group at the Georgia Institute of Technology since 2017. He received his B.E. degree in chemical engineering from Southeast University, China in 2017. His current research is focused on the synthesis and application of functional semiconducting nanomaterials, block copolymers, and polymer-based nanocomposites.



Mingyue Zhang received his B.S. and Master's in materials science and engineering from the Pennsylvania State University and University of Pennsylvania in 2016 and 2018, respectively. He is now a Ph.D. student in materials science and engineering at Georgia Institute of Technology. His research focuses on the synthesis of nonlinear block copolymers and nanocrystals using nonlinear block copolymer as nanoreactors.



Gill M. Biesold is a Ph.D. student in the Materials Science and Engineering department at Georgia Institute of Technology. He received his B.S. in materials science and engineering from Clemson University in 2017. His current research is focused on quantum dots and their potential applications in lasing and sensing.



Zhiqun Lin is a professor at the School of Materials Science and Engineering at the Georgia Institute of Technology. His research interests include solar energy conversion, batteries, electrocatalysis, semiconductor organic-inorganic nanocomposites, multifunctional nanocrystals, conjugated polymers, block copolymers, hierarchical structure formation and assembly, and surface and interfacial properties.